Mechanistic basis for the recognition of laminin-511 by α6β1 integrin

（α6β1 インテグリンによるラミニン-511 の認識機構）

A Doctoral Dissertation
Presented to Osaka University

2018

Mamoru Takizawa

Contents

Chapter 1: Introduction

Organization of cells is a fundamental process for building tissues in multicellular organisms. In vertebrates, there are four basic types of tissues; epithelial, connective, muscular, and nerve tissues. These tissues show a well-ordered spatial arrangement of diverse cell types and have functions beyond what single cell could accomplish. Extracellular matrix (ECM) helps these cells to bind together and harmonizes diverse cellular functions.

The emergence of ECM coincides with the origin of multicellular organisms (*1*). ECM is a generic term used to refer to the supramolecular complex of structural and regulatory ECM proteins occupying extracellular space in tissues. ECM proteins elicit a variety of cell behaviors such as cell adhesion, migration, proliferation, and survival. ECM has two basic forms; interstitial matrix and basement membrane (BM) (Fig. 1A). Interstitial matrix surrounds the cells in connective tissue and gives organs mechanical properties of tensile, compressive strength, and elasticity. On the other hand, BM is a sheet-like architecture of 50-100 nm in thickness that underlies most, if not all, epithelial/endothelial cells and surrounds muscle/adipose cells (Fig. 1B) (*2*).

1-1. Basement membrane

When viewed by transmission electron microscopy, BM is seen at the boundary between epithelial cells and connective tissue (Fig. 1C). BM consists of three layers; an electron-lucent layer (*lamina lucida*) adjacent to a plasma membrane, an electron-dense layer (*lamina densa*), and an anchoring fibril (*lamina fibroreticularis*) connecting with subjacent connective tissue (*3-5*). Although more than 50 BM proteins have been identified to date (*6*), BM is composed of a common set of proteins; laminins, collagen IV, nidogens, and perlecan (*7*). A number of in vitro studies has revealed that laminins and collagen IV are assembled into independent networks that act as frameworks for BM assembly (*7, 8*). In electron microscopic observations, laminin network is visualized as continuous lattice consisting of interconnecting struts with vertices that can be distinguished from the network of collagen IV (Fig. 1D) (*9*).

Collagen IV is a triple-helical molecule commonly composed of two α1 and one α2 subunits ($\alpha1_2\alpha2$[IV]). Collagen IV assembles into an interdigitating network through formation of C-terminal non-collagenous domain (NC1) dimers and N-terminal tetramers (7S domain) (Fig. 1E) (*8*). Gene ablation of α1[IV] and α2[IV] subunits in mice resulted in embryonic death (E10.5-11.5) characterized by abnormality of BMs including Reichert's membrane, despite no effect on the deposition of laminins and nidogens in the BM zones (*10*). Expression of laminins precedes the appearance of collagen IV in early embryonic stage (*11*), suggesting that collagen IV is required for BM stability, but dispensable for initiation of BM assembly.

Nidogens, containing nidogen 1 and nidogen 2, do not assemble into a network, but bind to laminins and collagen IV so as to link these independent networks together (Fig. 1E) (*8*). Nidogens consist of three globular domains (G1–3). Nidogens bind to LEb region of laminin γ1/γ3 chains through the G3 domain, and also bind to the triple-helical collagenous domain of collagen IV through the G2 domain (*12, 13*). The knock-

out of the nidogen genes had a mild consequence in mice because nidogen 1 and nidogen 2 compensate for each other. The single knockout in mice lacking either nidogen 1 or nidogen 2 showed no abnormality and were fertile (*14, 15*), whereas double deletion of nidogens resulted in a postnatal lethality associated with the phenotypes including impaired heart morphogenesis, delayed lung differentiation, and renal dysgenesis (*16-18*).

Perlecan is a major heparan sulfate proteoglycan (HSPG) that is situated in not only BMs but also cartilage. Perlecan null-mice showed a severe chondrodysplasia in embryonic development as well as deterioration of BMs with increased mechanical stress such as contracting myocardium (*19, 20*). The core protein of perlecan is divided into five domains (domains I–V) (Fig. 1E). Among these, domain IV interacts with the G2 domain of nidogens (*21*). Several lines of evidence show that HS chains in domain I not only interact with collagen IV but also bind a number of cytokines and growth factors (*22, 23*). Therefore, perlecan is assumed to provide a depot of the regulatory factors as well as a physical support for BMs.

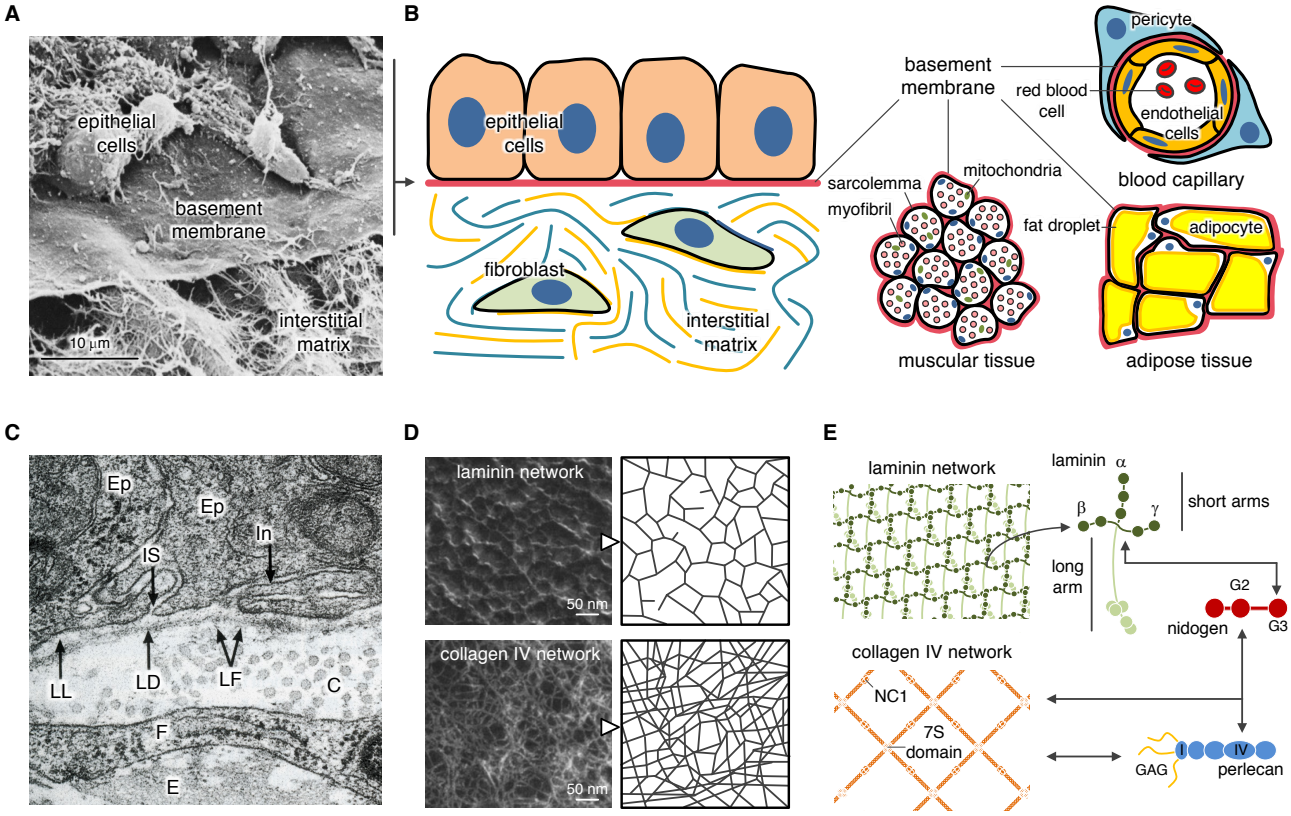

Fig. 1. Basement membrane.

(**A**) An electron microscopic image of the cornea in the chick embryo (B. Alberts *et al*., Molecular Biology of the Cell, 6th ed., with minor modifications). (**B**) Schematic diagrams of basement membrane. Basement membranes underlie epithelial/endothelial cells and surround muscle/fat cells. This figure is illustrated with reference to R. Jayadev and D. R. Sherwood, *Curr. Biol.* **27,** 207-211, 2017. (**C**) A high-magnification transmission electron microscopic image of mouse tracheal epithelium. LL, *lamina lucida*; LD, *lamina densa*; LF, *lamina fibroreticularis*; C, collagen fibril; E, elastic fiber; Ep, epithelial cell; F, fibroblast, IS, intracellular space (B. Young *et al*., Wheater's Functional Histology, 4th ed.). (**D**) Independent networks of EHS sarcoma-derived laminin and collagen IV (P. D. Yurchenco *et al*., *J. Cell Biol*. **117**, 1119-1133, 1992). (**E**) Laminin and collagen IV networks, which act as the BMs framework, associate with each other through the interactions with nidogen and perlecan.

1-2. Laminins

In 1979, laminin was isolated as a high molecular weight non-collagenous glycoprotein from Engelbreth-Holm-Swarm (EHS) sarcoma producing a copious amount of BM proteins (*24*). Laminins are composed of three chains, α, β, and γ. In mammals, 11 laminin chains (α1 to α5, β1 to β3, and γ1 to γ3) and 16 combinations of these have been identified (Fig. 2, A and B) (*25*). Laminin genes and/or proteins are widespread across metazoans (Fig. 2C) (*26*). The evolutionarily ancient one α and one β chain genes has been identified in the *Oscarella carmela* (sponge) (*27*) and *Hydra vulgaris* (hydra) (*28*). In *Caenorhabditis elegans* (nematodes) and insects such as *Drosophila melanogaster* (fruit fly), two α, one β, and one γ chains have been identified. Laminin chains of *C. elegans* are encoded by *lam-3* (the ancestral form of mammalian laminin α1and α2 chains, designated as "$\alpha_{1,2}$"), *Epi-1* (the ancestral form of mammalian laminin α3 and α5 chains, designated as "$\alpha_{3,5}$"), *lam-1* (β), and *lam-2* (γ). Laminin chains of *Drosophila* are encoded by *wing blister* ($\alpha_{1,2}$), *LanA* ($\alpha_{3,5}$), *LanB1* (β), and *LanB2* (γ). The orthologues of mammalian 11 laminin chains are conserved in vertebrates including zebrafish (*29*), but the physiological role of zebrafish laminin chains is not exactly the same as that of mammalian laminin chains. The laminin α2 chain (LMα2) is expressed in skeletal muscle and its gene ablation in zebrafish and mice caused muscular dystrophy (*30-32*). LMα5-null zebrafish died after birth due to defect in fin fold morphology (*33*), while LMα5-null mice showed embryonic lethality due to multiple defects including failure of neural tube closure and placental dysfunction (*34*). Thus, it seems likely that evolution of body plan leads to a functional diversification of laminin chains.

The biological function of laminins in mammals

Comprehensive immunohistochemical analyses and loss-of-function studies revealed distinctive spatiotemporal distributions and physiological roles of laminin isoforms in mice (*26, 35*). In the peri-implantation period, laminin-α1β1γ1 (LM111) and laminin-α5β1γ1 (LM511) are distributed in the embryonic BM surrounding the epiblast and Reichert's membrane supporting the outer layer of trophoblasts (Fig. 2D) (*36, 37*). Genetic ablation of LMβ1 or LMγ1 prevented BM assembly in mouse embryo, resulting in early embryonic lethality at embryonic day 5.5 (E5.5) (*37, 38*). LMα1-null mice died around E7 due to lack of Reichert's membrane, despite the presence of embryonic BM (*37, 39*). This delay of post-implantation death by ~1 day suggests that, although the absence of Reichert's membrane inflicts fatal damage on early embryonic development, LMα5 partially compensates the loss of the LMα1's function (*37*). On the other hand, LMα5-null mice died around E17 due to multiple developmental abnormalities such as failure of neural tube closure and digit separation as well as the abnormality of placental, kidney and lung morphologies (*34, 40, 41*). The presence of LMα1 allows the embryo to survive until the late stage of embryonic development, but could not compensate the dysfunction of the LMα5-null BM, resulting in failure of epiblast maintenance (*42-44*). The expression and distribution of LMα1 are firmly restricted in the adult mice to Bowman's capsules of the kidney (LM111) (*45*) and sinusoids of regenerating liver (LM121) (*46*). Conversely, LMα5-containing isoforms, i.e., LM511 and LM521, are ubiquitously distributed in adult mice (*47*). In addition, LMα2-containing isoforms (LM211/221) are clearly detected in BMs of skeletal muscle cells and pericytes (*48*), while LMα4-containing isoforms (LM411/421) are

A

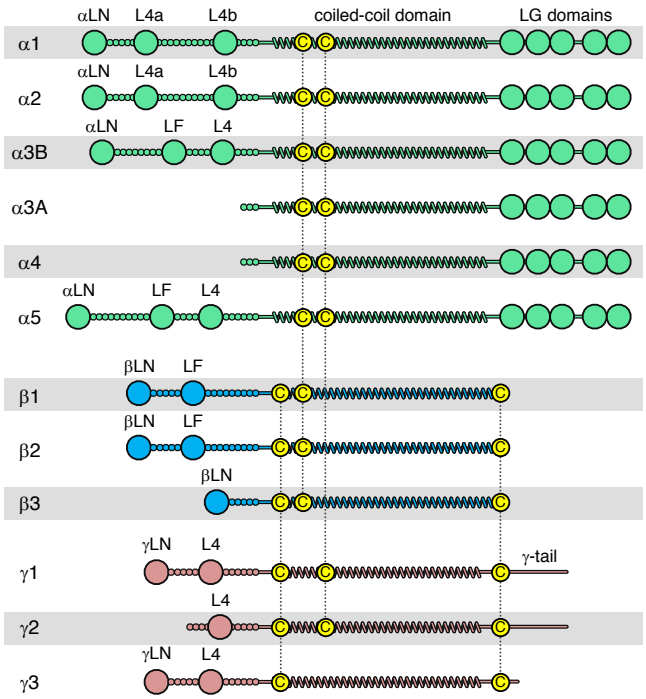

B

old nomenclature	chain composition	standard
laminin-1	α1 - β1 - γ1	laminin-111/LM111
laminin-2	α2 - β1 - γ1	laminin-211/LM211
laminin-3	α1 - β2 - γ1	laminin-121/LM121
laminin-4	α2 - β2 - γ1	laminin-221/LM221
laminin-5	α3A - β3 - γ2	laminin-332/LM332
laminin-5B	α3B - β3 - γ2	laminin-3B32/LM3B32
laminin-6	α3A - β1 - γ1	laminin-311/LM311
laminin-7	α3A - β2 - γ1	laminin-321/LM321
laminin-8	α4 - β1 - γ1	laminin-411/LM421
laminin-9	α4 - β2 - γ1	laminin-421/LM421
laminin-10	α5 - β1 - γ1	laminin-511/LM511
laminin-11	α5 - β2 - γ1	laminin-521/LM521
laminin-12	α2 - β1 - γ3	laminin-213/LM213
laminin-13	α3 - β2 - γ3	laminin-323/LM323
laminin-14	α4 - β2 - γ3	laminin-423/LM423
laminin-15	α5 - β2 - γ3	laminin-523/LM523

C

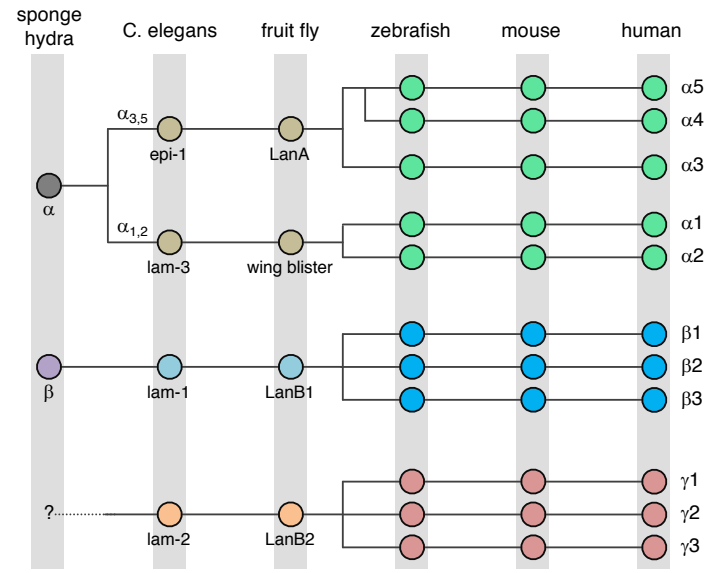

D

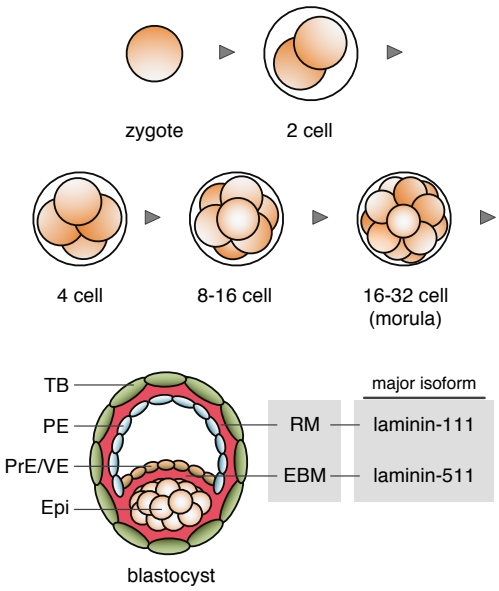

Fig. 2. Laminin chain structure and isoforms.

(**A**) Laminin chains contain tandem arrays of globular and rod-like domains. The α chains contain five laminin globular domains (LG1–5) at their C-termini. The N-termini of all laminin chains contain a variable number of laminin-type epidermal growth factor-like (LE) domains (LEa–c) and globular domains (LN, LF, L4). This figure is illustrated with reference to M. Aumailley, *Cell Adh. Migr.* **7**, 111-121, 2013. (**B**) Laminin heterotrimers. Combinations of α, β, and γ chains give rise to 16 isoforms. In 2005, the laminin nomenclature was simplified to avoid confusion and facilitate transfer of information (M. Aumailley *et al.*, *Matrix Biol.* **24**, 326-332, 2005). (**C**) Laminin chains in evolution (A. Domogatskaya *et al.*, *Annu. Rev. Cell Dev. Biol.* **28**, 523-553, 2012). (**D**) Early embryo development in mice. In the blastocyst, the embryonic basement membrane (EBM) surrounds epiblast (Epi), giving rise to all three embryonic layers, and separates these cells from primitive/visceral endoderm (PrE/VE). Parietal endoderm (PE) migrates around the inside of the trophoblasts (TB), making Reichert's membrane (RM).

abundant in endothelial BMs (*49*). LMα3-containing isoforms including LM332 are dominantly expressed in BMs underlying epidermal cells (*50*).

The role of short arms in network assembly

In vitro studies were undertaken soon after the discovery of LM111 from EHS sarcoma to characterize laminin's functions (*51, 52*). When viewed by rotary shadowing electron microscopy, the EHS sarcoma-derived LM111 had a cross-shape with three short arms (35~50 nm) and one long arm (~80 nm) (Fig. 3A) (*53, 54*). Enzymatic dissection of LM111 using cathepsin-G, pepsin, elastase, and trypsin identified the regions responsible for the laminin's functions including network formation, chain assembly, and cell-adhesive activity (Fig. 3B) (*51*). One of these fragments, C1-4 fragment, containing all three N-terminal short arms, retained a Ca^{2+}-dependent polymerization ability of laminins (*55*). The short arms are composed of a laminin N-terminal (LN) domain followed by tandem repeats of laminin-type epidermal growth factor-like (LE) domains, despite the absence of the LN domain in LMα3 splice variant (LMα3A), LMα4, and LMγ2 (Fig. 2A). Except for LMα3A, LMα4, and LMβ3 short arms, LE domain repeats are interrupted by one or two globular domains including L4 and LF domain (formerly known as domain IV) and are divided into tandem LE compartments, referred to as LEa, LEb, and LEc. Proteolytic fragments of short arms were also produced by elastase and pepsin digestion, yielding E1 (short arms lacking β1LN domain), E4 (N-terminal distal part of LMβ1 containing LN domain) and P1 (short arms lacking all LN domains) (Fig. 3B). Although E4 and P1 fragments do not polymerize, E1 fragment shows a weak polymerization activity that is significantly enhanced by the adding of E4 fragment (*56, 57*), suggesting that the laminin network is a consequence of formation of a ternary complex of three LN domains. Consistent with this scheme, deletion of each LN domain or replacement of the γ1LN domain with LN domains of LMα1 and LMβ1 abolished the polymerization ability of LM111 (*58*). Furthermore, LM211/221 from the murine muscular dystrophy strain (dy^{2J}/dy^{2J}), having a destabilizing mutation in the LN domain of LMα2, did not show any significant polymerization activity in vitro (*59, 60*). Finally, comprehensive analysis using recombinant N-terminal short arm fragments derived from laminin α, β, and γ chains detected four binary combinations of α-α/α-β/α-γ/β-γ and one ternary combination of α-β-γ (Fig. 3C) (*61, 62*). To date, the crystal structures of the LN domains of LMα5, LMβ1, and LMγ1 are available (*63, 64*), but it remains unclear how these LN domains recognize each other, due to the lack of structural information of their binary or ternary complexes.

The mechanism of laminin chain assembly

The assembly of laminin chains is mediated through the long arm that consists of a triple-stranded α-helical coiled-coil domain. Initial studies revealed that proteolytic fragments C8–9 and E8, which retain nearly 100 % and approximately 40 % of the coiled-coil domain of the long arm, respectively, showed a specific chain assembly among laminin α, β, and γ chains (Fig. 3B) (*65-67*). Several studies suggested that secretion of the three chains requires a dimerization of laminin β and γ chains followed by an assembly of the β-γ dimer with laminin α chain on the biosynthetic pathway of laminins (*68, 69*). Utani *et al*. demonstrated that approximately C-terminal 50 residues of the coiled-coil domain of each chain were required to initiate the chain assembly (*70, 71*). The helices of individual coiled-coil domains are comprised of multiple heptad repeats, i.e., a-b-c-d-e-f-g

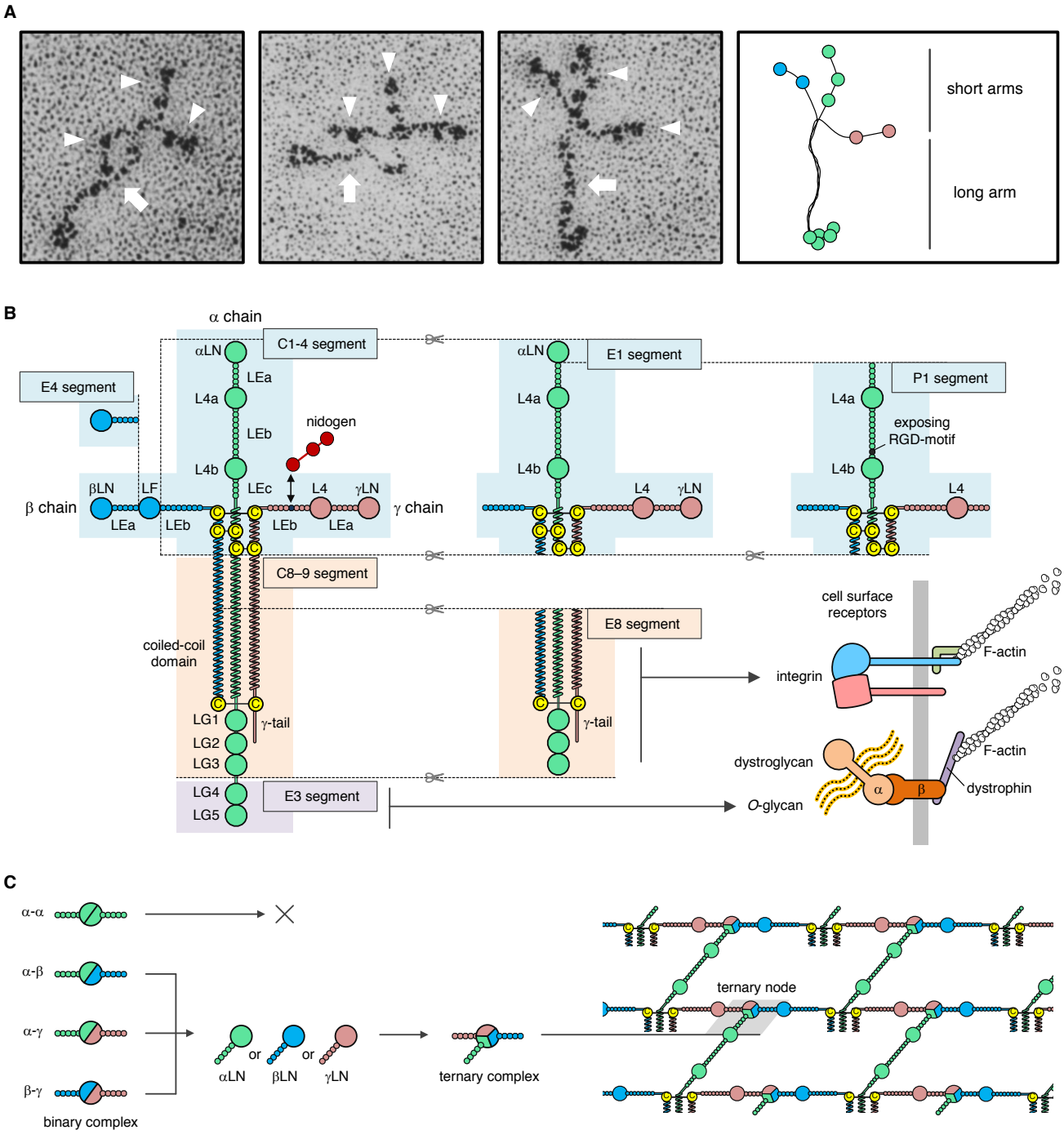

Fig. 3. Laminin segments recapitulating laminin's functions.

(**A**) The Rotary shadowing electron micrographs of EHS sarcoma-derived laminin (J. Engel *et al.*, *J. Mol. Biol.* **150**, 97-120, 1981; K. Beck *et al.*, *FASEB J.* **4**, 148-160, 1990). (**B**) Enzymatic dissection of EHS sarcoma-derived LM111 gives rise to a panel of functionally active fragments. N-terminal short arm segments including C1-4, E1, and E4 have polymerization activity, while long arm segments including C8-9 and E8 are involved in laminin chain assembly regulated by specific coiled-coil interactions. E8 and E3 segments have the cell-adhesive activity through the LG domains that interact with cell surface receptors including integrins and dystroglycan, respectively. (**C**) Network assembly of laminin through LN domains. A weak and transient interaction between βLN and γLN domains is consolidated by the Ca^{2+}-dependent interaction with αLN domain, resulting in formation of a ternary complex.

(Fig. 4A). Upon a lateral association of two or three chains, hydrophobic residues at the positions "a" and "d" form a core of the helical bundle, while some charged amino acid residues at positions "e" and "g" stabilize the helical bundle through ionic interactions (Fig. 4, B and C). Site-direct mutagenesis studies suggested that Ile at the positions "a" and "d" in the laminin α and γ chains contributed to a high thermal stability of three chains assembly (*72*). It has been suggested that acidic residues, i.e., Asp and Glu, at the positions "e" and "g" in the laminin β and γ chains form an acidic pocket together so as to attract the basic residues in the laminin α chain (Fig. 4B) (*73, 74*). The current model for chain assembly consists of following two steps (Fig. 4D): [1] laminin β and γ chains are assembled into a heterodimer with an acidic pocket arising from an electrostatic imbalance among the acidic residues at the positions "e" and "g"; [2] basic residues in laminin α chain interacts with the acidic residues in the β-γ dimer, leading to a stable heterotrimer formation. Additionally, disulfide bonds at N- and/or C-terminal ends of the coiled-coil domain stabilize the chain assembly (Fig. 3B) (*75, 76*).

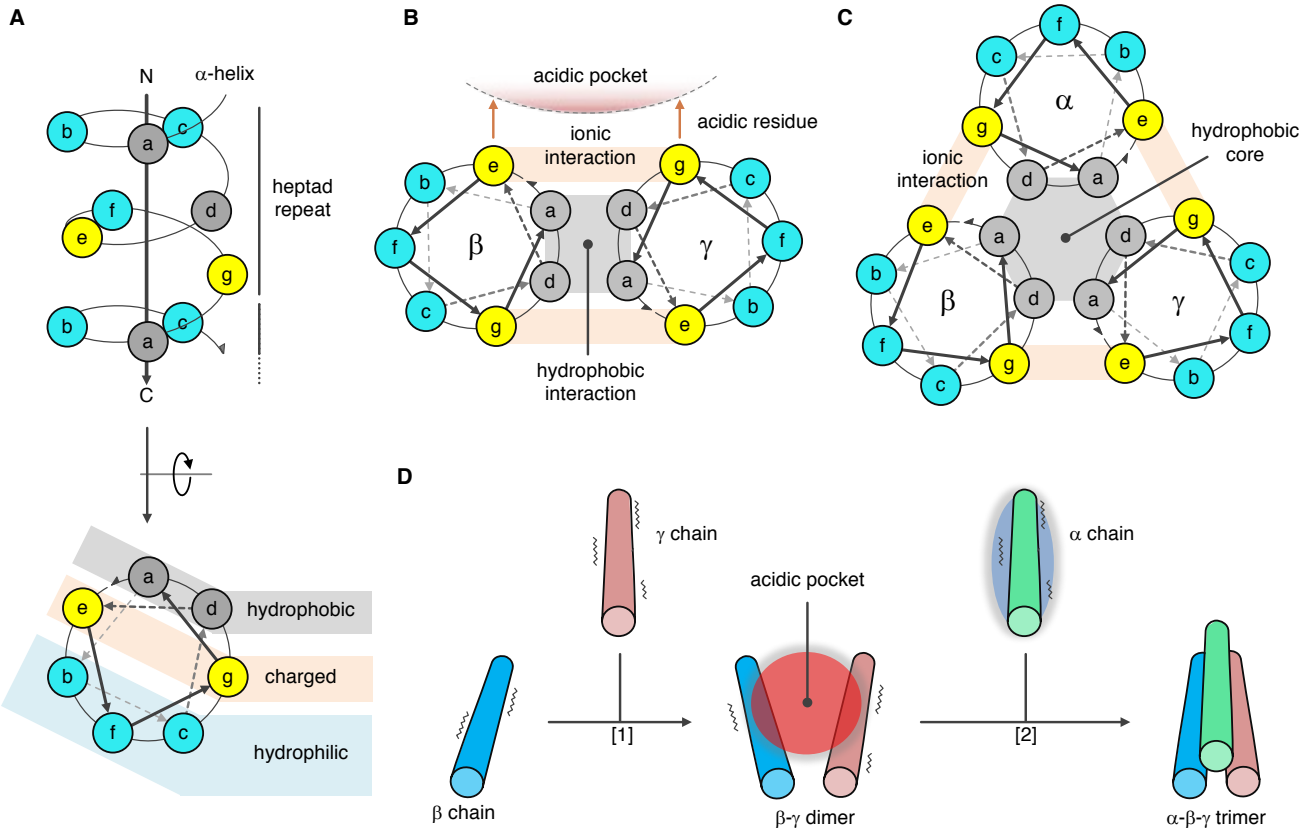

Fig. 4. Laminin chain assembly into a triple-stranded coiled-coil structure.

(**A**) A scheme of the heptad repeats. The hydrophobic amino acid residues forming a core of the helical bundle are positioned at "a" and "d" (grey). The charged amino acid residues stabilizing the coiled-coil assembly are positioned at "e" and "g" (yellow). (**B, C**) Coiled-coil helical wheel representation of the β-γ dimer (**B**) and α-β-γ trimer (**C**). (**D**) A model for laminin chain assembly into double- and triple-stranded coiled-coil structures: [1] β and γ chains interact with each other though hydrophobic/charged side chains. However, the resulting β-γ dimer is unstable because of the imbalance among the charged side chains at the positions "e" and "g"; [2] an interaction between basic residues of α chain and acidic pocket of β-γ dimer leads to a stable heterotrimer formation. Wavy lines mean a conformational instability of laminin chains. These figures are illustrated with reference to M. Nomizu *et al*., *Biochemistry* **35**, 2885-2893, 1996.

Cell-adhesive activity of laminin

Laminins make a major contribution to the cell-adhesive activity of the BM and elicit a variety of cellular responses through interaction with a panel of cell surface receptors including integrins and dystroglycan. A series of proteolytic digestion of LM111 identified P1, E3, and E8 fragments having the cell-adhesive activity (Fig. 3B). P1 fragment binds to integrins due to having the Arg-Gly-Asp (RGD) motif in the LEb region of LMα1 (*77*). However, this motif is not accessible to cells in intact LMα1 because of masking by an adjacent L4b domain, and becomes available to cells only after pepsin cleavage of the L4b domain (*78, 79*).

E3 fragment consists of LG4–5 that bind dystroglycan in a Ca^{2+}- and *O*-glycan-dependent manner (*80, 81*). Dystroglycan is a cell surface receptor that constitutes the dystrophin glycoprotein complex essential for the maintenance of the nervous system and the integrity of the skeletal muscle (*81*). Dystroglycan consists of a membrane-spanning β subunit (β-dystroglycan) and an extracellular α subunit (α-dystroglycan), which are derived from a single gene product by post-translational cleavage. α-Dystroglycan has a highly *O*-glycosylated mucin-like domain (*82, 83*). The laminin binding activity of α-dystroglycan requires heteropolysaccharides having alternating xylose (Xyl) and glucuronic acid (GlcA) moieties, which are added by the glycosyltransferase LARGE to the phosphorylated *O*-mannosyl glycan (*84*). On the other hand, the Ca^{2+} and surface-exposing basic residues in LG4 are requires for α-dystroglycan binding by LG4–5 (*85, 86*). Recently, the crystal structure of LG4–5 of LMα2 with a tetrasaccharide (GlcA-Xyl-GlcA-Xyl) revealed that the Xyl-GlcA disaccharide coordinates the Ca^{2+} in LG4 (Fig. 5) (*87*).

The integrin binding activity of laminins has been mapped within the E8 segment, comprising the distal part of the coiled-coil domain and three laminin globular domains (LG1–3) of the laminin α chain (Fig. 3B). There is compelling evidence that LG1–3 are required for laminin recognition by integrins. Deletion of LG1–3

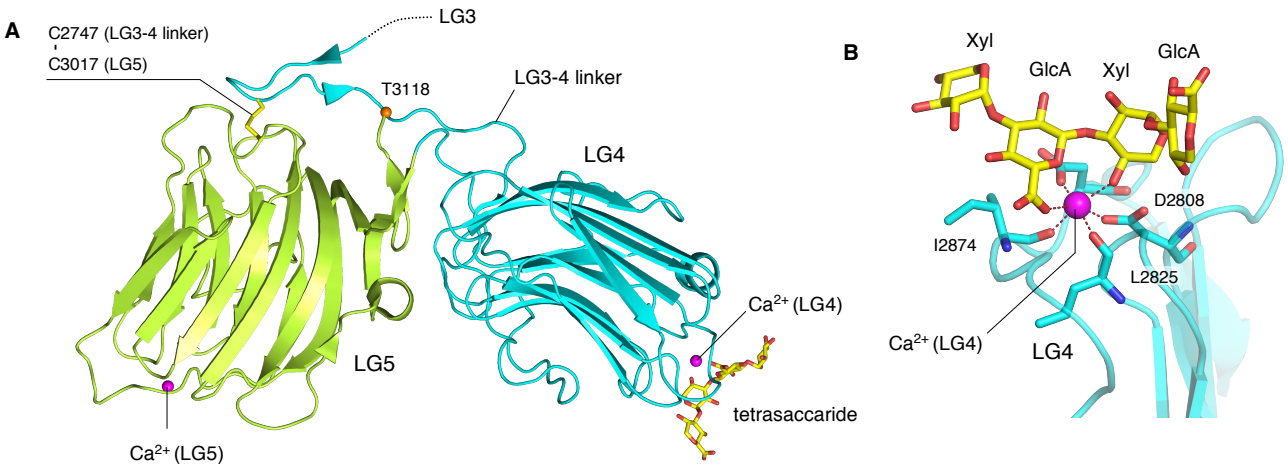

Fig. 5. The interaction of LG4–5 with α-dystroglycan-derived *O*-glycan.

(**A**) The crystal structure of LG4–5 complexed with tetrasaccharide GlcA-Xyl-GlcA-Xyl [Protein Data Bank (PDB) ID: 5IK5]. LG4–5 are colored in green-cyan (LG4) and yellow-green (LG5). (**B**) Ca^{2+} at LG4 is octahedrally coordinated with Xyl-GlcA disaccharide (D. C. Briggs *et al*., *Nat. Chem. Biol.* **12**, 810-814, 2016). A tetrasaccharide (GlcA-Xyl-GlcA-Xyl) is shown as yellow stick. A calcium ions at the LG4 and LG5 are shown as a magenta sphere; Cα atoms of C-terminal residues as orange spheres.

or substitution of any one of the LGs nullifies the integrin binding activity of laminins (Fig. 6A, top and middle) (*88-90*). Furthermore, the integrin binding specificity and affinity of laminin isoforms have been shown to be primarily defined by α chains (*91*). LG1–3 have been proposed to adopt a "cloverleaf" configuration based on electron microscopic observations (Fig. 6B) (*54*), although LG1–3 alone adopted an open configuration when determined by X-ray crystallography (Fig. 6C) (*92*). LG1–3 alone have no significant integrin binding activity, suggesting that β and/or γ chains facilitate the cloverleaf assembly of LG1–3 for integrin recognition. Ido *et al.* previously reported that the Glu residue at the third position from the C-termini of LMγ1 and LMγ2 is crucial for integrin binding (Fig. 6A, bottom) (*93*). Gln substitution for the Glu residue in the C-terminal region of the γ chain (designated the γ-tail) abrogated the integrin binding activity of LMγ1/LMγ2-containing laminin isoforms (e.g., LM511 and LM332). Although LM213 is incapable of binding to integrins because of lack of an

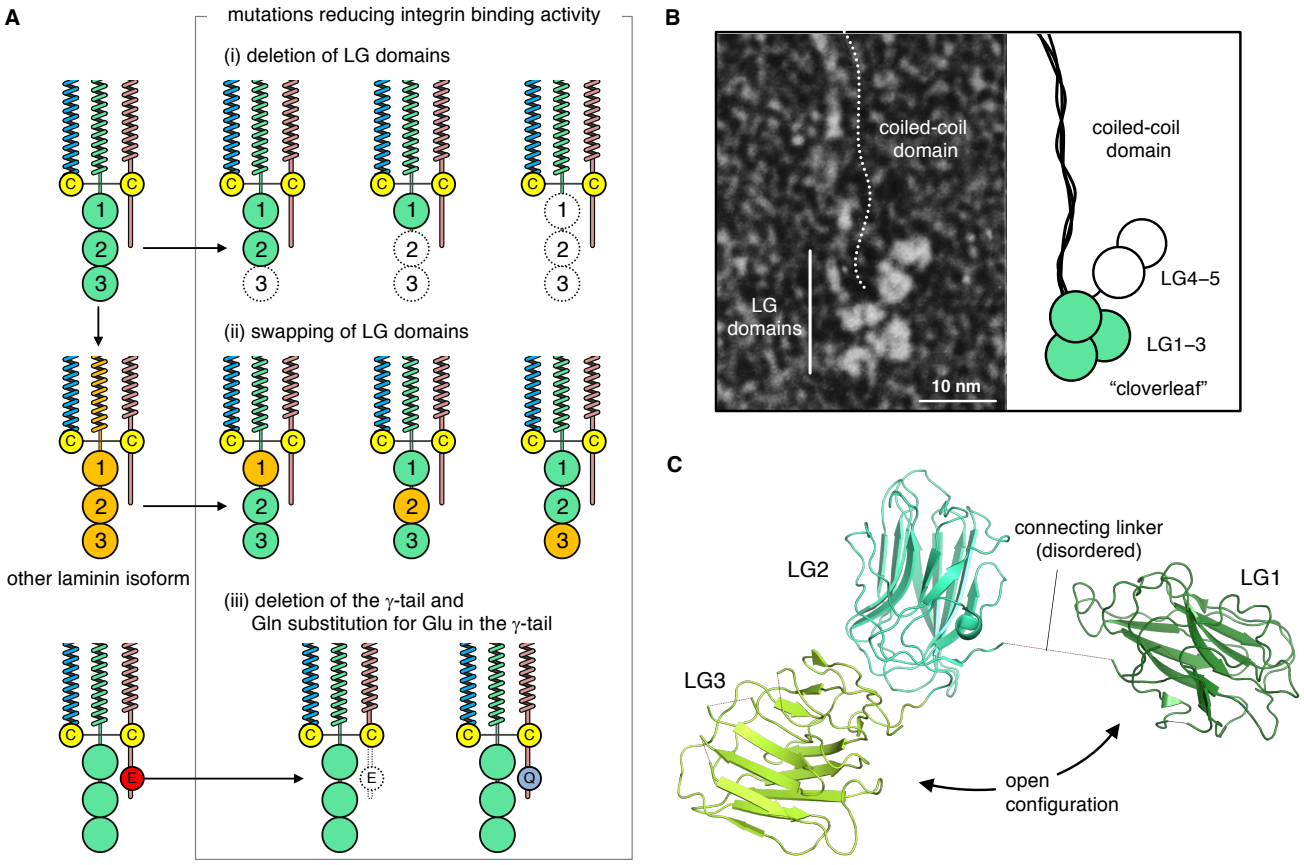

Fig. 6. Integrin binding region of laminin.

(**A**) A summary of previous studies on the role of α and γ chains in integrin binding. Following mutations resulted in a significant decrease in the integrin binding activity of LM511; (i) deletion of LG domains(s) of LMα5 (Ido *et al.*, *J. Biol. Chem.* **279**, 10946-10954, 2004), (ii) substitution of any one of LGs of the LMα5 with the counterparts of the LMα1 (Ido *et al.*, *Matrix Biol.* **25**, 112-117, 2006), (iii) deletion of the γ1-tail and Gln substitution for Glu residue in the γ1-tail (Ido *et al.*, *J. Biol. Chem.* **284,** 22786-22792, 2007). (**B**) The rotary shadowing electron micrograph (left) (K. Beck *et al.*, *FASEB J.* **4**, 148-160, 1990) and the interpretive drawing (right) of the C-terminal region of LM111. (**C**) The crystal structure of the LG1–3 of the LMα2 chain (PDB ID: 2WJS). LG1–3 are colored in deep-green (LG1), green-cyan (LG2), and yellow-green (LG3). LG1 was dissociated from LG2–3 (F. Carafoli, N. J. Clout, E. Hohenester, *J. Biol. Chem.* **284**, 22786-22792, 2009).

equivalent Glu residue in LMγ3, the chimeric LM213 mutant having the nine C-terminal residues of LMγ1 in place of the four C-terminal residues of LMγ3 became fully active in integrin binding (*94*). In addition, Navdaev *et al*. reported that C-terminal truncation of LMγ2 in LM332 resulted in an open configuration of LG1–3 of LMα3 (*95*), suggesting that the Glu residue in the γ-tail contributes to adopting an active LG1–3 conformation for integrin recognition (*8*). However, the mechanism by which integrin recognizes laminin remains to be elucidated due to the lack of structural information of laminin and its complex with integrin.

1-3. Integrin receptors

Integrins are heterodimeric membrane proteins composed of noncovalently associated α and β subunits. In mammals, 18 α and 8 β subunits have been identified, combination of which yields 24 distinct integrin heterodimers (Fig. 7A) (*96*). These integrins are classified into five subfamilies based on their ligand-binding properties. Laminin-binding integrins include α3β1, α6β1, α6β4, and α7β1 integrins, among which α6β1 integrin exhibits the highest binding affinity for the LMα5-containng laminin isoforms (i.e., LM511/521) (*91*). Human pluripotent stem cells express α6β1 integrin as a major integrin species and proliferate robustly on recombinant LM511/521 in an undifferentiated state, making these laminin isoforms and their fragments ideal substrates for expansion of these cells in regenerative medicine (*97-99*). A full picture of the ectodomain of integrins was first given by the determination of the crystal structure of αVβ3 integrin (Fig. 7, B and C) (*100*). The ectodomain of the α subunit is composed of a seven-bladed β-propeller domain, a thigh domain, and calf-1/2 domains. In half of the α subunits, the αI domain is inserted between blades 2 and 3 of the β-propeller domain. The ectodomain of the β subunit consists of a βI domain resembling the αI domain in function and

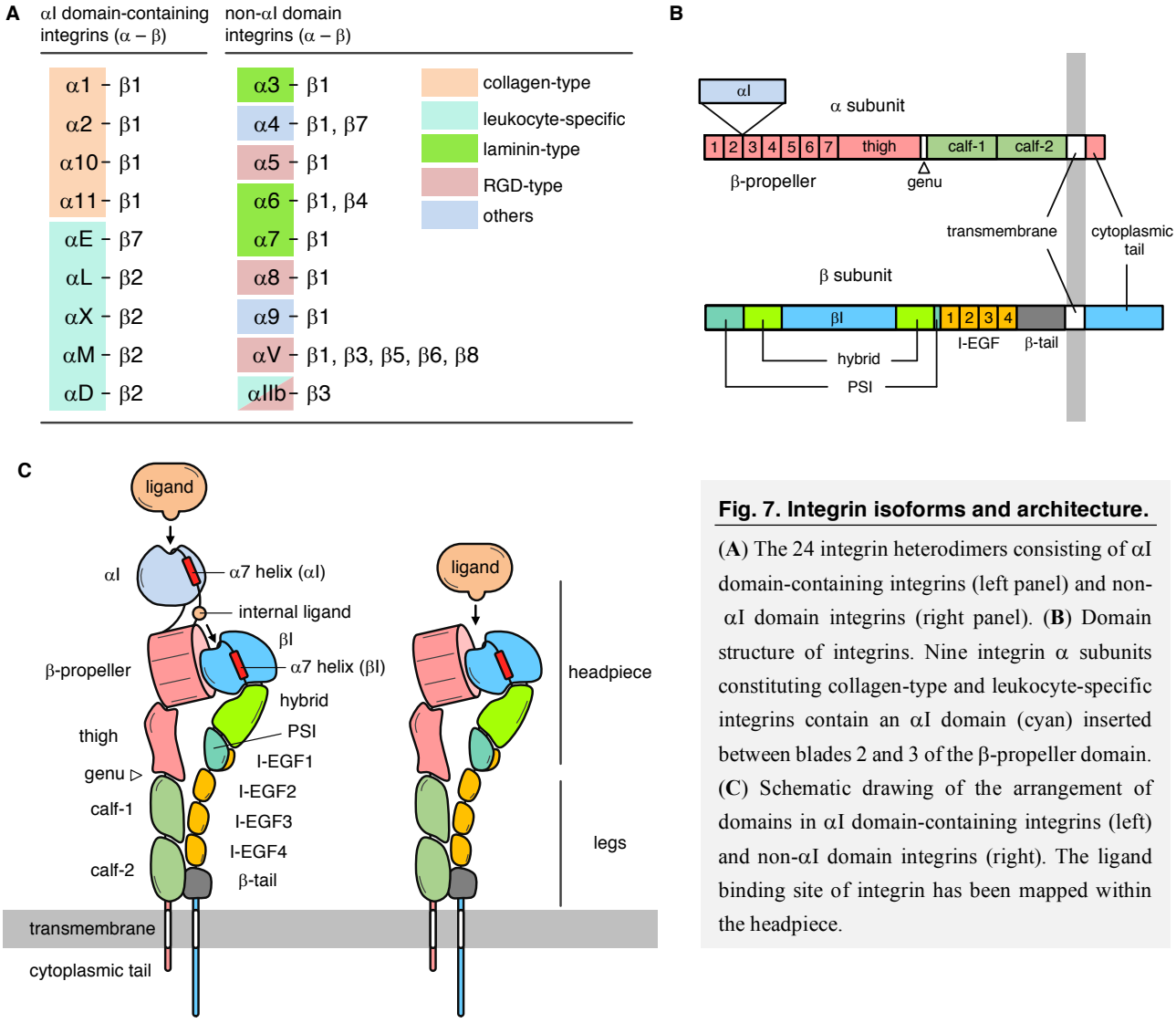

Fig. 7. Integrin isoforms and architecture.

(**A**) The 24 integrin heterodimers consisting of αI domain-containing integrins (left panel) and non-αI domain integrins (right panel). (**B**) Domain structure of integrins. Nine integrin α subunits constituting collagen-type and leukocyte-specific integrins contain an αI domain (cyan) inserted between blades 2 and 3 of the β-propeller domain. (**C**) Schematic drawing of the arrangement of domains in αI domain-containing integrins (left) and non-αI domain integrins (right). The ligand binding site of integrin has been mapped within the headpiece.

structure, a plexin-semaphorin-integrin (PSI) domain, a hybrid domain, four epidermal growth factor (EGF) repeats, and a β-tail. The N-terminal domains of α and β subunits associate to form the headpiece that contains the ligand recognition site (Fig. 7C).

Global change in ectodomain conformation

Based on early electron microscopic observations, integrins had been proposed to adopt an extended conformation, in which the headpiece stands on two legs consisting of four EGF repeats of α subunit and calf-1/2 domains of β subunit (*101-103*). However, the breakthrough crystal structure of αVβ3 integrin ectodomain revealed that the integrin has a severely bent conformation, in which the headpiece comes close to the two legs (Fig, 8A) (*100*). In addition, electron microscopic observations of αVβ3 integrin ectodomain demonstrated that activation by adding Mn^{2+} and/or a ligand mimetic peptide induces switchblade-like extension of the ectodomain with a swing-out of the hybrid domain, despite having a bent conformation without any ligands under physiological (Mg^{2+}/Ca^{2+}) conditions (*104*). Several lines of evidence suggest that integrins expressed on cell surfaces assume a bent conformation representing a low-affinity ligand binding (Fig. 8A). Cytoplasmic

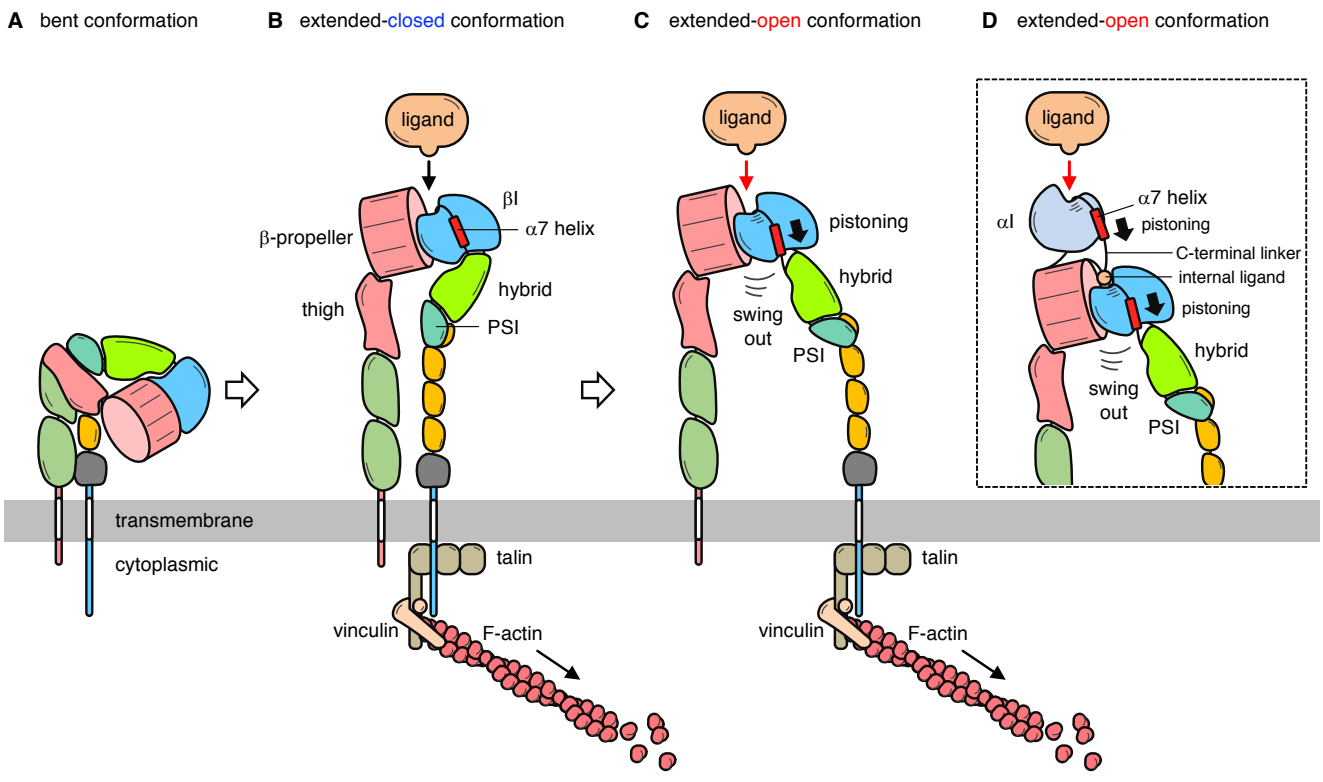

Fig. 8. Rearrangement of domains during activation of integrins.

(**A**) In a low-affinity state, integrins assume a bent conformation. (**B**, **C**) A physiological ligand binding to the headpiece as well as recruiting of the adaptor proteins (e.g., talin and vinculin) and actin cytoskeleton into the cytoplasmic tails facilitate the global change in the ectodomain conformation with the swing-out of the hybrid domain, making a high-affinity state of integrins. (**D**) The ligand binding activity of αI domain-containing integrin requires the relay between αI and βI domains.

proteins such as talin and vinculin mediate a physical linkage between an actin cytoskeleton and the cytoplasmic tail of integrins. A retractile force generated by actomyosin breaks a clasp between the cytoplasmic/transmembrane domains of α and β subunits, resulting in a switchblade-like extension with the swing-out of the hybrid domain sufficient for the ligand binding (Fig. 8, B and C). This process is known as "inside-out" signaling. Conversely, the interaction of ECM proteins with the headpiece induces an extended-conformation accompanied by the swing-out of the hybrid domain, and in turn opens the clasp between the cytoplasmic tails of α and β subunits, thereby helping to recruit the adaptor proteins and cytoplasmic actin filaments. This process is known as "outside-in" signaling. Together, integrins act as a bidirectional transducer of mechanical information between intracellular and extracellular environments (*105, 106*). It is of note that the global change in ectodomain conformation is tightly coupled with the conformational reshaping of the αI and βI domains having a critical ligand binding site.

Ligand recognition by the αI domain

The αI and βI domains adopt a typical Rossmann fold with α-helices surrounding six β-strands, and harbors a divalent metal ion binding site known as the metal-ion-dependent adhesion site (MIDAS). Several lines of evidence indicated that Mg^{2+} is the physiological metal ion comprising the MIDAS of the αI and βI domains (α-MIDAS and β-MIDAS) (*107, 108*), and is coordinated with an acidic residue in integrin ligands upon ligand binding (*109, 110*). Because the αI domain retains the ligand binding activity of αI-containing integrin even after isolating from other domains, researchers initially embarked on the determination of the crystal structures of the αI domains and their complexes with ligands (*111-113*). These structures showed two conformations of the αI domain, termed 'closed' and 'open', responsible for affinity maturation (Fig. 9, A-D). The crystal structure of the αI domain of α2 subunit (α2-I domain) has a closed conformation and houses an α-MIDAS metal ion at its apex (Fig. 9A). The metal ion in the α-MIDAS is ligated by 5 residues located in three loops as well as by water molecules (Fig. 9B). The β1-α1 loop provides three ligands, D151, S153, and S155, known as the Asp-X-Ser-X-Ser (DXSXS, X: any amino acid residue) motif. In addition, the α2-α3 and the β4-α5 loops provide coordinating ligands, T221 and D254, respectively. On the other hand, liganded α2-I domain has an open conformation showing distinct coordination geometry of the α-MIDAS (Fig. 9, C and D) (*112*). The α2-I domain recognizes the Gly-Phe-Hyp-Gly-Glu-Arg (GFOGER) motif in collagens (*114*), in which the Glu residue coordinates a divalent metal ion in the α-MIDAS. With the coordination by the extrinsic acidic ligand, D254 switches from the primary to the secondary coordination ligand, while T221 switches from the secondary to the primary coordination ligand, resulting in a movement of the metal ion with the β1-α1 loop away from D254 and toward T221. In addition, the change in coordination geometry of the α-MIDAS is accompanied by downward movement of the α7 helix (Fig. 9D). Such a large displacement of the α7 helix is essential for high-affinity ligand binding by the αI domains. The αI domain mutants containing disulfide bonds stabilizing the open conformation induced rearrangements of the α-MIDAS and a greater increase in affinity for ligands than wild-type αI domain (10,000-fold) (Fig. 9E) (*113*). Antagonists blocking ligand-binding activity of the αL-I domain, such as lovastatin, penetrate between the α7 helix and β-strands and allosterically prevented the downward displacement of the α7 helix (Fig. 9F) (*115-117*).

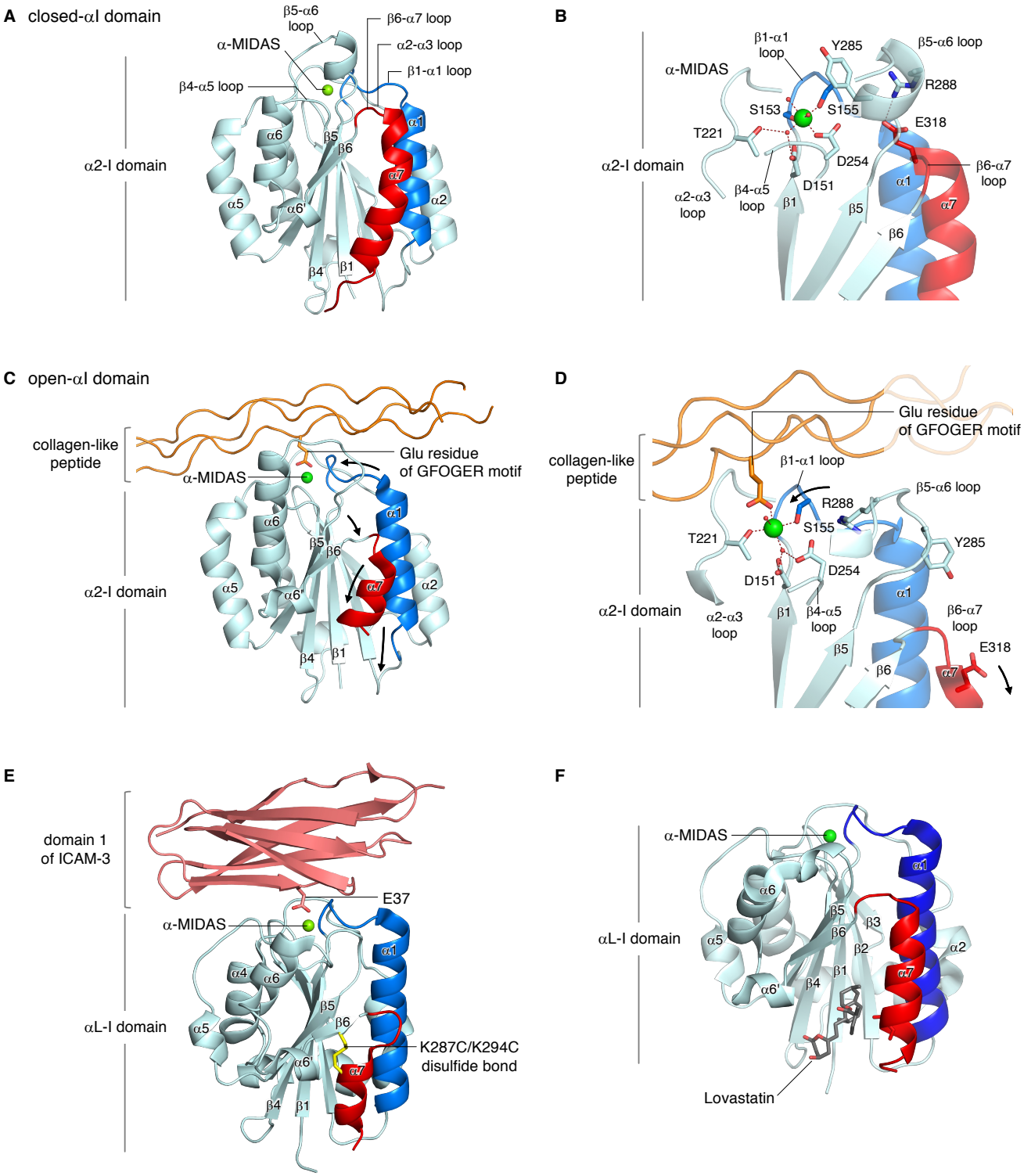

Fig. 9. Conformational change in αI domain.

(**A-D**) The crystal structures of the αI domain of integrin α2 (**A, B**) and its complex with collagen-like peptide (**C, D**) (PDB ID: 1AOX, 1DZI). (**E**) The crystal structure of the αI domain of integrin αL complexed with the domain 1 of ICAM-3 (PDB ID: 1T0P). (**F**) The crystal structure of the αI domain of integrin αL complexed with lovastatin (PDB ID: 1CQP). A metal ion in the α-MIDAS is shown as a green sphere; disulfide-linked Cys residues as yellow sticks. The α1 and α7 helices are colored in blue and red, respectively.

Ligand recognition by the βI domain

The molecular mechanism by which the βI domain recognizes integrin ligands was initially revealed by the crystal structure of the αVβ3 integrin in complex with an RGD peptide (Fig. 10A) (*118*). In this structure, the RGD peptide fits into a well-shaped pocket formed by the β-propeller and the βI domains, with the Arg residue forming a salt bridge to an acidic residue in the β-propeller domain and the Asp residue coordinating the β-MIDAS metal ion. The RGD motif was originally identified as the α5β1 integrin recognition site that is located at the 10th type III fibronectin repeat of fibronectin (Fig. 10B) (*119, 120*). To date, the RGD-binding integrins including αVβ3 integrin constitute the largest subgroup of integrins. While electron microscopic images of αVβ3 and α5β1 integrin ectodomains showed that the swing-out of the hybrid domain occurs upon binding to a fibronectin fragment or an RGD peptide (*104, 121*), the crystal structures of αIIbβ3 integrin and its complex with a ligand mimetic peptide revealed that ligand binding to the βI domain induces a conformational change in the domain with a downward movement of the α7 helix seen in the αI domain (Fig. 11, A-D) (*122, 123*). As is the case with the α-MIDAS, the β-MIDAS in integrin β3 (β3-MIDAS) is formed by a DXSXS motif in the β1-α1 loop (D119/S121/S123) and the two residues in the α2-α3/β4-α5 loops (E220/D251) (Fig. 11B). In addition, the βI domain contains two Ca^{2+} coordination sites flanking β-MIDAS, i.e., LIMBS (ligand-associated metal ion-binding site) and ADMIDAS (adjacent to MIDAS). Two residues in the α2-α3 loop (N215/E220) participate in LIMBS formation. The Ala substitutions for the corresponding residues in integrin β7 reduced the adhesive activity of α4β7 integrin because of a collapse of metal ion coordination geometry (*124*). On the other hand, ADMIDAS is formed by the residues in the β1-α1 (S123/D126), the β4-α5 (D251), and the β6-α7 (M335) loops. Particularly, Ca^{2+} coordination of the carbonyl oxygen of M335 secures the α7 helix at the side of the βI domain. αIIbβ3 integrin recognizes Lys-Gln-Ala-Gly-Asp-Val (KQAGDV) sequence in the C-terminal segment of fibrinogen γ chain, where the Asp residue coordinates a divalent metal ion in the β3-MIDAS (Fig. 11, C and D). The ligand binding to αIIbβ3 integrin breaks the coordination bond between the ADMIDAS

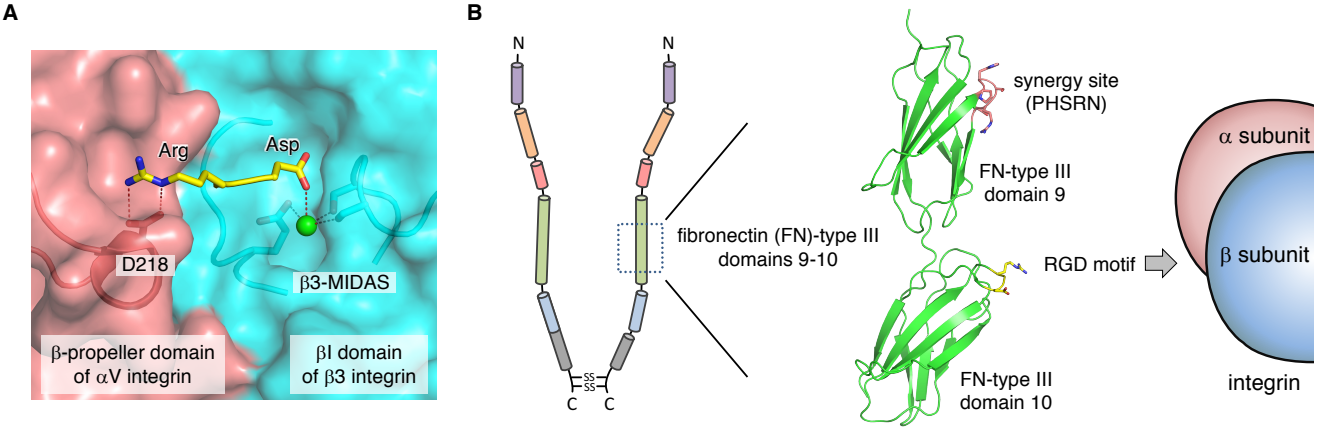

Fig. 10. RGD motif as the essential cell attachment site in fibronectin.

(**A**) The binding of an RGD peptide to the well-shaped pocket formed by the β-propeller and the βI domains (PDB ID: 1L5G). The β-propeller and the βI domains are colored in deep-salmon and cyan, respectively. (**B**) Schematic drawing of the arrangement of domains in fibronectin (left) and the crystal structure of the fibronectin-type III domains 9-10 (Protein Data Bank ID: 1FNF).

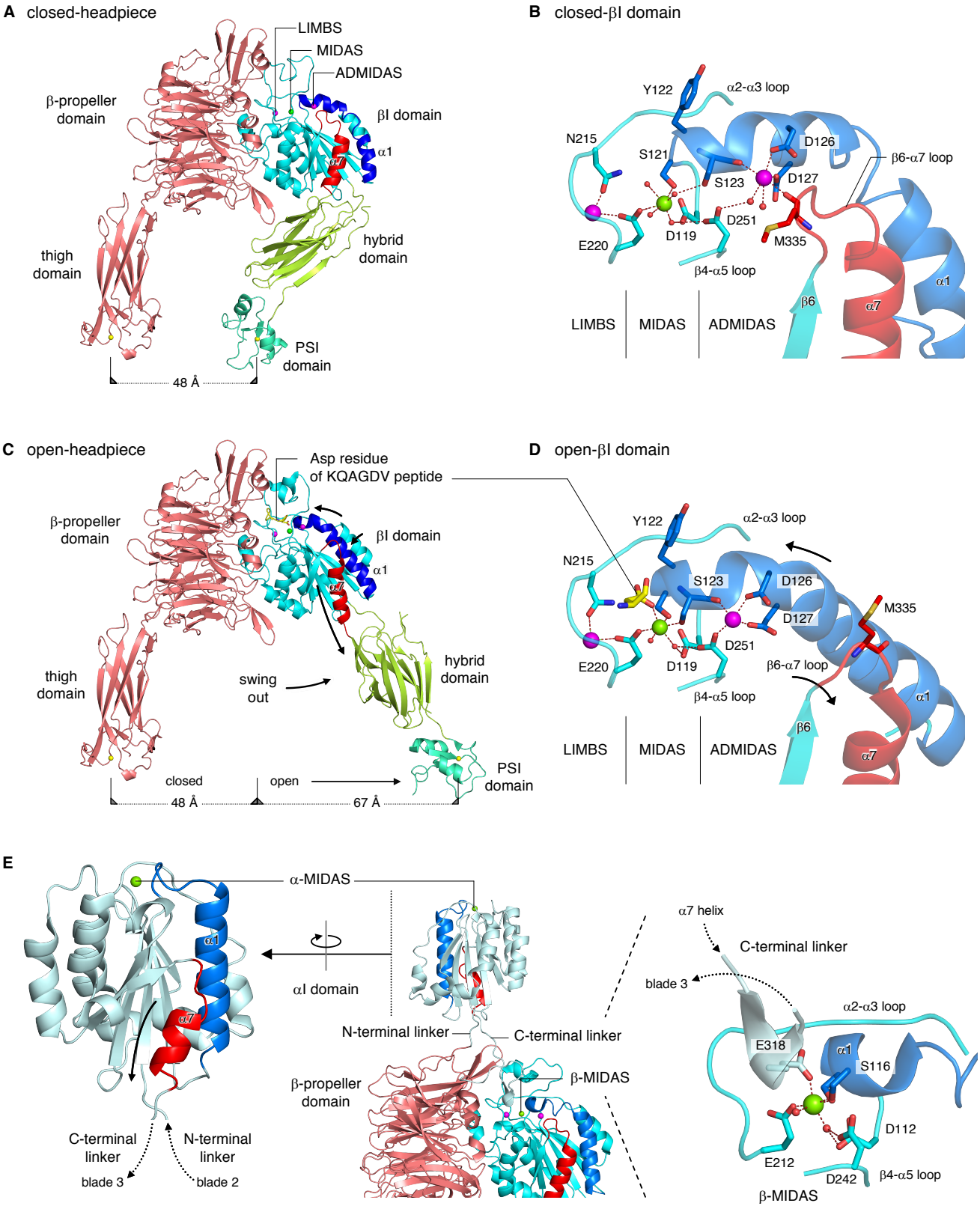

Fig. 11. Conformational change in the headpiece with a swing-out of the hybrid domain.

(**A-D**) The crystal structures of the headpiece of αIIbβ3 integrin (**A**, **B**) and its complex with fibrinogen γ chain–derived peptide (**C, D**) (PDB ID: 3FCS, 2VDR). (**E**) The crystal structure of the headpiece of αXβ2 integrin containing the αI domain, in which the Glu residue in the C-terminal linker of the αI domain coordinates the β3-MIDAS metal ion (Protein Data Bank ID: 4NEH). A metal ion in the β-MIDAS is shown as a green sphere. Metal ions in the ADMIDAS and LIMBS are shown in magenta spheres. The α1 and α7 helices are colored in blue and red, respectively.

metal ion and the β6-α7 loop, leading to downward movement of the α7 helix. This enables the β1-α1 loop coordinating both the ADMIDAS and MIDAS metal ions to move toward the β-propeller domain (Fig. 11D). Because of the topology of the βI domain inserted into the hybrid domain, the downward displacement of the α7 helix causes the hybrid domain to swing-out by an approximately 60 degrees, resulting in an approximately 70 Å movement of the PSI domain (Fig. 11C). In support of the requirement of the swing-out of the hybrid domain for eliciting high-affinity binding of integrins, mutational insertion of a "glycan wedge" into the hybrid–βI domain interface led to a significant increase in ligand-binding affinity (*125*). Inhibitory anti-integrin β1 antibodies, such as mAb13 and SG19, bind to the lateral face of the βI domain and allosterically block the swing-out of the hybrid domain (*126-128*). Recent studies indicated that the relay between αI and βI domains pulls downward the α7 helix and favors high-affinity ligand binding of the αI-containing integrins (Fig. 8D) (*110*). The αI domain contains an invariant Glu residue located in its C-terminal linker between the C-terminal α7 helix and the blade 3 of the β-propeller domain. The Glu residue coordinates the β-MIDAS metal ion similar to the ligand binding in αI-less integrins, resulting in the downward displacement of the α7 helix and activation of the αI domain (Fig. 11E) (*129-131*).

1-4. Aim of this study

Adhesion of cells to the basement membrane (BM) is a fundamental biological process essential for tissue development and maintenance. Although laminins in BMs have an essential role in a regulation of diverse cellular functions through the interaction with integrins, the mechanistic basis for the recognition of laminins by integrins remains to be elucidated. Given that two regions of laminins—LG1–3 and the γ-tail—are required for integrin binding, it is conceivable that the two regions configure a composite integrin binding interface. However, it has long been an open question of how the γ1-tail contributes to the integrin binding activity of laminins. As described above, the studies on the mechanisms of integrin-ligand interactions have shown that an acidic side chain in the ligand coordinates the MIDAS metal ion, leading to the hypothesis that the Glu residue in the γ-tail directly interacts with integrins by coordinating the metal ion in the β-MIDAS. This hypothesis disapproves the conventional notion that the Glu residue in the γ-tail contributes to adopting an active LG1–3 conformation for integrin recognition. Here, I sought to determine the role of the γ-tail in the laminin-integrin interaction by X-ray crystallography combined with a series of biochemical analyses.

Chapter 2: Results

2-1. Crystal structure of the integrin binding segment of LM511

Production of truncated LM511E8 fragments

The E8 fragment of LM511 (LM511E8) consists of three chains, LMα5E8 (A2534-A3327), LMβ1E8 (L1561-L1786), and LMγ1E8 (N1364-P1609). LM511E8 is sufficient for recapitulating the integrin binding activity of LM511 because of including LG1–3 of LMα5 and the C-terminal region of the β1-γ1 dimer (*93, 132*). Electron microscopic imaging performed by Dr. Yukimasa Taniguchi (Osaka University) revealed that LM511E8 has a long (approximately 30 nm) and flexible coiled-coil extension (Fig. 12, A and B). Therefore, I sought to produce a smaller LM511 fragment having a shorter coiled-coiled domain amenable to crystallization. Through phased truncation/deletion mutagenesis, I found that deletions of N-terminal segments, i.e., A2534-Q2640 (LMα5), L1561-A1713 (LMβ1) and N1364-L1527 (LMγ1), made little influence on the secretion of LM511E8 from FreeStyle™ 293-F cells ("truncation-0" in Fig. 12, C and D). Further deletion of the coiled-coil domains of LMβ1E8 and LMγ1E8 resulted in a decrease in the secretion level, while the D2641-Q2654 segment of LMα5E8 could be additionally deleted without compromising the secretion level ("truncation-2" in Fig. 12, C and D). The resulting truncated LM511E8 (designated as tLM511E8) has a coiled-coil domain of approximately 10 nm long (Fig. 12, E and F).

tLM511E8 is composed of three chains, termed tLMα5E8 (E2655-A3327), tLMβ1E8 (D1714-L1786), and tLMγ1E8 (D1528-P1609) (Fig. 12G). To prevent unexpected destabilization or dissociation of heterotrimeric coiled-coil assembly under various solvent conditions (i.e., pH, ionic strength, and temperature) used for initial screening for crystallization, an interhelical disulfide linkage was introduced into the coiled-coil structure by Cys-substitutions for α5-I2723 and γ1-D1585 (Fig. 12G and H). Additionally, a TEV protease recognition sequence (ENLYFQ ↓ G) was introduced immediately after the N-terminal tag to avoid the tags hindering crystallization of tLM511E8 (Fig. 12G). Regardless of the treatment with a TEV protease, tLM511E8 has an α6β1 integrin binding activity equivalent to that of wild-type LM511E8 (Fig. 12, I and J)

Fig. 12. Preparation of tLM511E8.

(**A, B**) Electron microscopic images and averaged dimensions (n=50) of LM511E8. (**C**) N-terminal amino acid sequences of truncated LMα5E8, LMβ1E8, and LMγ1E8. (**D**) A series of truncated LM511E8s were subjected to SDS-PAGE under nonreducing conditions, followed by immunoblotting with anti-5×His mAb. (**E, F**) Electron microscopic images and averaged dimensions (n=50) of tLM511E8 corresponding to truncation-2. (**G**) Schematic drawing of tLM511E8. To prevent unexpected dissociation of the heterotrimeric coiled-coil assembly in various solvent conditions, an additional disulfide bond was introduced into the coiled-coil by Cys substitutions for residues α5-I2723 and γ1-D1585. (**H**) Purified LM511E8, tLM511E8 and tLM511E8 containing an additional disulfide bond were subjected to SDS-PAGE under nonreducing conditions, followed by Coomassie Brilliant Blue staining. (**I**, **J**) Microtiter plates were coated with LM511E8, tLM511E8, and TEV protease-treated tLM511E8, and then incubated with α6β1 integrin in the presence of 1 mM $MnCl_2$. The bound integrins were quantified with biotinylated anti-Velcro pAb and HRP-conjugated streptavidin as described in "Materials and Methods". The amounts of integrin bound in the presence of 10 mM EDTA were used as negative controls and subtracted as background. The results are means ± S.D. of three independent experiments.

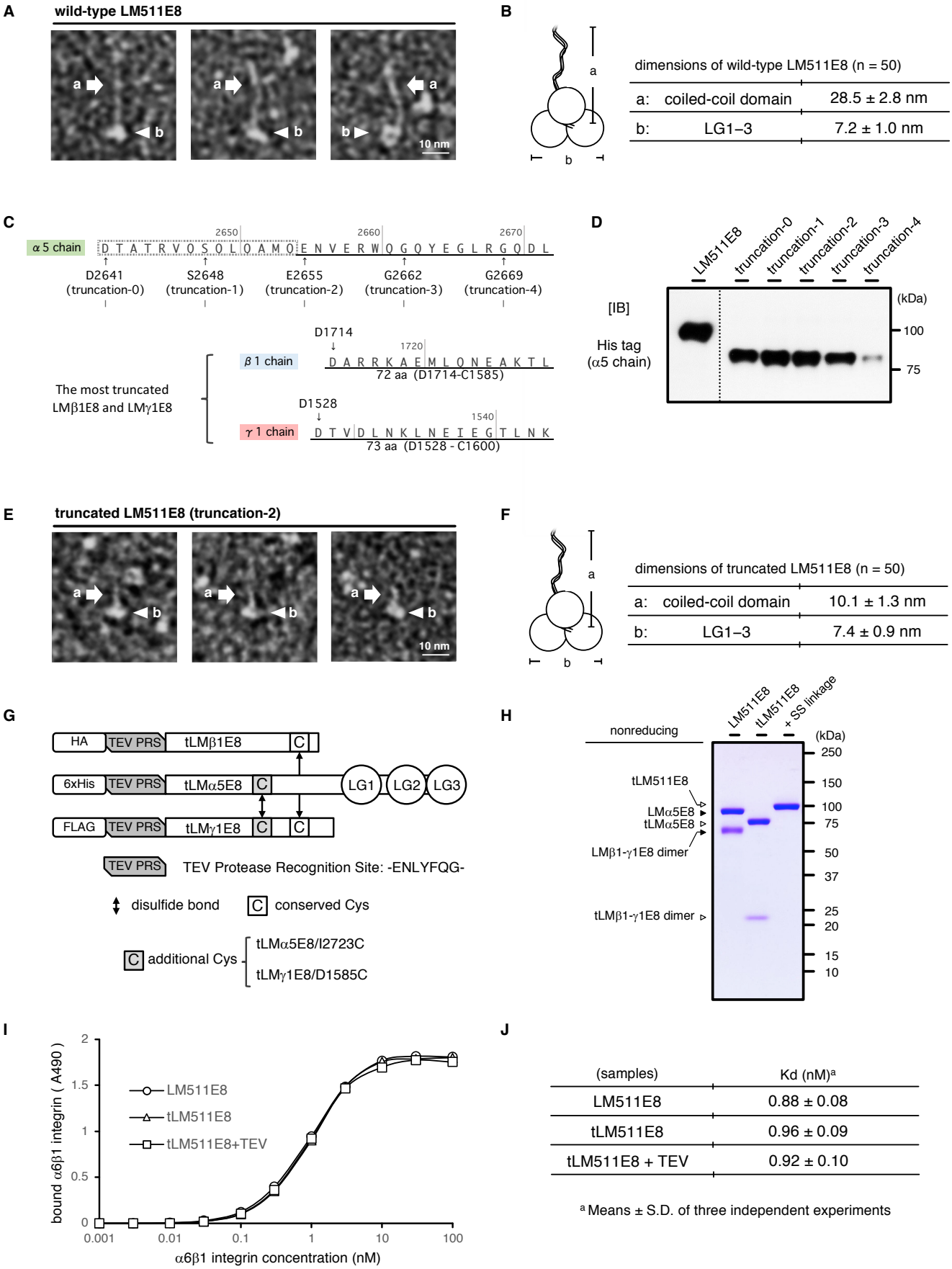
A
wild-type LM511E8
a
b
10 nm
B
a
b
dimensions of wild-type LM511E8 (n = 50)
a: coiled-coil domain 28.5 ± 2.8 nm
b: LG1–3 7.2 ± 1.0 nm
C
α 5 chain
2650
2660
2670
D T A T R V Q S Q L Q A M Q E N V E R W Q G Q Y E G L R G Q D L
D2641 (truncation-0)
S2648 (truncation-1)
E2655 (truncation-2)
G2662 (truncation-3)
G2669 (truncation-4)
D1714
1720
β 1 chain
D A R R K A E M L Q N E A K T L
72 aa (D1714-C1585)
The most truncated LMβ1E8 and LMγ1E8
D1528
1540
γ 1 chain
D T V D L N K L N E I E G T L N K
73 aa (D1528 - C1600)
D
LM511E8
truncation-0
truncation-1
truncation-2
truncation-3
truncation-4
[IB]
His tag (α5 chain)
(kDa)
100
75
E
truncated LM511E8 (truncation-2)
a
b
10 nm
F
a
b
dimensions of truncated LM511E8 (n = 50)
a: coiled-coil domain 10.1 ± 1.3 nm
b: LG1–3 7.4 ± 0.9 nm
G
HA
TEV PRS
tLMβ1E8
C
6xHis
tLMα5E8
LG1
LG2
LG3
FLAG
tLMγ1E8
TEV PRS
TEV Protease Recognition Site: -ENLYFQG-
disulfide bond
conserved Cys
additional Cys
tLMα5E8/I2723C
tLMγ1E8/D1585C
H
nonreducing
LM511E8
tLM511E8
+ SS linkage
(kDa)
250
150
100
75
50
37
25
20
15
10
tLM511E8
LMα5E8
tLMα5E8
LMβ1-γ1E8 dimer
tLMβ1-γ1E8 dimer
I
bound α6β1 integrin (A490)
2
1.5
1
0.5
0
LM511E8
tLM511E8
tLM511E8+TEV
0.001
0.01
0.1
1
10
100
α6β1 integrin concentration (nM)
J
(samples) Kd (nM)[a]
LM511E8 0.88 ± 0.08
tLM511E8 0.96 ± 0.09
tLM511E8 + TEV 0.92 ± 0.10
[a] Means ± S.D. of three independent experiments

Structure determination and refinement

tLM511E8 for crystallization was produced using FreeStyle™ 293-F cells and purified by affinity chromatography as for LM511E8 (described in detail in "Chapter 5: Materials and Methods"). TEV protease-treated tLM511E8 was subjected to gel filtration (Fig. 13A). Upon SDS-polyacrylamide gel electrophoresis (SDS-PAGE), the resulting tLM511E8 gave a single band migrating at ~100 kDa under nonreducing conditions, which dissociated into two bands (~80 kDa of tLMα5E8; ~10 kDa of tLMβ1E8/tLMγ1E8) under reducing conditions (Fig. 13B). Crystals of tLM511E8 were grown by vapor diffusion using 0.2 M ammonium sulfate, 0.1 M sodium acetate adjusted to pH 4.2 with acetic acid, and 19% polyethylene glycol 4000 as a precipitant (Fig. 13C). Solving the structure by the molecular replacement method using the LG1–3 of mouse LMα2 as a template failed because of low sequence homology between mouse LMα2 and human LMα5. Thus, the

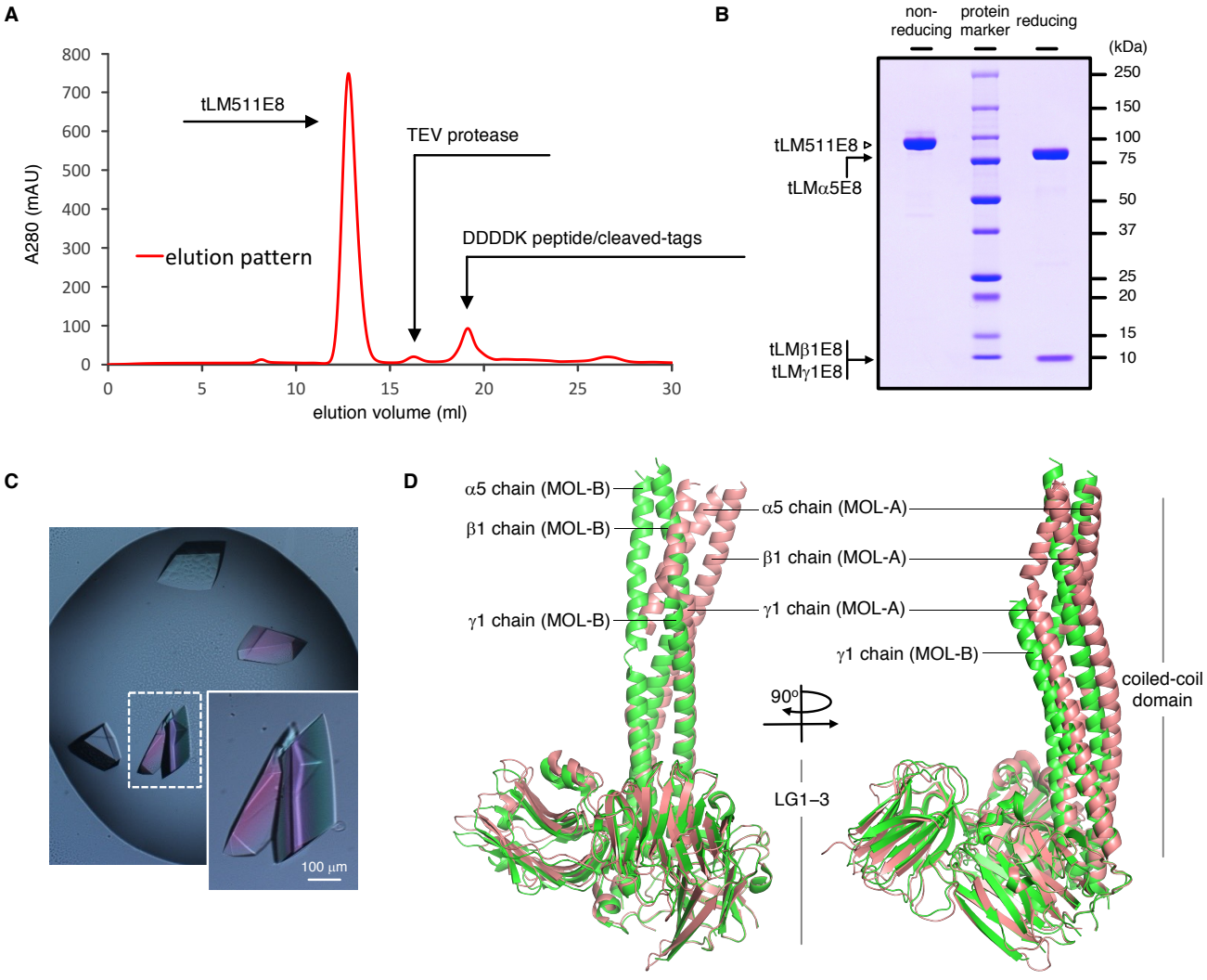

Fig. 13. Crystallization and structure determination of tLM511E8.

(**A**) Gel filtration chromatography of TEV protease-treated tLM511E8. (**B**) The peak fraction containing the cleaved tLM511E8 was subjected to SDS-PAGE under nonreducing and reducing conditions. (**C**) Crystals of tLM511E8. (**D**) Superposition between MOL-A (salmon) and MOL-B (green).

structure was solved by the single wavelength anomalous dispersion method using native crystals (S-SAD method). The final model was refined to the R/R_{free} factors of 0.202/0.237 at 1.80 Å resolution (deposited in the Protein Data Bank with accession code 5XAU). Diffraction data and refinement statistics are described in Table 1. Two structures were contained in one crystallographic asymmetric unit [designated as MOL-A consisting of chains 'A' (LMα5), 'B' (LMβ1), and 'C' (LMγ1); MOL-B consisting of chains 'D' (LMα5), 'E' (LMβ1), and 'F' (LMγ1)]. LMα5 in both structures contain one calcium ion and four *N*-glycans with either one or two *N*-acetylglucosamine (GlcNAc). Because MOL-A and MOL-B are essentially identical except that the coiled-coil domain of MOL-A is in slight flexion, I describe the structure of MOL-B (green-colored structure in Fig. 13D).

Table 1. Data collection and refinement statistics.

Data name	LM511E8 (for S-SAD)[a]	LM511E8
PDB ID		5XAU
Data collection		
Source	PF BL-1A	SPring-8 BL44XU
Space group	*C*2	*C*2
Cell dimensions		
a, *b*, *c* (Å)	175.4, 122.0, 107.7	175.0, 121.6, 107.6
β (°)	127.6	127.6
Wavelength (Å)	2.7	0.9
Resolution (Å)	50.0 - 2.48 (2.54 - 2.48)	50.0 - 1.80 (1.83 - 1.80)
R_{merge} or R_{sym} (%)[b]	10.3 (133)	6.5 (114)
$\langle I/\sigma(I)\rangle$	20.9 (0.87)	16.7 (1.4)
Completeness (%)	98.3 (87.1)	99.9 (100.0)
Redundancy	16.4 (3.7)	3.8 (3.8)
Refinement		
Resolution (Å)		49.41 - 1.80
No. of reflections		155,954
R_{work} / R_{free} (%)[c]		20.2/23.7
No. of atoms		
Protein		11,383
Ca^{2+}		2
Water		591
Average *B* factors (Å^2)		
Protein		36.2
Ca^{2+}		33.7
Water		36.6
r.m.s. deviations		
Bond length (Å)		0.011
Bond angle (°)		1.47

Values in parentheses correspond to the highest resolution shell.

[a]Three datasets collected from the same crystal were merged.

[b]$R_{sym} = 100\times\Sigma|I_{hkl}-\langle I_{hkl}\rangle|\Sigma I_{hkl}$, $\langle I_{hkl}\rangle$ is the mean value of I_{hkl}.

[c]$R_{work} = 100\times\Sigma||F_o|-|F_c||/\Sigma|F_o|$. R_{free} was calculated from the test set (5% of the total data).

The crystal structure of tLM511E8

The structure of tLM511E8 exhibits a "ladle" shape with LG1–3 adopting a compact triangular "cloverleaf" configuration, where LG1 is in direct contact with LG3 (Fig. 14, A and B). Each LG adopts a canonical β-sandwich fold consisting of 12 (LG1, LG2) or 14 (LG3) β-strands. The C-terminal end of individual LGs is brought into close proximity with their N-terminus by disulfide bonds: C2899–C2929 (LG1), C3090–C3115 (LG2), and C3261–C3292 (LG3). The C-terminal region of the coiled-coil domain of tLM511E8 lies between LG1 and LG2, where the C-termini of LMβ1 and LMγ1 helices are connected by a disulfide bond between β1-C1585 and γ1-C1600. There are four *N*-glycans attached to N2707 (coiled-coil domain of tLMα5) and N3209/N3257/N3287 (LG3), which are exposed to lateral faces. Although N3107 in LG2 is a potential *N*-glycosylation site, an attached *N*-glycan to its site could not be identified in this structure because of a very weak electron density. LMα5 contains one calcium ion at the LG1–LG3 interface, where its octahedrally coordinating ligands are provided by the residues within LG1 and LG3 as well as one water molecule (Fig. 15A). LG1 provides four ligands including side chains of D2793 and N2868 and carbonyl oxygens of residues 2810 and 2866, while LG3 provides D3219 as the fifth calcium-ligand from the protruding β9-β10 loop that is firmly anchored to the β7-β8 loop by hydrogen bonds among D3198, H3202, and D3218 (Fig. 15B).

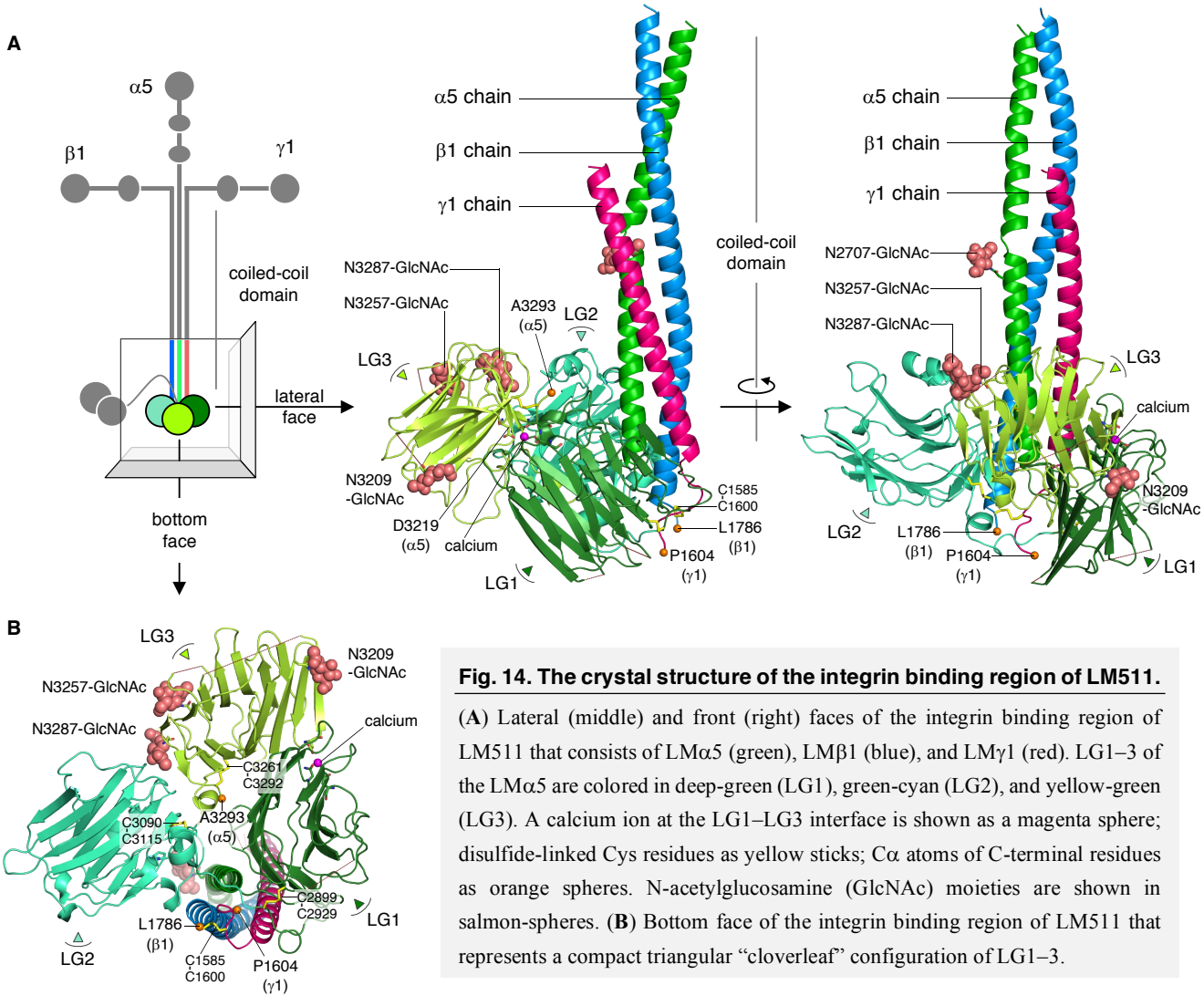

Fig. 14. The crystal structure of the integrin binding region of LM511.

(**A**) Lateral (middle) and front (right) faces of the integrin binding region of LM511 that consists of LMα5 (green), LMβ1 (blue), and LMγ1 (red). LG1–3 of the LMα5 are colored in deep-green (LG1), green-cyan (LG2), and yellow-green (LG3). A calcium ion at the LG1–LG3 interface is shown as a magenta sphere; disulfide-linked Cys residues as yellow sticks; Cα atoms of C-terminal residues as orange spheres. N-acetylglucosamine (GlcNAc) moieties are shown in salmon-spheres. (**B**) Bottom face of the integrin binding region of LM511 that represents a compact triangular "cloverleaf" configuration of LG1–3.

The coiled-coil domain of tLM511E8

When the triple-stranded coiled-coil domain of tLM511E8 is viewed from its N-terminus, tLMα5, tLMβ1, and tLMγ1 are arranged in an anticlockwise order. The coiled-coil domain consists of repeats of heptad sequence in which hydrophobic residues at the positions "a" and "d" form the core of the helical bundle, except for an interrupting segment with N2702-A2711 of tLMα5 (Fig. 15, C and D). In MOL-A, the N2702-A2711 segment is not integrated into the coiled-coil rod due to its flexibility, leading to a slight flexion of the coiled-coil domain (Figs. 13D and 15C). The following residues in MOL-A interact with the β1-γ1 dimer via the π-π face-to-face interaction of α5-H2706 with β1-Y1747 and initiates a triple-stranded coiled-coil assembly (Fig. 15C). In MOL-B, the N2702-A2711 segment is integrated into the coiled-coil rod through the hydrogen bond with β1-Y1747, allowing α5-V2705 to form the core of the helical bundle (Fig. 15D). The β1-γ1 dimer forms an acidic pocket attracting basic residues of LMα5 including R2718, R2720, and R2727 (Fig. 15E). These residues, particularly R2720 and R2727, are highly conserved in human laminin α chains (Fig. 15F). Ala substitutions for K2127 and R2134 in mouse LMα2 (equivalent to K2131 and R2138 in human LMα2) resulted

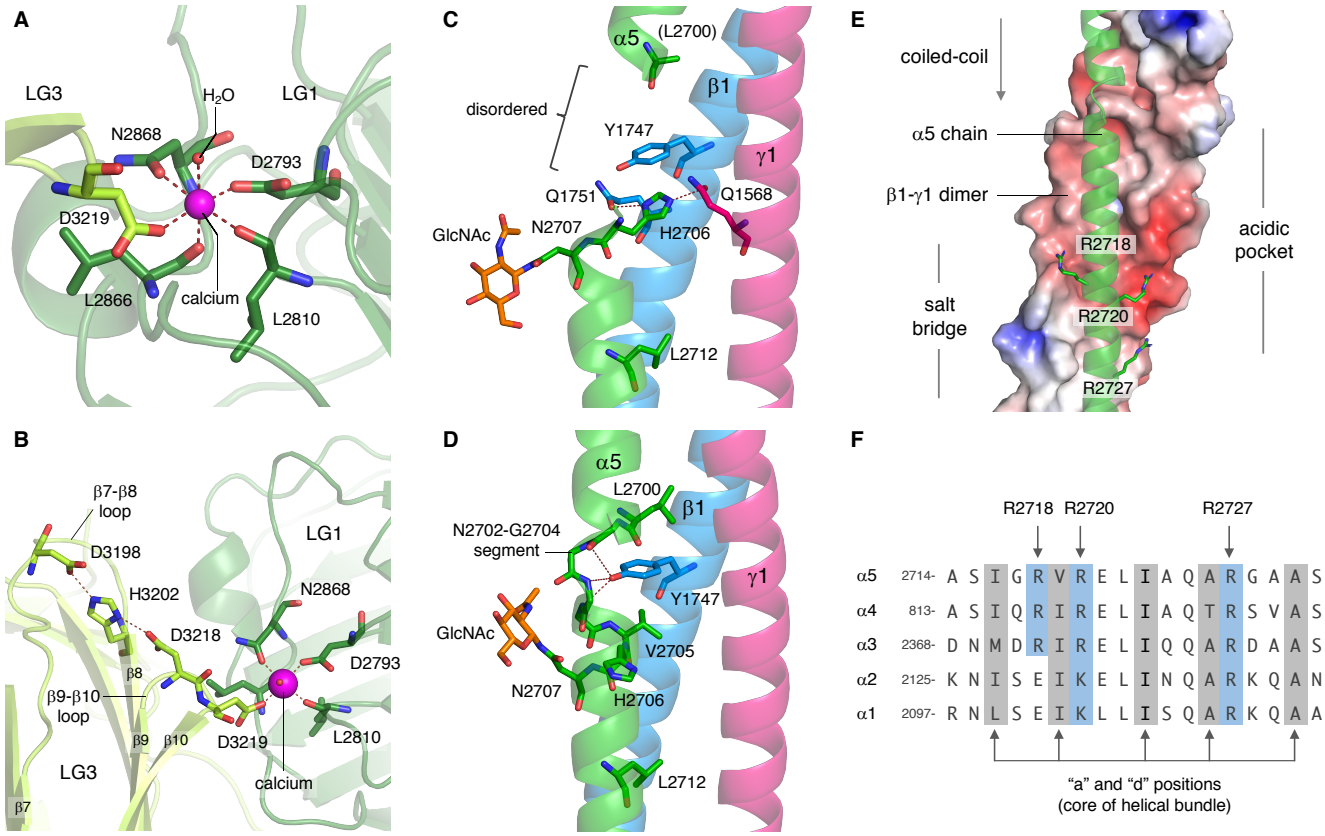

Fig. 15. Structural features of tLM511E8.

(**A**) Octahedral calcium coordination in the LG1–LG3 interface. (**B**) Hydrogen bonds among D3198, H3202, and D3218. (**C**, **D**) The structure of coiled-coil domain surrounding GlcNAc attached to N2707 in MOL-A (**C**) and MOL-B (**D**). GlcNAc is shown as an orange stick. Hydrogen bonds are shown as dashed lines. (**E**) Electrostatic potentials of β1-γ1 dimer countered from -5 kT/e (red) to +5 kT/e (blue) and ribbon presentation of LMα5. For the electrostatic potential calculation, γ1-C1585 was substituted by Asp. (**F**) Amino acid sequences of the coiled-coil domain of human laminin α chains. Amino acid residues at the positions "a" and "d" are colored in grey.

in decreased efficiency of trimer assembly with the β1-γ1 dimer (*71*), implying that electrostatic interaction between the basic residues of the LMα5 chain and the acidic pocket of the β1-γ1 dimer is required for coiled-coil assembly of LM511.

Association of LG1–3 with the β1-γ1 dimer

The overall arrangement of LG1–3 is in sharp contrast to that seen in the same fragment of LMα2 reported previously in isolation, which adopted an open configuration with LG1 completely dissociated from LG3 (Fig. 6C) (*92*). Thus, the cloverleaf assembly of LG1–3 in tLM511E8 should have been brought about by the heterotrimeric assembly of LMα5 with β1-γ1 dimer, rather than by the direct contact between LG1 and LG3 (Fig. 16A). Notably, LG1 and LG2 clamp the C-terminal region of the β1-γ1 dimer (Fig. 16B). LG1 contains a

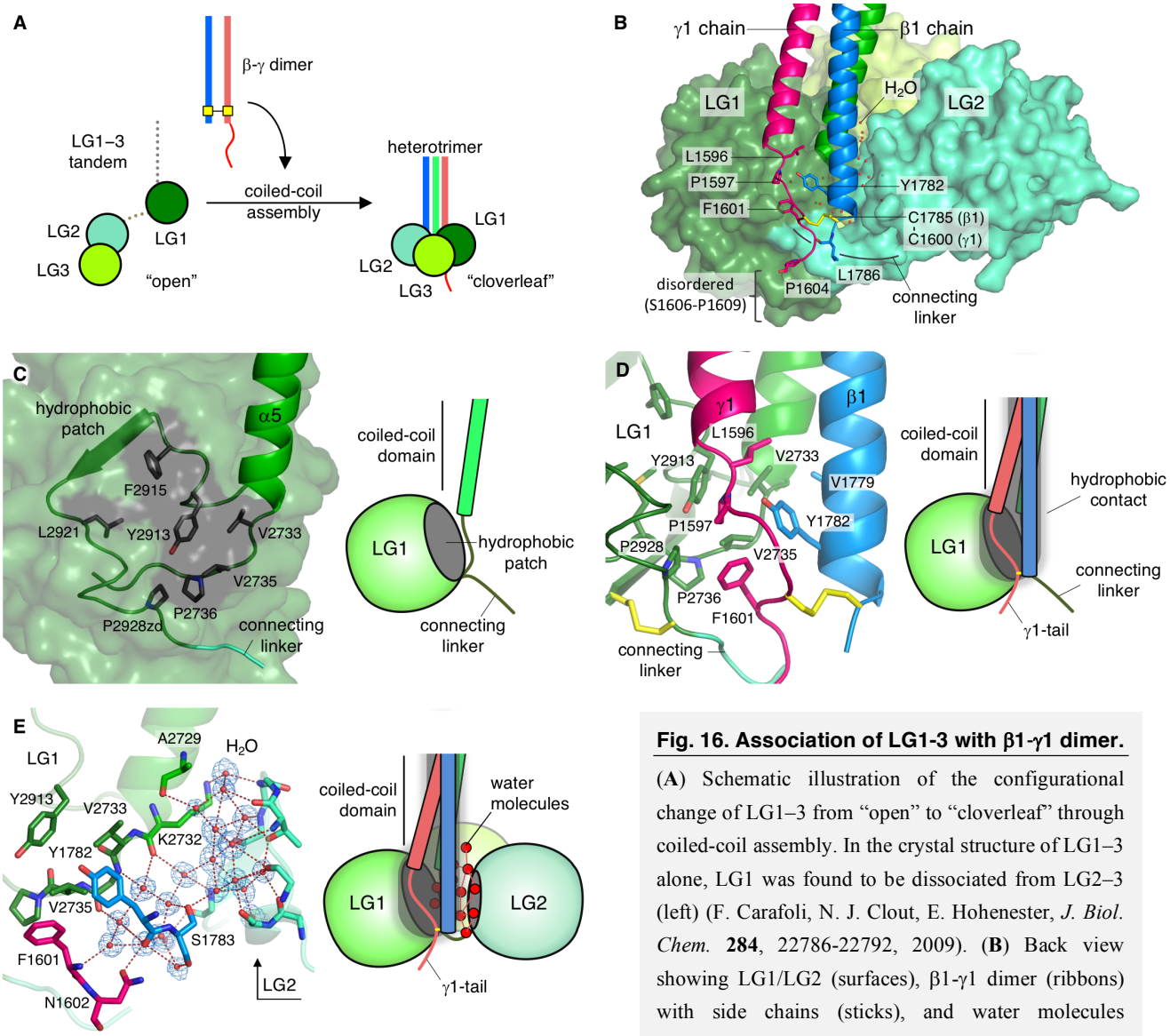

Fig. 16. Association of LG1-3 with β1-γ1 dimer.

(**A**) Schematic illustration of the configurational change of LG1–3 from "open" to "cloverleaf" through coiled-coil assembly. In the crystal structure of LG1–3 alone, LG1 was found to be dissociated from LG2–3 (left) (F. Carafoli, N. J. Clout, E. Hohenester, *J. Biol. Chem.* **284**, 22786-22792, 2009). (**B**) Back view showing LG1/LG2 (surfaces), β1-γ1 dimer (ribbons) with side chains (sticks), and water molecules (spheres). (**C**) Hydrophobic patch on LG1. (**D**) Hydrophobic interaction between the hydrophobic patch of LG1 and the C-terminal regions of the β1–γ1 dimer. (**E**) The interaction between LG2 and LMβ1 mediated by a layer of hydrogen-bonded water molecules. $2F_o$-F_c electron density map countered at 1.0 σ is shown as blue mesh around water molecules.

hydrophobic patch consisting of residues V2733, V2735, P2736, Y2913, F2915, L2921, and P2928 (Fig. 16C). Following the heterotrimeric assembly, the hydrophobic patch is brought into direct contact with the side chains of V1779/Y1782 of LMβ1 and L1596/P1597/F1601 of LMγ1. As a result, LG1 is fastened to the LMβ1 pillar through the hydrophobic side chain interactions (Fig. 16D). LG2 faces the LMβ1 pillar from the opposite side, but there are no obvious side chain interactions at the interface. Instead, water molecules fill the gap by forming a hydrogen-bonded network and secure the contacts of LG2 with the β1-γ1 dimer (Fig. 16E). Thus, heterotrimeric assembly may impose conformational restriction on LG1–2 to appose the LMβ1 pillar and lead to the cloverleaf assembly of LG1–3. It has been proposed that the Glu residue in the γ-tail associates with LG1–3 to ensure their functional triangular assembly (*95*). However, the five C-terminal residues of the γ1 chain, including γ1-E1607 that is the critical residue for integrin binding, are disordered in this structure and have no direct contact with LG1–3 (Fig. 16B), arguing against its role in stabilizing the functionally active conformation of LG1–3.

Comparison of the integrin binding region of LM511 and LM111

Recently, Pulido *et al.* reported a high-resolution crystal structure of the integrin binding segment of mouse LM111 using a truncated-LM111E8 having a shorter coiled-coil domain of approximately 50 residues long (described as "mini-E8" in their report) (*133*). Although LMα1 is the laminin chain phylogenetically distant from LMα5 (Fig. 2C), the global structure of LM111 is essentially the same as that of LM511 shown here,

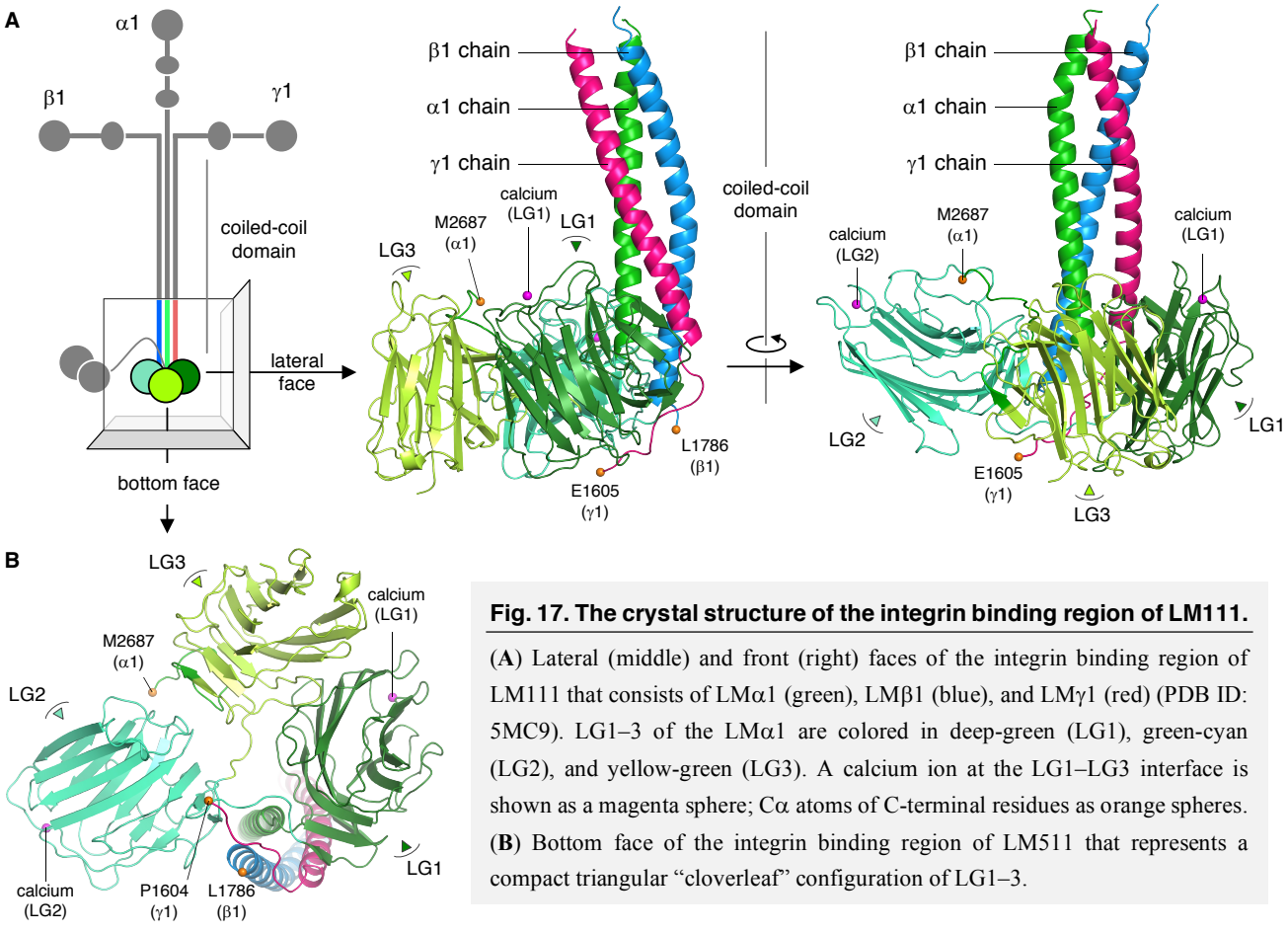

Fig. 17. The crystal structure of the integrin binding region of LM111.

(**A**) Lateral (middle) and front (right) faces of the integrin binding region of LM111 that consists of LMα1 (green), LMβ1 (blue), and LMγ1 (red) (PDB ID: 5MC9). LG1–3 of the LMα1 are colored in deep-green (LG1), green-cyan (LG2), and yellow-green (LG3). A calcium ion at the LG1–LG3 interface is shown as a magenta sphere; Cα atoms of C-terminal residues as orange spheres. (**B**) Bottom face of the integrin binding region of LM511 that represents a compact triangular "cloverleaf" configuration of LG1–3.

exhibiting a triangular configuration of LG1–3 with the β1-γ1 dimer clamped between LG1 and LG2 (Figs. 18A). Particularly, LG1 of LMα1 is associated with the β1-γ1 dimer through hydrophobic interaction in a way comparable to that of LMα5 (Fig. 18B). One interesting difference is that the LG3 in LM111 is positioned so as to make the transverse plane of LG1–3 orthogonal to the coiled-coil domain and does not provide a Ca^{2+} ligand to LG1, whereas LG3 in LM511 forms a beveled plane of LG1–3 and provides a Ca^{2+} ligand to LG1 (Fig. 18C). Pullido *et al*. noted that amino acid residues constituting each LG1–LG3 interface are not conserved in other laminin isoforms (*133*). Therefore, each α chain is assumed to have a specific LG1–LG3 interface depending on the interactions between surface-exposing side chains in LG1 and LG3. Nevertheless, the γ1-tail in the LM111 structure is oriented toward the bottom face of LG1/LG2 with the main chain of E1605 (equivalent to γ1-E1607 in human) and the following residues disordered in the crystal structure (Figs. 17 and 18A). The consistency in terms of the position of the γ1-tail relative to LG1–3 corroborates the notion that the γ1-tail directly interacts with integrin β1, with the Glu residue coordinating the metal ion in the β-MIDAS during formation of the laminin–integrin complex.

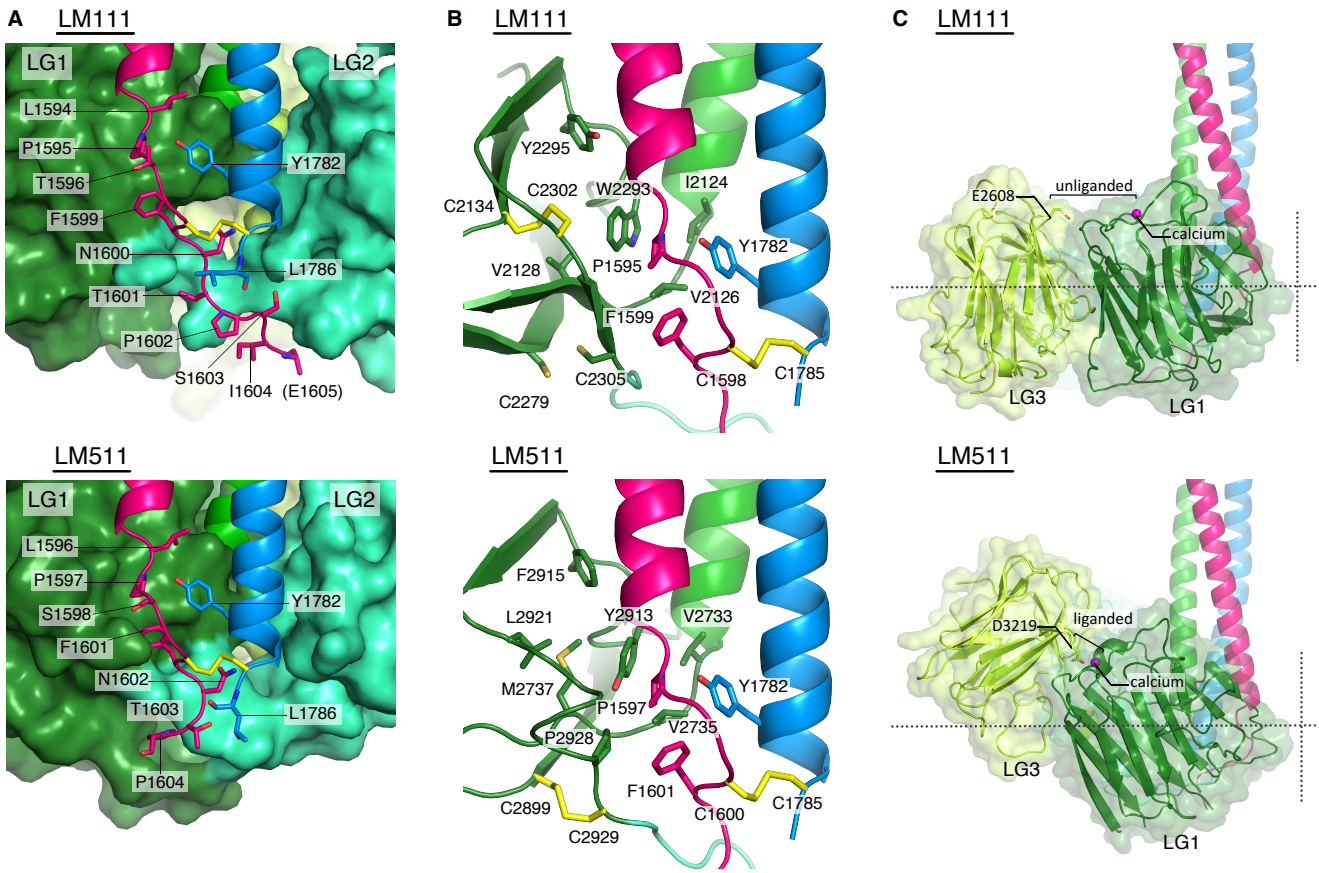

Fig. 18. Similarities and differences between the structures of LM111 and LM511E8.

(**A**) The β1-γ1 dimer clamped between LG1 and LG2 in LM111 (top) and LM511 (bottom). (**B**) Hydrophobic interaction between the hydrophobic patch of LG1 and the C-terminal regions of the β1-γ1 dimer in LM111 (top) and LM511 (bottom). The C2279-C2305 disulfide bond in LM111 is reduced due to radiation damage. (**C**) The LG1–LG3 interface of LM111 (top) and LM511(bottom).

2-2. Elucidation of the role of the γ1-tail in integrin recognition by LM511

LG1–3 do not provide an acidic residue coordinating the β1-MIDAS metal ion

The crystal structure of the integrin binding fragment of LM511 indicated that γ1-E1607 is quite unlikely to contribute to integrin binding through securing the functionally active conformation of LG1–3. The ligand-binding site of integrins has been mapped to the upper face of the integrin's headpiece that consists of the β-propeller domain of the α subunit and the βI/hybrid/PSI domains of the β subunit. It is generally accepted that recognition of physiological ligands by integrins relies on an acidic residue in the ligands, coordinating a divalent metal ion in the β-MIDAS (*109, 110*). Consistent with this scheme, the Glu residues in the γ1-tail (E1607) and γ2-tail (E1191) are essential for integrin binding by laminins, except for LMγ3 that does not contain a Glu residue in the γ-tail (*93, 94*), pointing toward the possibility that γ1-E1607 directly coordinates with the β-MIDAS. Laminin has a number of acidic residues within LG1–3 besides the Glu residue in the γ-tail. In the case of LMα5, LG1–3 contain 54 acidic residues (Fig. 19). Thus, there remains another possibility that one of

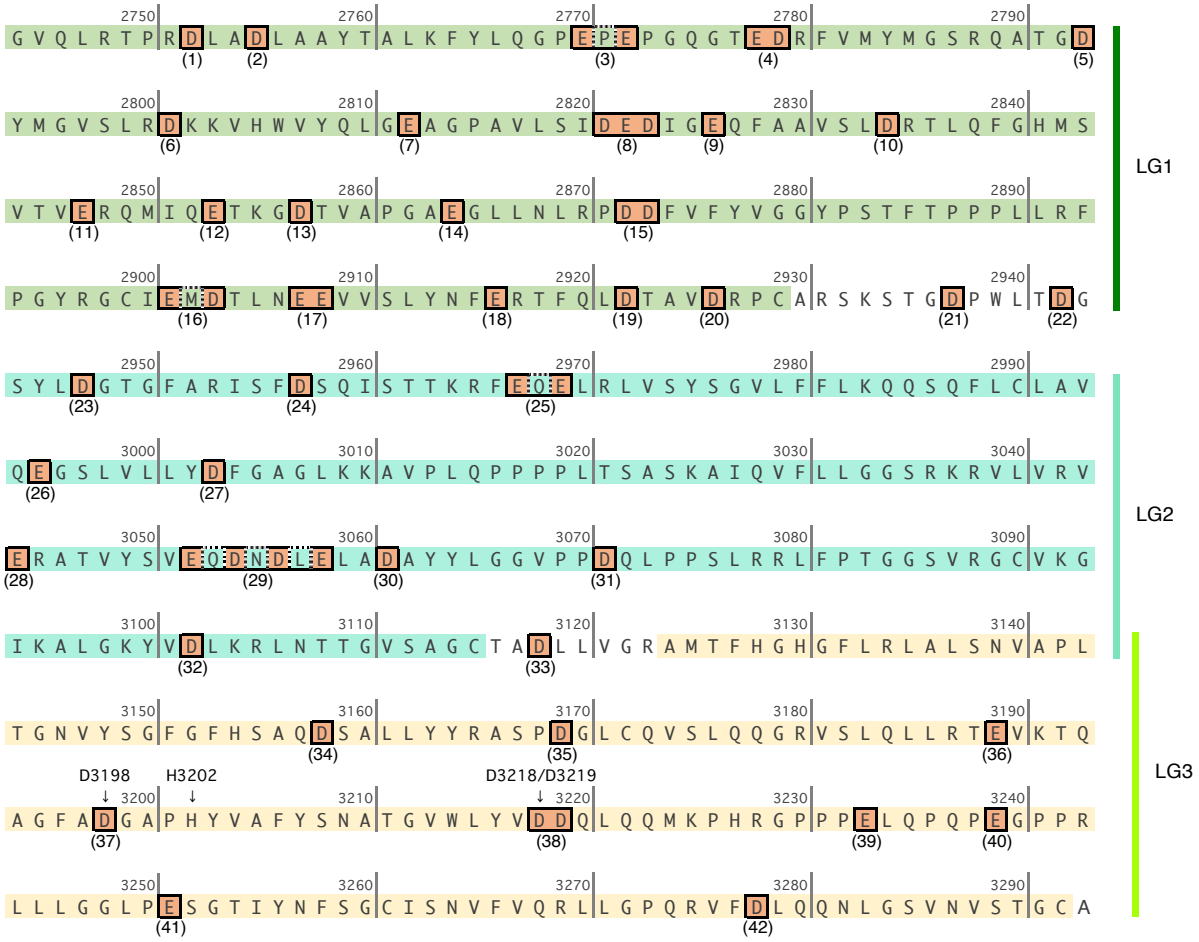

Fig. 19. A series of Ala mutagenesis.

Amino acid sequences of LG1, LG2, and LG3 are colored in deep-green, green-cyan, and yellow-green, respectively. The 54 targeted acidic residues are colored in orange and boxed.

these acidic resides directly coordinates with the β1-MIDAS metal ion. Therefore, I sought to probe the role of these acidic residues in LG1–3 in integrin binding by LM511. To achieve this, forty-two Ala substituted LMα5E8 mutants, covering all 54 acidic residues within LG1–3 (Fig. 19), were individually coexpressed in FreeStyle™ 293-F cells with wild-type LMβ1E8 and LMγ1E8. Wild-type and mutant LM511E8s in the culture supernatant were subjected to the solid-phase binding assay using α6β1 integrin (Fig. 20). The amounts of captured wild-type and mutant LM511E8s on a microtiter plate were equalized on the basis of LM511E8 concentrations in conditioned media determined by sandwich ELISA. A series of Ala mutagenesis and assessment of the integrin binding activity of LM511E8 mutants revealed that #37 (D3198A) and #38 (D3218A/D3219A) mutants were less active in binding to α6β1 integrin than wild-type LM511E8 (Fig. 21A). Particularly, D3218A/D3219A double mutation resulted in complete loss of the activity, as was the case for mutant LM511E8 having a E-to-Q mutation in the γ1-tail (LM511E8/EQ). To assess the impact of individual Ala mutation on the activity, LM511E8/D3218A and LM511E8/D3219A were prepared and subjected to the solid-phase integrin binding assay (Fig. 21B). As a result, D3218A mutation abrogated the α6β1 integrin binding activity of LM511E8, despite a partial decrease with D3219A mutation. The crystal structure of tLM511E8 demonstrated that D3219 contributes to forming the LG1–LG3 interface by coordinating a Ca^{2+} in LG1, while D3218 is directly involved in the integrity of LG3 through the interaction with H3202 (Fig. 15, A and B). Notably, H3202A mutation also nullified the integrin binding activity (Fig. 21B), suggesting that a break of hydrogen bond between H3202 and D3218, not between H3202 and D3198, leads to a fatal misfolding of LG3 and perturbs the assembly of LG1–3, thereby resulting in reduced α6β1 integrin binding activity. Consistent with this possibility, both H3202A and D3218A mutations caused a significant reduction in the

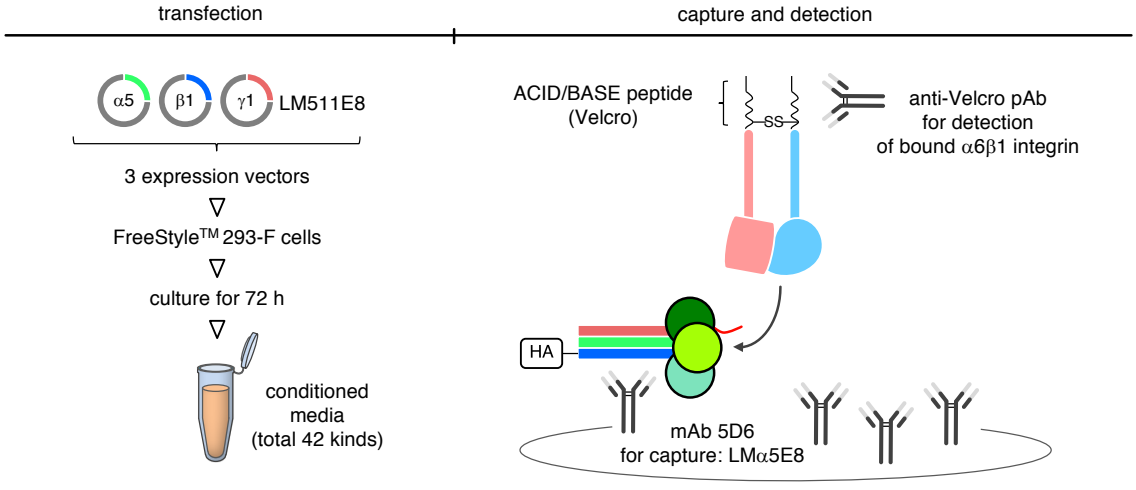

Fig. 20. Assessment of the integrin binding activity.

Schematic diagram of the assessment of the integrin binding activity of LM511E8 mutants. LMα5E8 mutants and wild-type LMβ1E8/LMγ1E8 were coexpresed in FreeStyle™ 293-F cells (left). The secreted LM511E8 mutants were captured on the mAb 5D6-coated plate, and then incubated with α6β1 integrin in the presence of 1 mM $MnCl_2$. The bound integrins were quantified with biotinylated anti-Velcro pAb and HRP-conjugated streptavidin as described in "Materials and Methods".

secretion of level of LM511E8 with concomitant intracellular accumulation of mutated LM511E8s (Fig. 21C). It is of note that an Asn substitution for D3218 did not severely compromise the integrin binding activity nor the secretion level of LM511E8 (*134*), indicating that the carboxylate of D3218 contribute to the maintenance of the functionally active conformation of LG1–3, but not to coordinating the β1-MIDAS metal ion. Together, I concluded that none of the 54 acidic residues within LG1–3 but E1607 in the γ1-tail is directly involved in integrin binding by LM511.

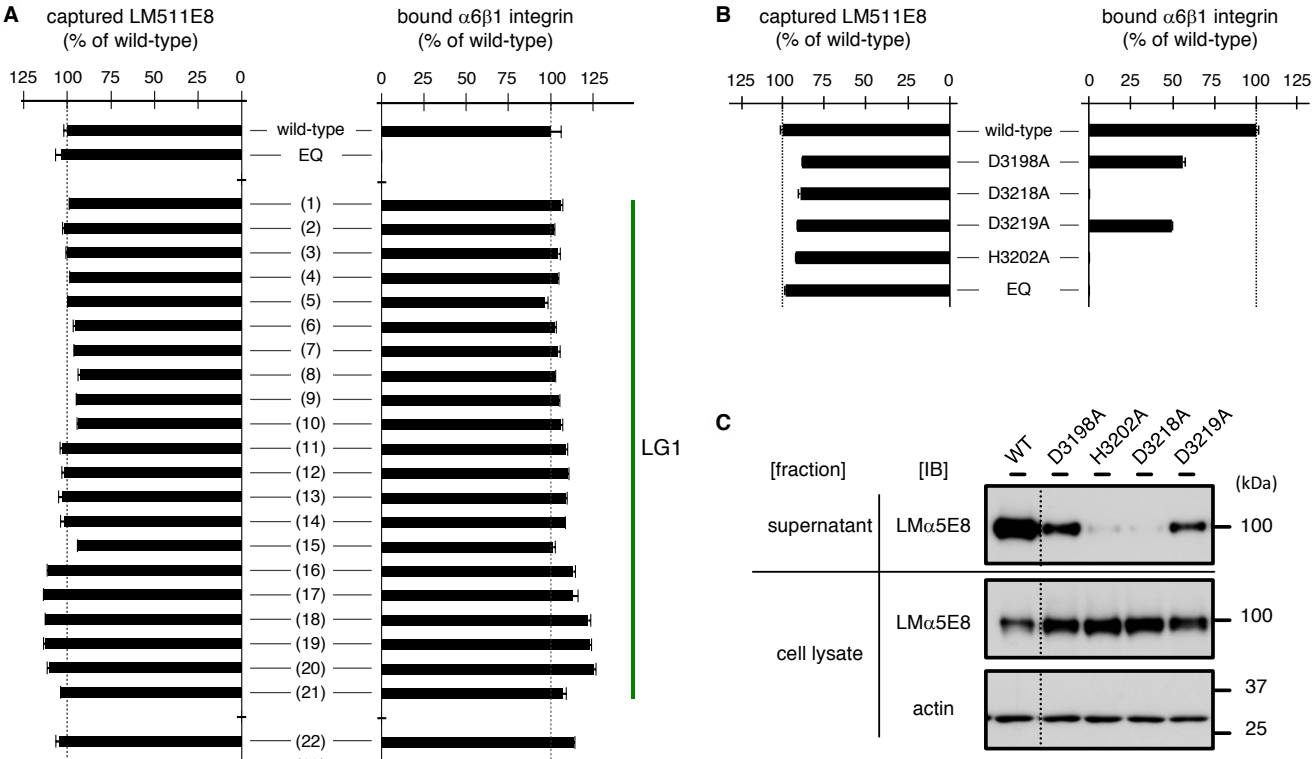

Fig. 21. Binding activities of LM511E8 and its mutants to α6β1 integrin.

(**A**) The captured amounts (left) and the binding activities (right) of LM511E8 mutants to α6β1 integrin are expressed as percentages relative to the amount/activity of wild-type LM511E8. (**B**) The captured amounts (left) and the integrin binding activities (right) of LM511E8/D3198A, /D3218A, /D3219A, /H3202A and the Gln substituted mutant for γ1-E1607 (LM511E8/EQ) are expressed as percentages relative to the amount/activity of wild-type LM511E8. Each column represents the mean ± S.D. of three independent experiments. (**C**) The supernatants and cell-lysates derived from FreeStyle™ 293-F cells expressing LM511E8 mutants were subjected to SDS-PAGE under reducing condition, followed by immunoblotting with anti-5×His mAb and anti-actin pAb.

The γ1-tail is positioned close to the metal ion of the β1-MIDAS

A gallery of electron microscopic images of the LM511E8-α6β1 integrin complex, which were obtained by Dr. Yukimasa Taniguchi, revealed that the headpiece of α6β1 integrin always bound to LM511E8 in an orientation opposing to the filament-like coiled-coil extension (Fig. 22A). These findings indicate that LM511 binds to α6β1 integrin via the bottom face of LG1–3 where the disordered C-terminal five residues of the γ1-tail are predicted to reside (Fig. 22B). To corroborate the direct contact of the γ1-tail with α6β1 integrin, I simultaneously introduced Cys substitutions into the γ1-tail and the βI domain of integrin β1 and then performed exhaustive screening for the intermolecular disulfide formation between the Cys-substituted LM511E8 and the α6β1 integrin. I reasoned that, if the γ1-tail directly interacts with integrin β1, a Cys residue introduced adjacent to γ1-E1607 would become cross-linked to a Cys residue introduced near the β1-MIDAS. Thus, residues I1606

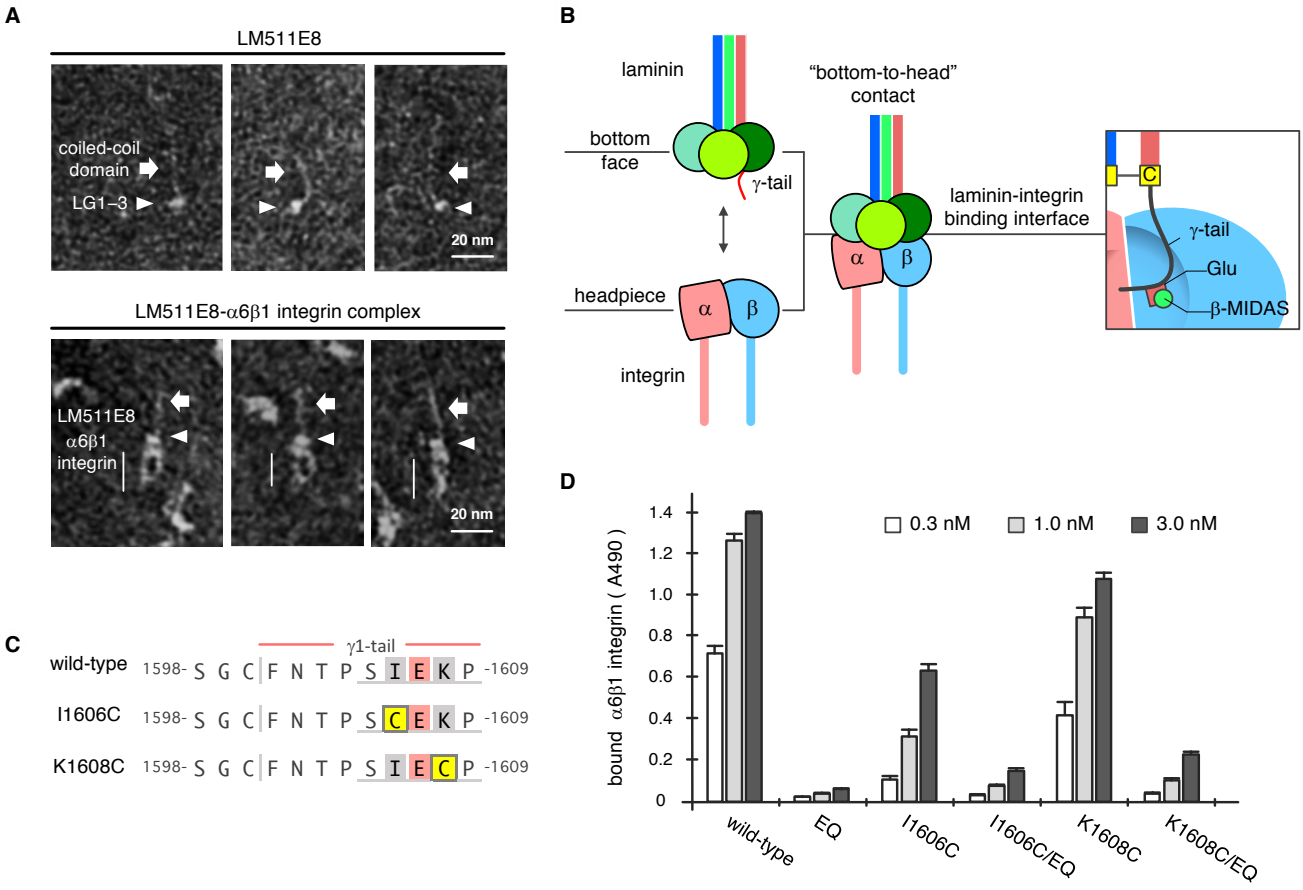

Fig. 22. Exhaustive cross-link screening between γ1-tail and integrin β1.

(**A, B**) Galleries of electron microscopic images of LM511E8 (**A**) and LM511E8-α6β1 integrin complex (**B**). (**C**) Schematic illustration of the interaction between LM511E8 and α6β1 integrin. (**C**) Amino acid sequences of wild-type and Cys-substituted γ1-tails. Cys-substituted residues are shown in yellow. (**D**) Integrin binding activity of wild-type and Cys-substituted LM511E8s. Microtiter plates were coated with LM511E8/wild-type, LM511E8/I1606C, LM511E8/K1608C, and their E to Q mutants and then incubated with α6β1 integrin in the presence of 1 mM $MnCl_2$. Bound integrins were quantified using biotinylated anti-Velcro pAb and HRP-conjugated streptavidin as described in "Materials and Methods". The amounts of integrin bound in the presence of 10 mM EDTA were used as negative controls and subtracted as background. Each column represents the mean ± S.D. of three independent experiments.

and K1608 of the γ1-tail (Fig. 22C) and residues in the βI domain that are predicted to be surface-exposed near the β1-MIDAS (Fig. 22E) were subjected to Cys-substitutions. LM511E8 with γ1-I1606C and -K1608C substitutions (designated LM511E8/I1606C and LM511E8/K1608C, respectively) retained integrin binding activity, whereas those having additional Gln substitutions for γ1-E1607 (designated LM511E8/I1606C/EQ and LM511E8/K1608C/EQ) were almost devoid of the integrin binding activity (Fig. 22D). Coexpression of Cys-substituted LM511E8 and α6β1 integrin in mammalian cells and subsequent immunoprecipitation of secreted LM511E8, followed by SDS-PAGE under nonreducing conditions (Fig. 22F), identified a total of seven

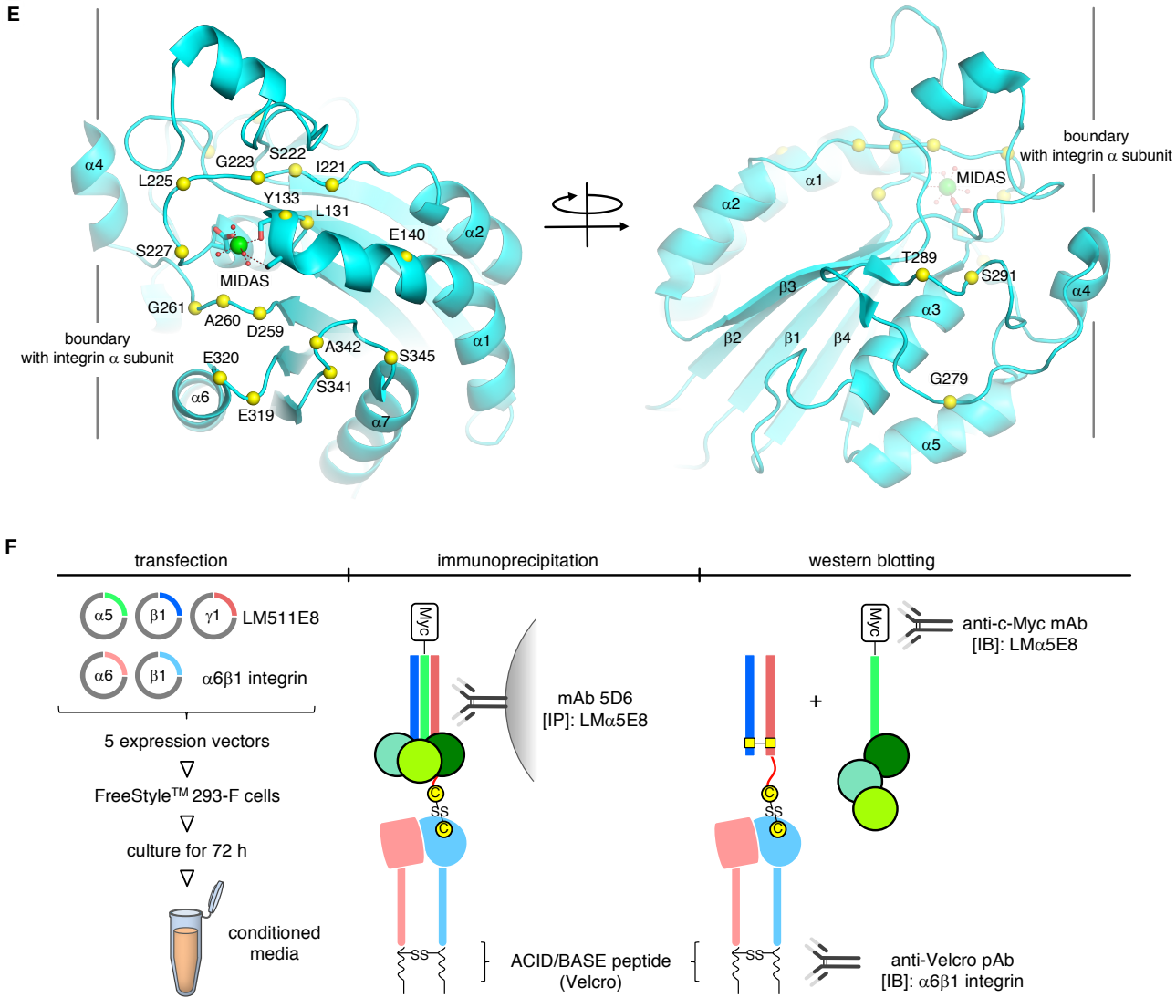

(**E**) Cys-substituted residues on βI domain. Cα atoms of 19 Cys-substituted residues are marked with yellow spheres on the crystal structure of the βI domain of human integrin β1 (PDB ID: 4WJK). The metal ion in the β1-MIDAS is shown as a green sphere. (**F**) Schematic diagram of the disulfide cross-link assay. LM511E8 and α6β1 integrin were coexpressed in FreeStyle™ 293-F cells (left) followed by immunoprecipitation of the secreted LM511E8-α6β1 integrin complex with mAb 5D6 against human LMα5 (middle). Immunoprecipitates were subjected to SDS-PAGE in nonreducing conditions and subsequent immunoblotting with anti-Velcro pAb or anti-c-Myc mAb (right).

disulfide-linked products between LM511E8 and α6β1 integrin, depending on the position of the Cys substitution within the γ1-tail (Fig. 23, A-C). LM511E8/I1606C was disulfide-linked to four Cys-substituted integrin β1 residues: 133, 221, 222, and 223 (Fig. 23A); LM511E8/K1608C was disulfide-linked to three Cys-substituted residues: 133, 223, and 225 (Fig. 23B). The ability of both laminin mutants to form disulfide bonds with integrin β1 residues 133 and 223 is consistent with the fact that these residues are closest to the MIDAS metal ion, with which γ1-E1607 is predicted to ligate (Fig. 23C). In contrast, residues 221 and 222, which are located further away from the α subunit, preferentially cross-linked to LM511E8/I1606C, while residue 225,

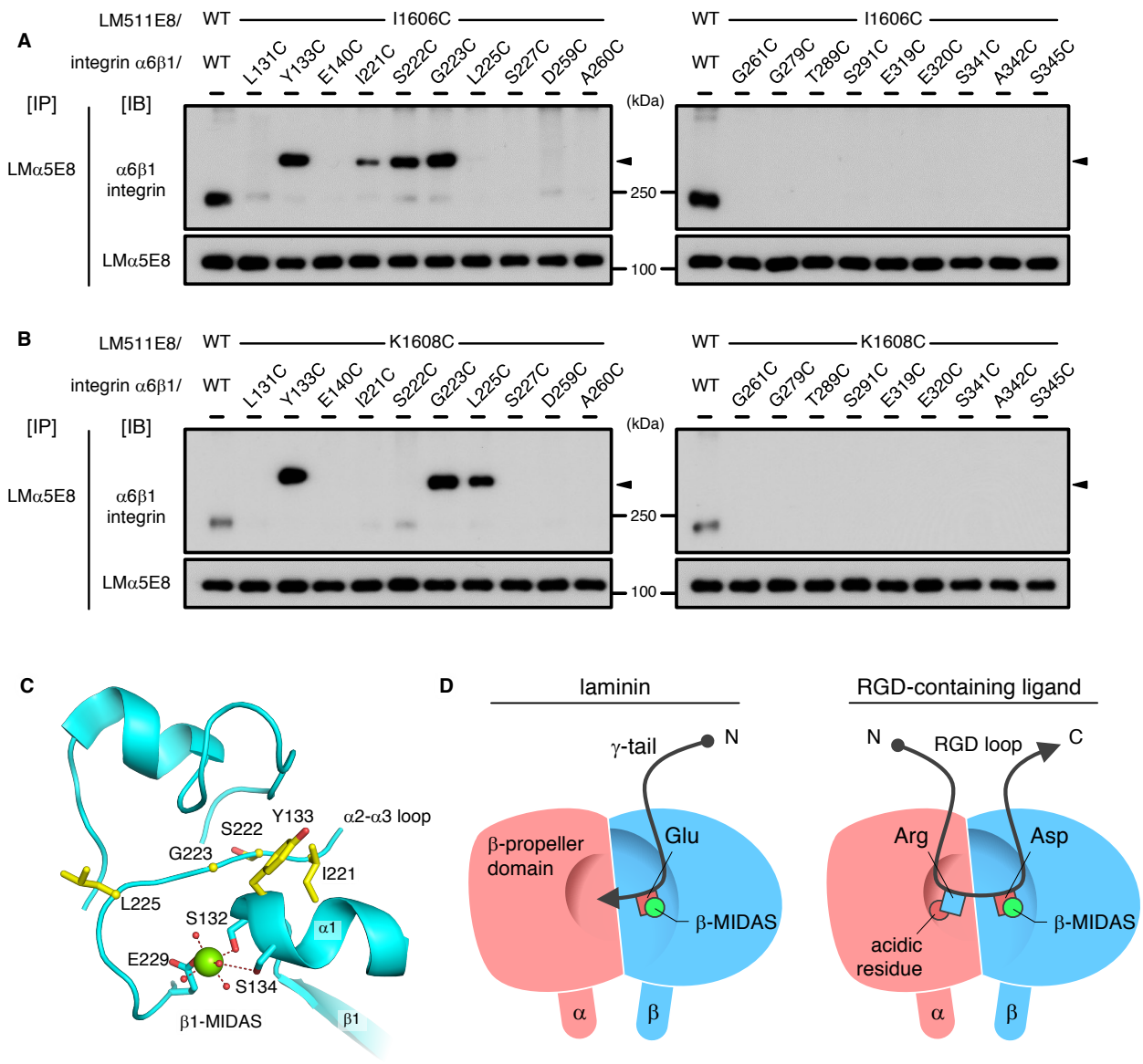

Fig. 23. Disulfide formation between Cys-substituted LM511E8 and α6β1 integrin.

(**A, B**) The results of intermolecular disulfide cross-linking of Cys-substituted α6β1 integrins with LM511E8/I1606C (**A**) and LM511E8/K1608C (**B**). Arrow heads indicate disulfide-linked products. (**C**) The residues cross-linked to the γ1-tail (yellow sticks) lie near the metal ion (green sphere) in the β1-MIDAS. The β1-MIDAS metal ion and water molecules are depicted as green and red spheres, respectively. (**D**) Distinct topologies of the γ-tail (left) and the RGD motif (right) on the integrin's headpiece.

situated closer to the α subunit, efficiently cross-linked to LM511E8/K1608C (Fig. 23C). These results suggest that the I1606-E1607-K1608 segment of the γ1-tail is aligned parallel to the segment with residues 221 to 225 of the α2-α3 loop of integrin β1, with the C-terminal end of the former pointing toward the β-propeller domain of integrin α6 when γ1-E1607 coordinates with the β1-MIDAS metal ion (Fig. 23D, left). This is in sharp contrast to the common mode of the RGD motif recognition by many integrins, because the RGD-containing peptide segment is docked at the α–β interface in the N→C direction with the side chains of Arg and Asp being recognized by the α- and β-subunits of integrin, respectively (Fig. 23D, right) (*135, 136*). To confirm the specificity of the intermolecular disulfide formation between the Cys-substituted LM511E8 and α6β1 integrin, I performed disulfide cross-link assays using laminin mutants carrying an inactivating Gln mutation at γ1-E1607 (Fig. 24). The Gln substitution resulted in a significant reduction in the disulfide formation though the disulfide bonds involving Y133 of integrin β1 form to some extent in the absence of γ1-E1607, suggesting that efficient disulfide bond formation requires correct steering of the γ1-tail guided by the γ1-E1607-MIDAS interaction.

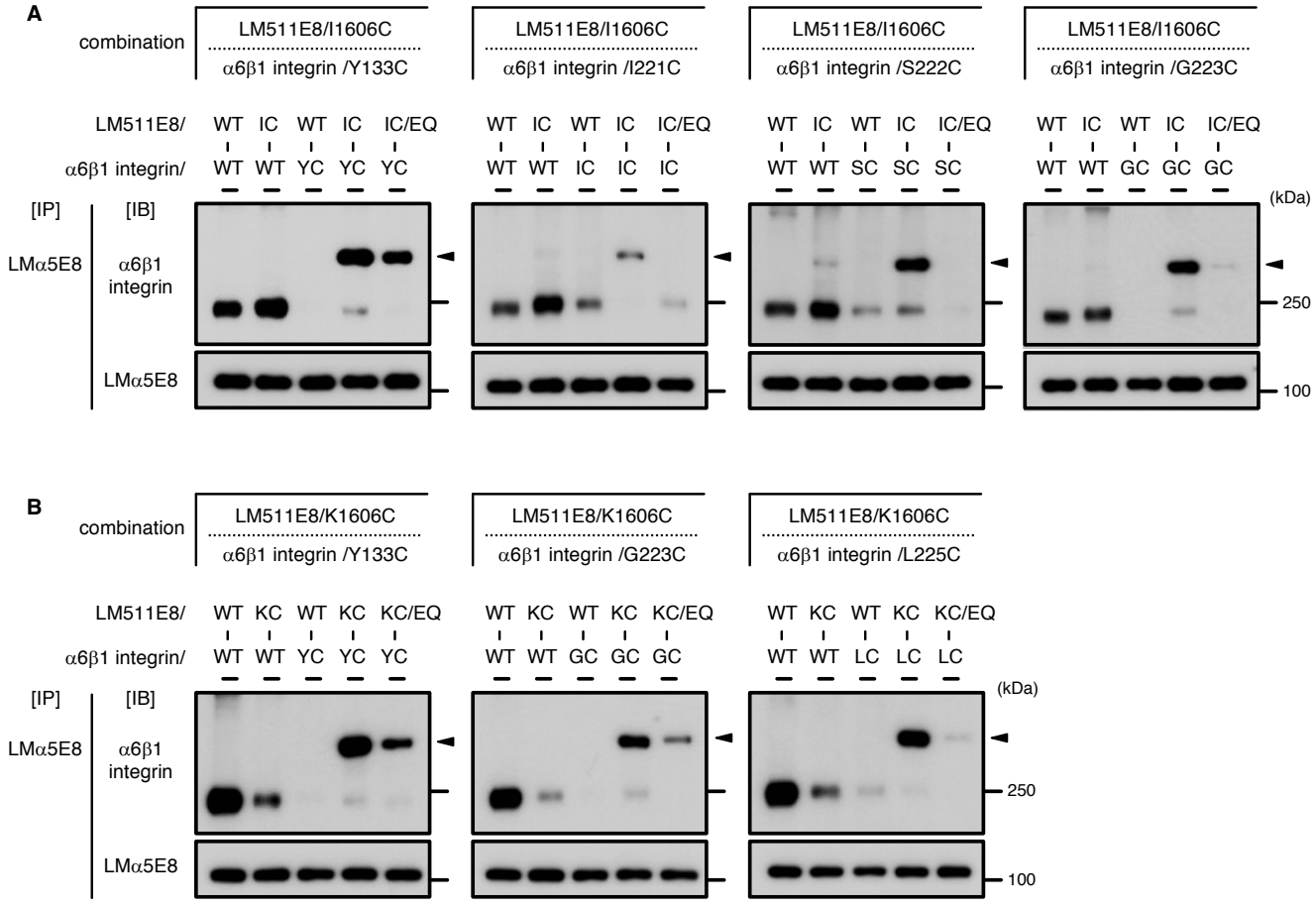

Fig. 24. Disulfide cross-link assays using LM511E8/I1606C/EQ and LM511E8/K1608C/EQ.

(**A**) Effects of E-to-Q mutation on disulfide formation between LM511E8/I1606C and Cys-substituted α6β1 integrins (Y133C, I221C, S222C, and G223C). (**B**) Effects of the E-to-Q mutation on disulfide formation between LM511E8/K1608C and Cys-substituted α6β1 integrins (Y133C, G223C, and L225C).

The γ1-tail and LG1–3 provide independent binding sites for integrin

It has been repeatedly observed that the ligand binding activity of RGD-recognizing integrins was inhibited by RGD and related peptides (*137*). However, previous study (*93*) was unable to demonstrate the competitive inhibition of the interaction of LM511 with α6β1 integrin by the γ1-tail–derived octapeptide NTPSIEKP (designated γ1C8). When a reduced concentration of the α6β1 integrin was used in the inhibition assay, however, I noticed that γ1C8 was weakly inhibitory to the binding of α6β1 integrin to LM511E8 in a γ1-E1607 dependent manner (Fig. 25A). To revisit the effect of synthetic γ1-tail peptides on the laminin-integrin interaction, I performed inhibition assays using a γ1-tail-derived pentapeptide SIEKP corresponding to the five residues disordered in the crystal structure of tLM511E8 (designated γ1C5) and its E-to-Q mutant (SIQKP) under the conditions where α6β1 integrin was rendered conformationally active by the activating anti-integrin β1 antibody TS2/16. I reasoned that, if γ1-E1607 coordinates with the β1-MIDAS metal ion, saturation binding of TS2/16 would render α6β1 integrin in a high-affinity state to γ1C5, as seen in the affinity state of α5β1 integrin toward the RGD peptide (Fig. 25B). While γ1C5 was only weakly inhibitory to α6β1 integrin binding to LM511E8 in the absence of TS2/16 (Fig. 26A, left and middle), it exerted a significant inhibitory activity in the presence of TS2/16 with half-maximal inhibitory concentration (IC_{50}) of 25.2 ± 0.5 μM (Fig. 26A, right). The inhibitory activity of γ1C5 was abrogated by the E-to-Q substitution. These results indicate that the γ1-E1607 in the γ1-tail is directly recognized by α6β1 integrin, though insufficient for recapitulating the integrin binding activity of LM511. These findings also point to the scheme that the γ1-tail comprises a bipartite integrin recognition site together with LG1–3 (Fig. 26B), although the direct interaction of LG1–3 with integrin has not

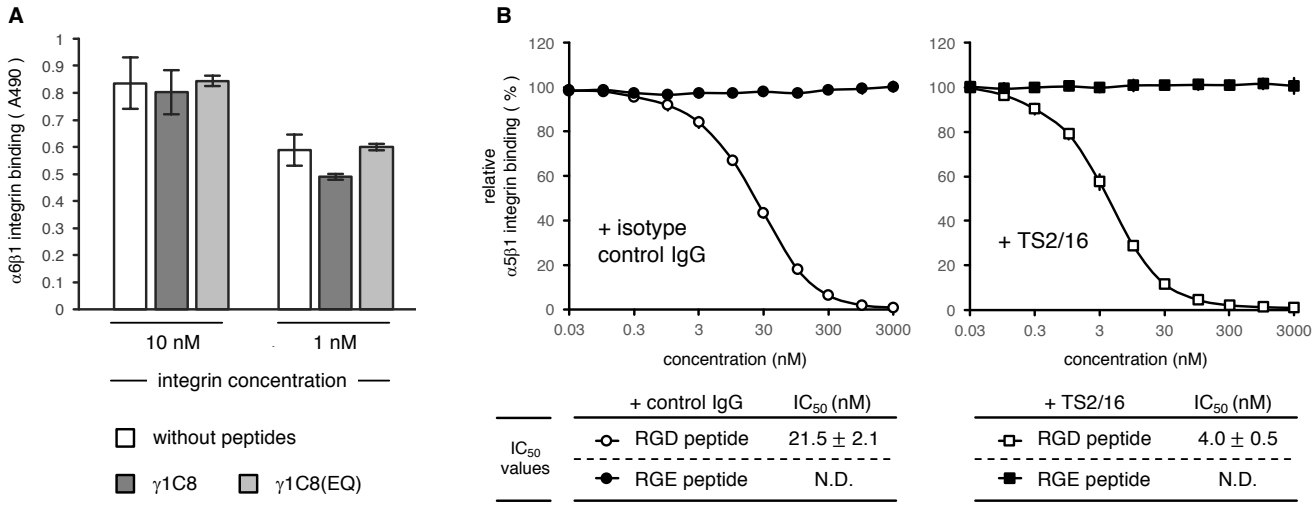

Fig. 25. Reassessment of inhibitory activity of γ1-tail–derived peptide.

(**A**). α6β1 integrin (1 or 10 nM) was incubated with 100 μM γ1-tail–derived octapeptide (NTPSIEKP, designated γ1C8) or its E-to-Q mutant [NITSIQKP, designated γ1C8 (EQ)] in the presence of 1mM $MnCl_2$, then added to LM511E8-coated plates and allowed to bind to LM511E8. Bound integrins were quantified using biotinylated anti-Velcro pAb and HRP-conjugated streptavidin as described in "Materials and Methods". (**B**) Inhibition of the fibronectin–α5β1 integrin interaction by RGD (white) and RGE (black) peptides in the absence (circle) or presence (square) of the integrin β1 activating mAb TS2/16. IC_{50} values of peptides (means ± S.D. of three independent experiments) are shown in tables. N.D., not determined.

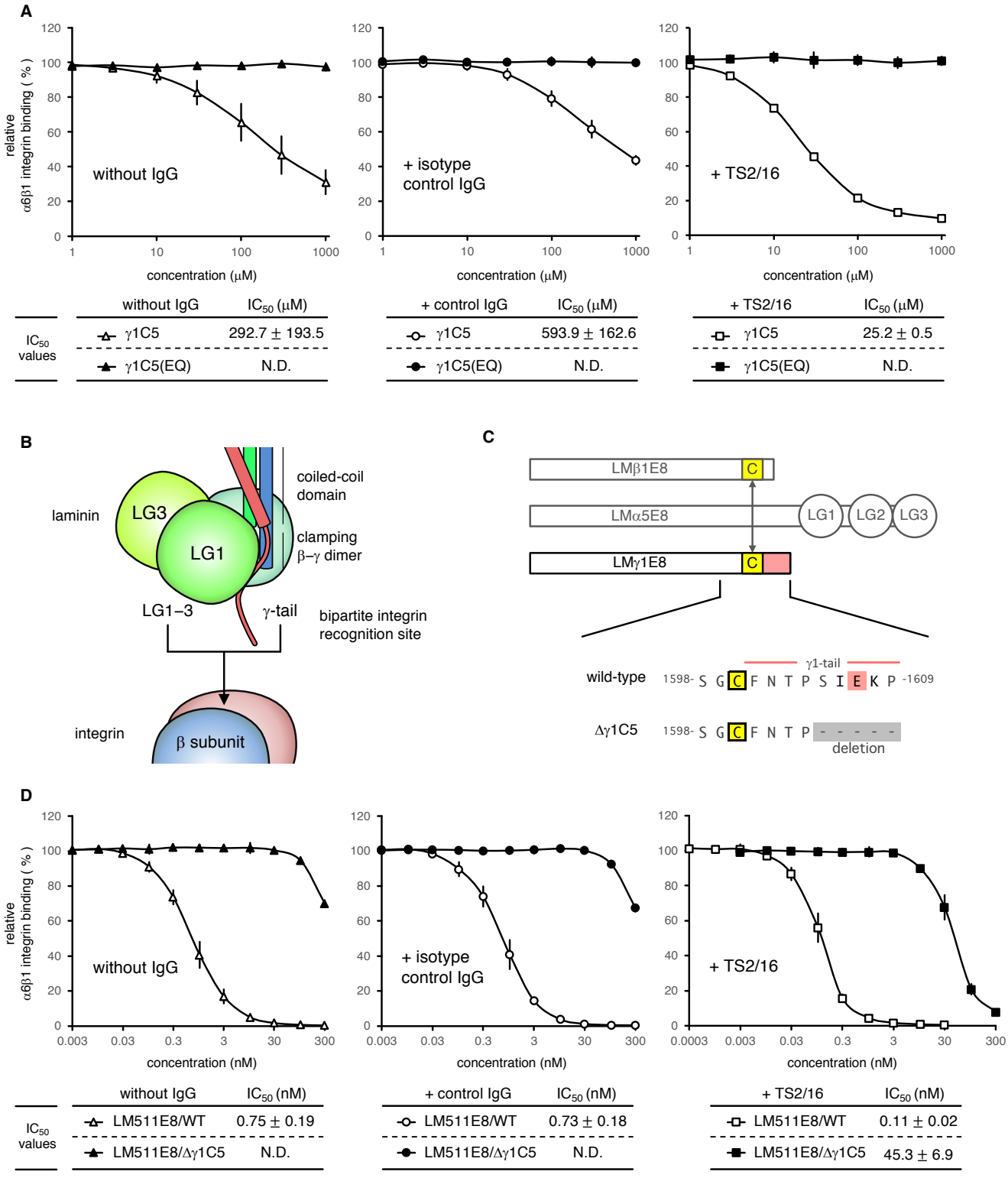

Fig. 26. Direct contribution of γ1-E1607 and LG1–3 to laminin-integrin interaction.

(**A**) Inhibition of the LM511E8–α6β1 integrin interaction by γ1-tail–derived peptides [white, γ1C5; black, γ1C5(EQ)] in the absence (triangle/circle) or presence (square) of mAb TS2/16. (**B**) A model for the integrin recognition by the composite binding interface of laminins. (**C**) Schematic illustration of wild-type and Δγ1C5 LM511E8. (**D**) Inhibition of the LM511E8-α6β1 integrin interaction by wild-type (white) or Δγ1C5 (black) LM511E8, in the absence (triangle/circle) or presence (square) of integrin β1 activating mAb TS2/16. IC_{50} values of peptides or LM511E8 (means ± S.D. of three independent experiments) are shown in tables. N.D., not determined.

been demonstrated (*89, 93*). To corroborate the direct involvement of LG1–3 in laminin recognition by integrins, I performed inhibition assays using mutant LM511E8 lacking the five C-terminal residues of the γ1-tail (designated LM511E8/Δγ1C5) in place of synthetic peptides (Fig 26C). LM511E8/Δγ1C5 was inhibitory to the binding of α6β1integrin to LM511E8 with an IC_{50} of 45.3 ± 6.9 nM, which was two orders of magnitude higher than that of intact LM511E8 (IC_{50} = 0.11 ± 0.02 nM) (Fig. 26D, right), suggesting that LM511E8 devoid of γ1-E1607 has weak but appreciable binding affinity toward α6β1 integrin. Consistent with these results, the intermolecular disulfide bonds in the exhaustive cross-link screening, particularly involving β1 residue 133, were formed to some extent in the absence of γ1-E1607. Taken together, full integrin binding activity of LM511 is defined by a combination of the two weak interactions involving the γ1-E1607 and LG1–3, of which the residues(s) involved in the latter remain to be identified.

Chapter 3: Discussion

Despite the requirement for the Glu residue within the γ-tail in integrin recognition by laminins, it has remained unsettled whether the γ-tail is required for the maintenance of a functionally active conformation of LG1–3 of the α chain or it directly interacts with integrin by coordinating the metal ion in the β-MIDAS. Several lines of evidence obtained in this study support the latter possibility. First, the γ1-tail of tLM511E8 was found disordered in the crystallized structure and therefore does not seem to contribute significantly to the maintenance of LG1–3 conformation. Furthermore, the C-terminal region of the β1-γ1 dimer is clamped between LG1 and LG2, thereby confining the disordered γ1-tial to the bottom face of the ladle-shaped tLM511E8. This finding is in agreement with the fact that LM511E8 binds to α6β1 integrin via the bottom face of LG1–3. Second, intermolecular disulfide crosslink screening with a panel of Cys-substituted LM511E8s and α6β1 integrins demonstrated that the γ1-tail is selectively disulfide-linked to residues near the β1-MIDAS, supporting the direct interaction of the γ1-tail with integrin's β1-MIDAS. Finally, the γ1C5 peptide SIEKP inhibited the binding of LM511E8 to α6β1 integrin but its E-to-Q mutant did not, corroborating the direct interaction of the γ1-tail with α6β1 integrin, in which γ1-E1607 is prerequisite. These findings together lead me to conclude that the γ1-tail directly interacts with integrin's β1-MIDAS, with γ1-E1607 serving as the critical acidic residue that coordinates the metal ion in the β1-MIDAS.

Common features between the γ-tail and other integrin recognition sites

The γ-tail having a Glu residue is found in both vertebrates and invertebrates except for the γ3-tail (Fig. 27A). In addition, two hydrophobic residues corresponding to F1601 and I1606 in the human γ1-tail are well conserved among these animals. The crystal structure of the integrin binding segment of LM511 revealed that the aromatic side chain of γ1-F1601 is in direct contact with LG1 through hydrophobic side chain interactions (Fig. 16), suggesting that the former hydrophobic residue contributes to the maintenance of the functionally active conformation of LG1–3, but not to the integrin binding of laminin. On the other hand, the latter hydrophobic residue (i.e., γ1-I1606) is located on the disordered γ1-tail and precedes the critical Glu residue. Notably, Cys substitution for γ1-I1606 made a greater impact on the integrin binding activity than that for γ1-K1608 (Fig. 22D), suggesting that the hydrophobic side chain of γ1-I1606 participates in integrin binding together with the carboxylate of γ1-E1607. Non-RGD ligands for α4- and α9-integrins as well as the internal ligands in αI domain-containing integrins often contain a hydrophobic residue that precedes the acidic residue critical for the β-MIDAS metal ion coordination (Fig. 27B). α4-integrins (i.e., α4β1 and α4β7 integrins) recognize an I/L-D-T/S motif located in a surface-exposed loop of vascular cell adhesion molecule-1 (VCAM-1) and mucosal addressin cell adhesion molecule-1 (MAdCAM-1) (*138, 139*) as well as a LDV motif in the alternatively spliced connecting III segment (IIICS) of fibronectin (*140, 141*). α9β1 integrin recognizes a D/E-X-ϕ-E motif, in which ϕ indicates a hydrophobic residue, in elastin microfibril interfacer protein (EMILIN)-1 (*142-144*), polydom (*145*), tenascin-C (*146*) and ADAM family proteases except for ADAM-10/17 (*147*). The αI domain in the collagen-type/leukocyte-specific integrins contains an invariant Glu residue in their C-terminal linker that binds to an interface between the β-propeller and the βI domains similar to the ligand binding of non-

αI domain integrins (Fig. 11E) (*129-131*). The α subunits of these integrins are associated with any one of the following β subunits: β1, β2 and β7 subunits (Fig. 7A). These β subunits constitute a major group in a phylogenetic tree of β subunits of integrins (Fig. 28A) (*148*). The ligand-binding grooves of integrin β2 (Fig. 28B) and β7 (Fig. 28C) contain a hydrophobic pocket-like depression formed by β1-α1/β2-β3/α2-α3 loops, similar to that of integrin β1 (Fig. 28D). Upon the coordination of E318 in the αX-I domain with the metal ion in the β2-MIDAS, the depression on the integrin β2 accommodates I317 in the C-terminal linker of the αX-I domain (Fig. 28E), indicating that the strength of the interaction between the internal ligand of the αX-I domain and the β2-I domain is increased by a burial of I317 in the hydrophobic depression of the ligand-binding groove of integrin β2 (*131*). Consistent with this scheme, small molecules that block the relay between the αI and βI domains require a hydrophobic moiety that precedes the free carboxyl group critical for binding to the integrin β2 (*149*). As is the case with the antagonist of the internal ligand of the αI domain, α4-integrin-targeted antagonists have been shown to contain an aliphatic/aromatic moiety adjacent to the carboxyl group that coordinates the β-MIDAS metal ion (*150-152*). Among these antagonists, the crystal structure of RO0505376 complexed with α4β7 integrin revealed how the antagonist binds to the β7-I domain at the atomic resolution

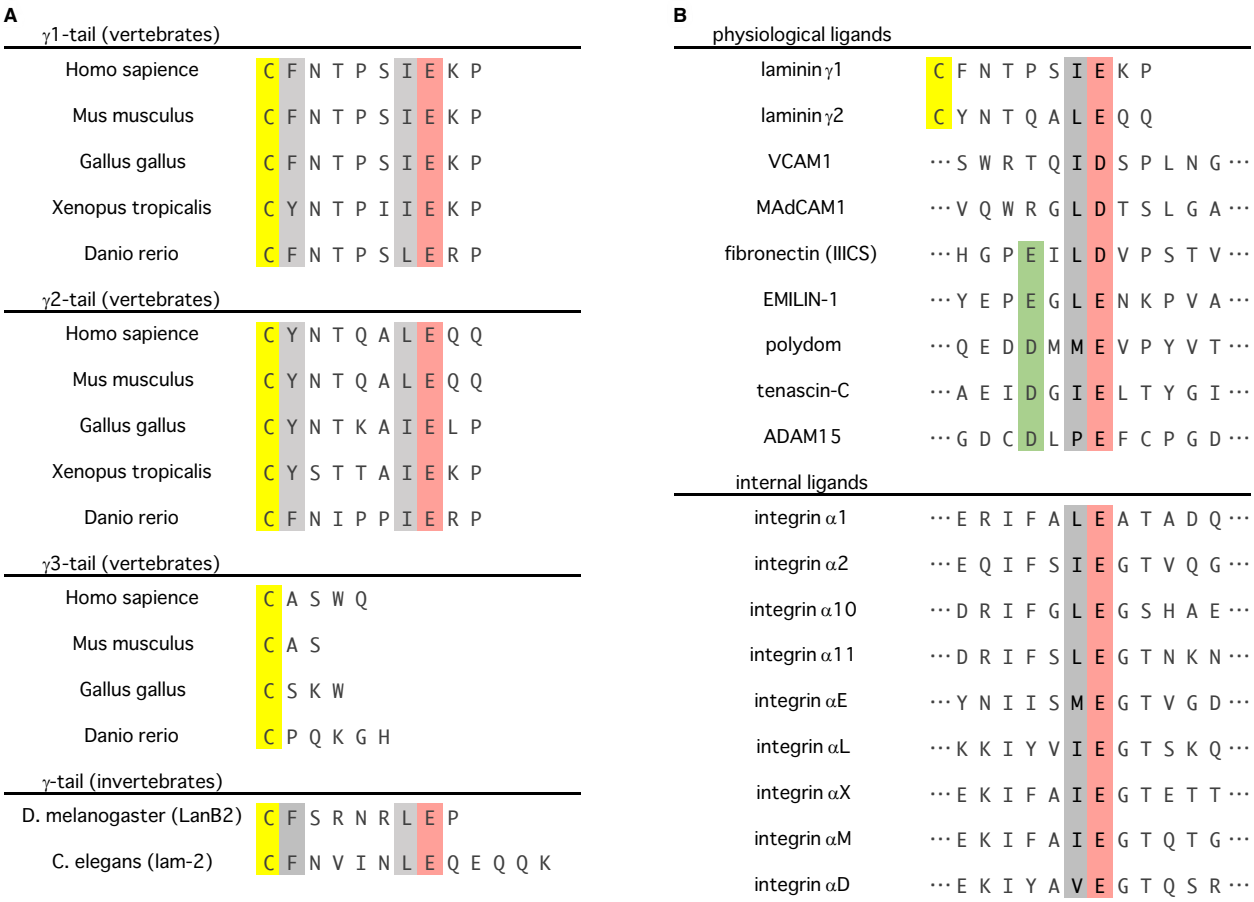

Fig. 27. Amino acid sequences of integrin recognition sites.

(**A**) Sequence alignment among the γ-tails of different species. (**B**) Sequence alignment of recognition site by integrin β subunits. The Cys residue cross-linked to laminin β chain is colored in yellow; conserved hydrophobic residues in grey; acidic residues essential for the ligand recognition by integrins in red.

(Fig. 28F) (*153*). As seen in the structure of the internal ligand-bound αXβ2 integrin, the amide-linked hydrophobic aromatic ring (dichlorobenzoyl) extends toward the pocket-like depression and is engaged in the hydrophobic interaction with the β7-I domain. Despite the lack of the structural information of α4-integrins

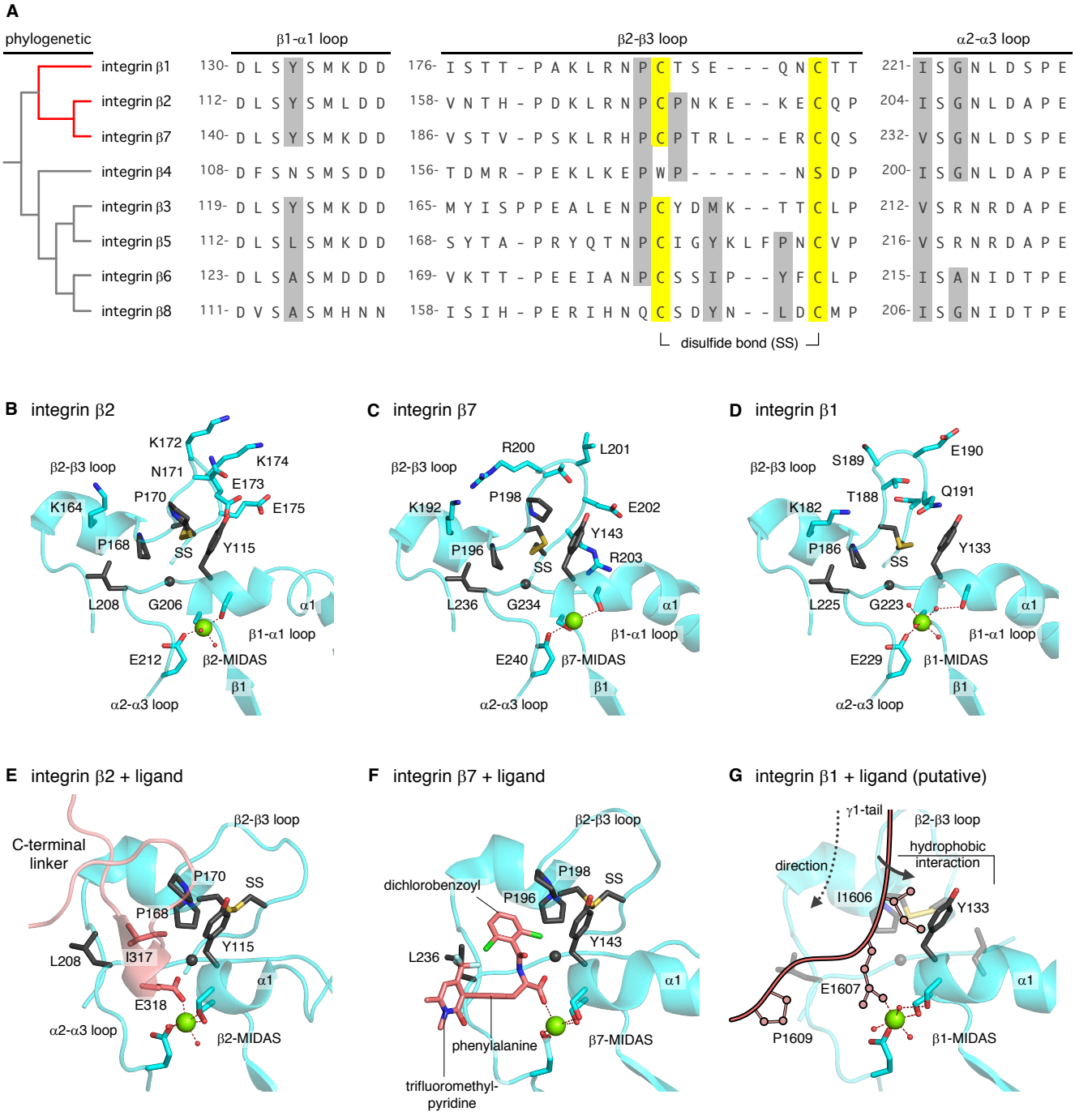

Fig. 28. Contribution of the hydrophobic residue to the ligand-integrin interaction.

(**A**) Phylogenetic tree for the amino acid sequences of the β1-α1/β2-β3/α2-α3 loops in the β-I domains. Hydrophobic residues and disulfide-linked Cys residues near the β-MIDAS are colored in grey and yellow, respectively. (**B-F**) Crystal structures of β2-I (**B, E**), β7-I (**C, F**), and β1-I domains (**D**) in the absence (**B-D**) or presence of ligands (**E**, **F**) (Protein Data Bank ID: 4NEH, 3V4V, 4WJK). Hydrophobic residues located near the metal ion (green sphere) are colored in grey. (**G**) A model for the γ1-tail binding to the β1-MIDAS.

complexed with physiological ligands, electron microscopic observations combined with docking simulations indicated that the key hydrophobic side chain of I39 that precedes D40 in VCAM-1 falls precisely in the position of the amide-linked hydrophobic aromatic ring of RO0505376 (*153*). Thus, it seems likely that γ1-I1606 directly interacts with the hydrophobic depression of integrin β1 (Fig. 28G).

The involvement of LG1–3 in laminin recognition by integrin

LMα5-null and integrin α3/α6-null mice share common developmental defects such as an absence of neural tube closure, a failure of digit separation, and an abnormality of lung morphology (*154*), indicating that LM511 engages α3/α6 integrins as specific receptors during embryonic development. Interestingly, Kikkawa *et al*. reported that a high level expression of LMα5 chimera, in which LG3–5 of LMα5 were replaced with the counterpart of LMα1, rescued multiple defects in LMα5-null mice and allowed to survive for several months, while a direct expression of another LMα5 chimera having LG1–5 of LMα1 could not complement the absence of the endogenous LMα5 expression (*155*). These observations raise the possibility that LG1–2 and the γ-tail comprise the minimum region for the recognition of LM511 by integrins. However, in vitro experiments revealed that recombinant LM511 mutant having LMα1's LG3 showed only marginal integrin binding activity (*89, 90*), suggesting that LG3 provides a structural integrity of active LG1–2 conformation and/or additional integrin recognition site(s) for retaining the integrin binding activity of LM511. Given the fact that LM511E8 binds to α6β1 integrin in a bottom-to-head manner (Fig. 22, A and B), it is conceivable that LG1–3 harbor an auxiliary integrin recognition site(s) at their bottom face that can complement the primary site involving the γ1-tail. Nishiuchi *et al*. previously reported that specificity and affinity of the laminin-integrin interactions depend on the combination of laminin α chain and integrin α subunit (*91*). Thus, LMα5-containing laminins (LM511/521) bind to α6β1 integrin with the highest affinity and to α3β1 and α7X1β1 integrins with moderate affinity, while the LMα1/α2-containing isoforms (LM111/121 and 211/221) bind preferentially to α7X2β1 integrin. Notably, the binding specificity of α7β1 integrin for laminins is determined by the alternatively spliced X1/X2 region of integrin α7 located between blades 3 and 4 in the β-propeller domain (Fig.29, A and B) (*156, 157*), suggesting that LG1–3 are recognized by the β-propeller domain of integrin α subunit. In addition to these findings, the present study provides a strong support for the involvement of LG1–3 in laminin recognition by integrins. The LM511E8 mutant lacking the C-terminal five residues of the γ1-tail competitively inhibited the binding of α6β1 integrin to LM511E8, albeit at a much higher concentration than intact LM511E8 (Fig. 26D). Furthermore, the exhaustive disulfide crosslink screening with Cys-substituted LM511E8s and α6β1 integrins showed that the γ1-tail came into close contact and cross-linked to integrin β1 residue 133 near the β1-MIDAS even after Gln substitution for γ1-E1607 (Fig. 24). These results suggest that the interaction of α6β1 integrin with the bottom face of LG1–3 brings the γ1-tail into close contact with the β1-MIDAS, thereby stabilizing the laminin-integrin complex through the coordination of γ1-E1607 with the metal ion in the β1-MIDAS (Fig. 29C). It is of note that, despite the absence of γ1-E1607, the inhibitory activity of LM511E8/Δγ1C5 was enhanced by addition of the activating anti-integrin β1 antibody TS2/16 (Fig. 26D, right). Recently, Su *et al*. demonstrated by electron microscopic examination of the complexes between α5β1 integrin and function-modulating antibodies that most activating integrin β1 antibodies perturb the conformational equilibrium by stabilizing

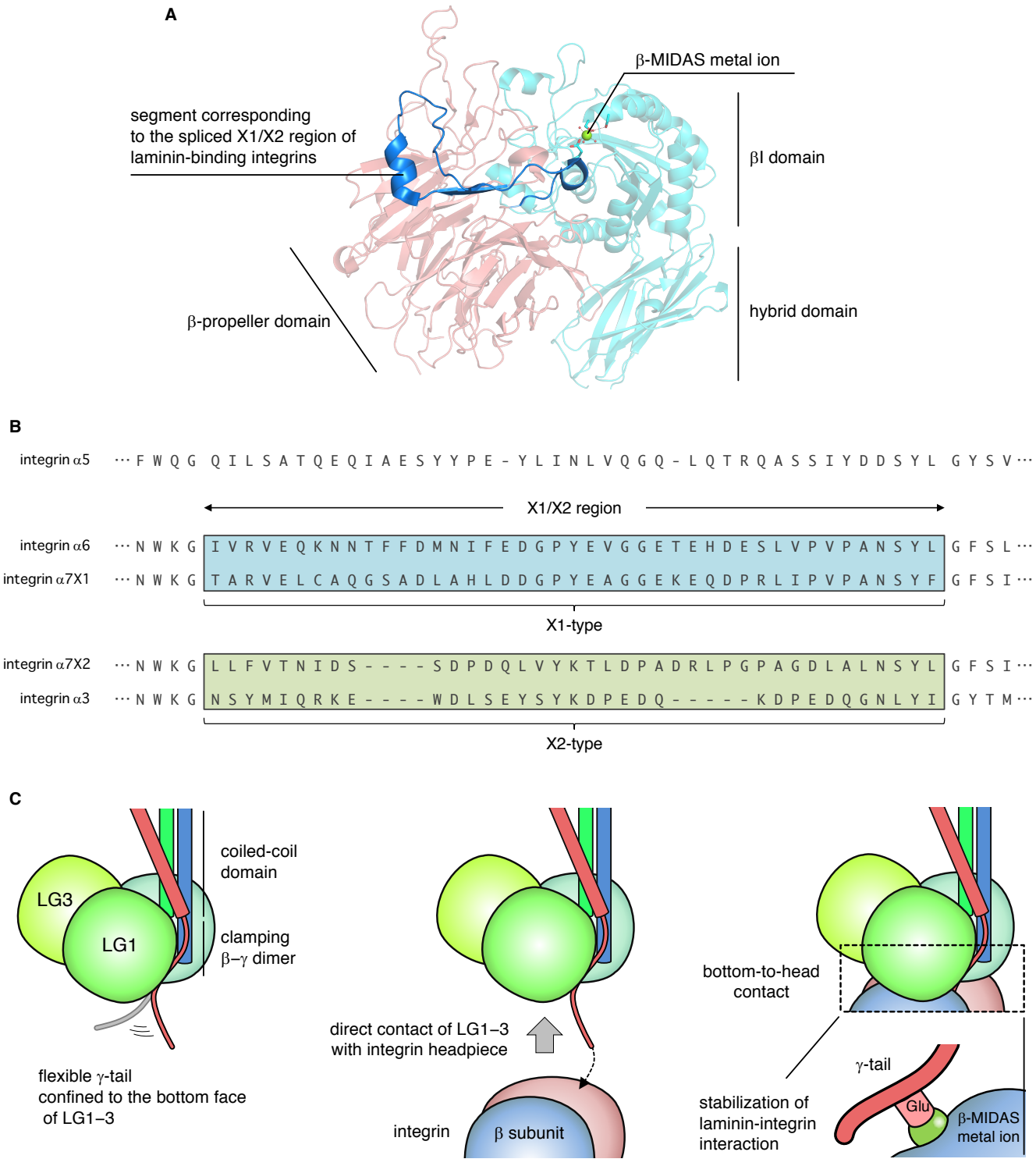

Fig. 29. Involvement of LG1–3 in laminin recognition by integrin

(**A**) The segment corresponding to the variable region of integrin α3, α6, and α7 subunits (blue) in the crystal structure of α5β1 integrin (Protein Data Bank ID: 4WJK). A metal ion in the β1-MIDAS is shown as green sphere. (**B**) Sequence alignment of the variable regions of integrin α3, α6, and α7 subunits and the corresponding region of integrin α5. X1 and X2-type variable regions are colored in blue and green, respectively. (**C**) Schematic model for the mechanism by which integrin recognizes laminin.

the extension of integrin's legs or the headpiece opening with the swing-out of the hybrid domain (*128*). However, the conformation of α5β1 integrin complexed with TS2/16 could not be distinguished from that of α5β1 integrin alone, suggesting that TS2/16 stabilizes a specific conformation of the β1-I domain in which only α1 helix moves, thereby eliciting the high-affinity ligand binding of α5β1 integrin. By analogy, the interaction of LG1–3 with α6β1 integrin is likely to be sensitive to a change in the conformation of the β1-I domain. It is generally accepted that a conformational change in the headpiece of integrin is induced by the ligand–β-MIDAS interaction (*104, 158, 159*). I propose a model in which LM511 interacts with α6β1 integrin through the following three steps: (i) a weak contact between LG1–3 and the headpiece of α6β1 integrin brings the γ1-tail into close contact with the β1-MIDAS; (ii) a coordination bond formed between γ1-E1607 and β1-MIDAS metal ion allosterically enhances the integrin binding by LG1–3 through a conformational change in the β1-I domain; (iii) LG1–3 allowed to stay on the integrin's headpiece ensures an intermittent coordination of γ1-E1607 with β1-MIDAS metal ion. Together, LG1–3 and the γ1-tail synergistically amplify their integrin binding activities, and achieve the high-affinity binding of LM511 by integrins. The identification of the residues within LG1–3 involved in integrin binding will provide an important clue to elucidate the role of LG1–3 in integrin recognition by laminins.

Functions of β chain as a structural support and an activity modulator for laminins

The LMβ1 helix is continuous all the way to the C-terminal β1-γ1 disulfide bond and most of it is engaged in the coiled-coil assembly with the helices of LMα5/LMγ1 (Figs. 14A and 16B). In the C-terminal segment of the LMβ1 helix, an aromatic ring of β1-Y1782, which is completely conserved in vertebrates (Fig. 30A), contributes to securing LG1 to the LMβ1 pillar and bringing the γ1-tail close to LG1–2 (Fig. 16D). In addition to the hydrophobic side chain, β1-S1776 and β1-S1783 are integrated into the hydrogen-bonded network among water molecules filling the gap between the β1-γ1 dimer and LG2, enabling LG2 to be apparently in contact with the LMβ1 pillar (Fig. 30B). These findings indicate that LMβ1 acts as a structural backbone supporting the ladle-shaped structure competent for integrin binding.

LMβ1 and LMβ2 exhibit high sequence homology and share the same domain structure (Fig. 2A). LMβ2 is abundantly distributed in glomerular BMs (GBMs) of the kidney and the neuromuscular junctions (NMJs) (*160, 161*). Gene ablation of LMβ2 in mice results in a progressive debility starting from postnatal day 7 (P7) and ultimately death between P15 and P30 due to a podocyte defect associated with a disorganization of GBMs and a paucity of active zones/junctional fold at the NMJs (*162-164*), suggesting that LMβ2 is required for postnatal maturation of the kidney GBMs and NMJs but not embryonic development. Taniguchi *et al*. reported that LMβ2-containing laminins (LM121/221/521) bound to α3β1/α7X2β1 integrins with higher affinity than LMβ1-containing laminins (LM111/211/511), whereas α6β1/α6β4/α7X1β1 integrins did not show any preference toward LMβ2-containing laminins (*132*). These findings are in good agreement with the fact that α3β1 integrin is dominantly expressed in podocytes that need to tightly adhere to LMβ2-abundant GBMs for maintaining the filtration barrier of glomeruli (*165*). Notably, Taniguchi *et al*. found that the LM511E8 chimera, in which C-terminal 22 residues of LMβ1 were replaced with the counterparts of LMβ2, showed high affinities for α3β1/α7X2β1 integrins compared with LM511E8 without compromising the binding activities

toward α6β1/α6β4/α7X1β1 integrins (*132*). The integrin α3 gene contains only the X2-like exon and has been classified an X2-type integrin along with integrin α7X2 (Fig. 29, A and B) (*166*). Thus, the C-terminal region of β2 chain has an ability to increase the binding affinity toward X2-type integrins. Interestingly, amino acid residues facing LG2 differ considerably between LMβ1 and LMβ2. LMβ2 has two Asn residues (β2-N1788/N1795) in place of two Ser residues in LMβ1 (β1-S1776/S1783) that participate in the hydrogen-bonded network formation for securing LG2 to the LMβ1 pillar (Fig. 30, A-C). In addition to these Asn residues, LMβ2 also contains two Gln residue (β2-Q1792/Q1798) corresponding to β1-A1780/L1786 (Fig. 30, A-C), raising the possibility that the presence of polar/bulky side chains at the interface between β chain and LG2 breaks the hydrogen-bonded network seen at the LMβ1-LG2 interface and changes the position of LG2 relative to the pillar of β chain (Fig. 30D). Furthermore, because of the topology of the LG2 adjacently connected to LG3 by a short linker segment, the distortion of the arrangement of LG1 and LG2 that clamp the β2-γ1 dimer causes an impact on the position of LG3 relative to LG1, resulting in distinct geometry of the integrin binding sites within LG1–3, thereby exerting strong influence on the preference toward X2-type integrins (Fig. 30D).

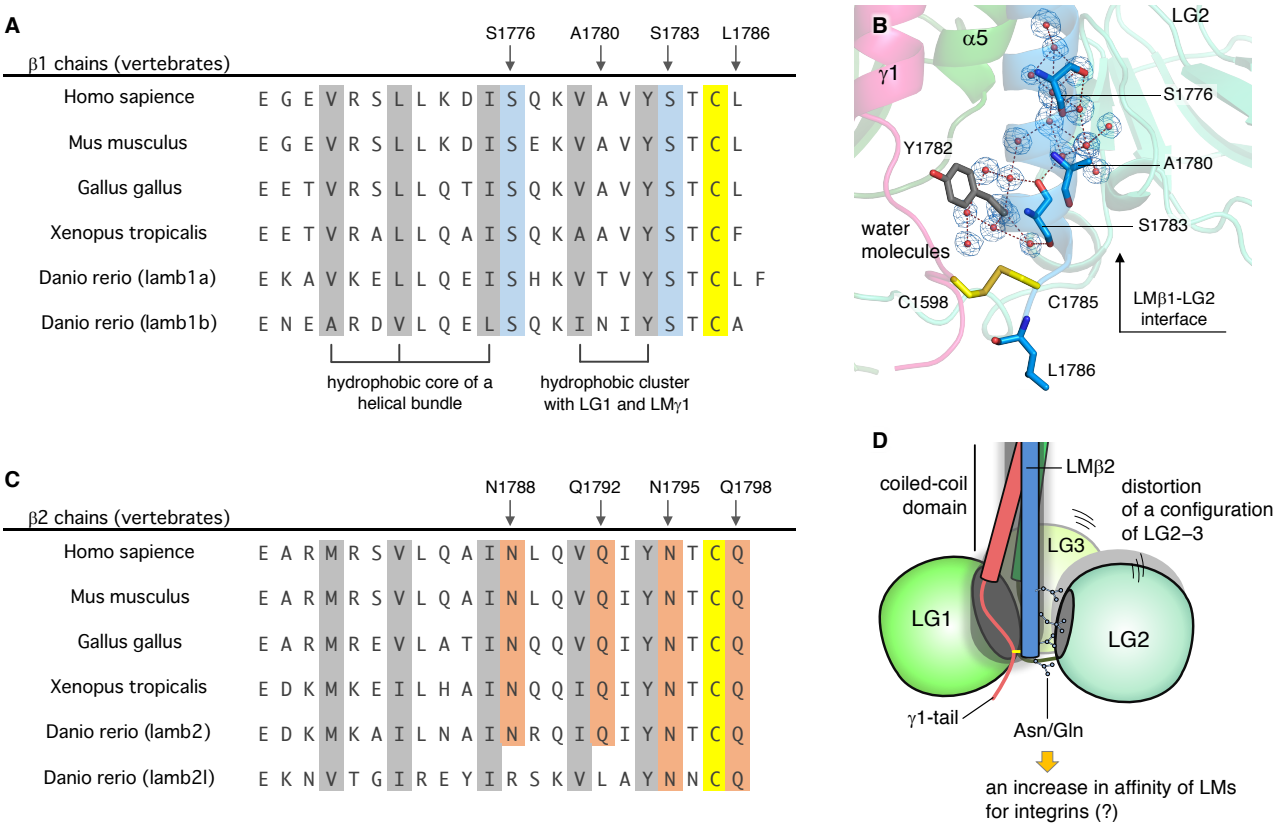

Fig. 30. Involvement of laminin β chain in laminin recognition by integrin.

(**A, B**) Sequence alignment among the C-terminal segments of LMβ1 (**A**) and LMβ2 (**B**) of different species. The Cys residue cross-linked to laminin γ chain is colored in yellow. Amino acid residues involved in the formation of the hydrophobic core and hydrogen bonded network are colored in grey and blue, respectively. Polar/bulky residues in LMβ2 assumed to face LG2 are colored in orange. (**C**) The interaction between LG2 and LMβ1 mediated by a layer of hydrogen-bonded water molecules. $2F_o$-F_c electron density map countered at 1.0 σ is shown as blue mesh around water molecules. (**D**) A model for the mechanism by which LMβ2 potentiates the binding affinity toward X2-type integrins.

Chapter 4: Conclusion

The present study addressed the long-standing question of how integrins recognize laminins. Laminins are the cell-adhesive proteins comprising BMs and regulate diverse cellular functions through the interaction with integrins. Among 16 laminin isoforms, I focused on LM511 which is the dominating laminin isoform in the embryonic BM and is ubiquitously distributed in the BMs maintaining the several types of tissues. Pluripotent stem cells express α6β1 integrin as a major integrin species, and hence the interaction of LM511 with α6β1 integrin has a significant impact on embryonic development as well as stem cell manipulation in vitro.

Understanding of the mechanism by which non-αI domain integrins recognize their ligands has been grown through the studies based on the interactions with RGD-containing ligands. Crystal structures of integrins complexed with the ligands or ligand mimetic peptides revealed that the carboxylate of the Asp residue in the RGD motif coordinates a metal ion in the MIDAS, thereby securing the integrin-ligand interaction. The acidic residues critical for the recognition by integrins have been identified in a number of non-RGD ligands, suggesting that a coordination bond between the integrin's MIDAS and a carboxylate from the ligand plays a central role in the integrin-ligand interaction. However, location of such acidic residues on laminins remains controversial. There are two candidate integrin-binding sites in laminins: one is LG1–3 and the other is the γ-tail. Previous studies found that the Glu residue in the γ-tail is required for integrin binding by laminins, although the current model for the laminin-integrin interaction assumes that the γ-tail is required for stabilizing the functionally active conformation of LG1–3.

The present study provides empirical support for the direct contribution of the γ1-tail to the recognition of LM511 by α6β1 integrin, employing (i) X-ray crystallography of the integrin binding site of LM511; (ii) comprehensive probing of the critical acidic residue within the integrin binding segment of LM511; (iii) exhaustive screening for intermolecular disulfide formation between the γ1-tail and the ligand binding site of the integrin β1 subunit; and (iv) the first discovery of a synthetic peptide derived from the γ1-tail capable of competing with the LM511-α6β1 integrin interaction. Four lines of evidence lead to the conclusion that the γ-tail directly interacts with the integrin's MIDAS, with the Glu residue in the γ-tail coordinating the metal ion. Furthermore, the additional finding that LM511E8 has integrin binding capability even after deletion of the Glu residue in the γ1-tail corroborates the scheme that the γ-tail comprises the bipartite integrin recognition site together with LG1–3.

There are still questions that need to be answered: 1) where is the integrin recognition site(s) within LG1–3 and 2) how do the three regions—LG1–3, the C-terminal segment of β chain, and the γ-tail—cooperatively achieve the integrin binding specificity and affinity of laminin isoforms. Answers to these questions will not only advance the understanding of the mechanistic basis of the integrin-mediated adhesion of cells to the BMs essential for tissue homeostasis and embryonic development but also promote the development of physiologically relevant scaffolds for manipulating stem cells in vitro.

Chapter 5: Materials and Methods

Antibodies and reagents

Horseradish peroxidase (HRP)-conjugated mouse anti-5×His monoclonal antibody (mAb) was from QIAGEN. Monoclonal ANTI-FLAG® M2 antibody was purchased from Sigma-Aldrich. HRP-conjugated mouse anti-c-Myc mAb (clone, 9E10) was purchased from Abcam. HRP-conjugated Rabbit polyclonal antibody (pAb) against the ACID/BASE coiled-coil region (designated Velcro) was produced by immunization with ACID/BASE coiled-coil peptides as described previously (*167*). The anti-Velcro pAb was biotinylated using EZ-Link™ Sulfo-NHS-Biotin reagents (Thermo Fisher Scientific) according to the manufacturer's instructions. mAb 5D6 against the human LMα5 was generated in our laboratory as described previously (*168*). mAb 4C7 against the LG of human LMα5 (*89, 169, 170*) was from Merck Millipore. Mouse immunoglobulin G (IgG) was from Thermo Fisher Scientific. The rabbit anti-actin pAb was purchased from Sigma-Aldrich. HRP-conjugated mouse anti-HA tag mAb (clone, HA-7) was from Sigma-Aldrich. HRP-conjugated goat anti-mouse IgG pAb and HRP-conjugated goat anti-human IgG Fc pAb were from Jackson ImmunoResearch. HRP-conjugated streptavidin was from Thermo Fisher Scientific. The mAb TS2/16 against human integrin β1 was purified on a Protein G Sepharose™ 4 Fast Flow column (GE Healthcare) from the conditioned media of hybridoma cells obtained from the American Type Culture Collection. Restriction enzymes Nhe I, Bam HI and Not I were obtained from New England BioLabs. AcTEV™ protease, which is an enhanced form of tobacco etch virus (TEV) protease, was purchased from Thermo Fisher Scientific. Human plasma fibronectin was purified as described previously (*171*). GRGDSP and GRGESP peptides were purchased from BACHEM. Synthetic peptides derived from the C-terminal 8 residues of human LMγ1, namely γ1C8 and γ1C8(EQ) were prepared as described previously (*93*). Synthetic peptides derived from the five C-terminal residues of the human LMγ1, namely γ1C5 and γ1C5(EQ), were purchased from Greiner Bio-One.

Construction of expression vectors

Expression vectors for recombinant E8 fragments of human LMα5, LMβ1, LMγ1, and mutant LMγ1 having a Gln substitution for γ1-E1607 (designated LMα5E8, LMβ1E8, LMγ1E8, and LMγ1E8/EQ) were prepared as described previously (*93*). 6×His, hemagglutinin (HA), and FLAG tags were added to the N termini of LMα5E8, LMβ1E8 and LMγ1E8, respectively. Thirty-three expression vectors for Ala-substituted LMα5E8 were kindly provided by Dr. Shaoliang Li, while nine expression vectors including #1 (D2752A), #2 (D2755A), #4 (E2778A/D2779A), #6 (D2801A), #16 (E2901A/D2903A), #18 (E2916A), #28 (E3044A), #29 (E3052A/D3054A/D3056A/E3058A), #38 (D3218A/D3219A) were generated by extension polymerase chain reaction (PCR). An expression vector for LMα5E8 in which the 6×His tag was replaced with a c-Myc tag was generated by extension PCR using 6×His tag-conjugated LMα5E8 expression vector as the template. Expression vectors for LMγ1E8/I1606C, LMγ1E8/I1606C/EQ, LMγ1E8/K1608C, and LMγ1E8/K1608C/EQ were generated by extension PCR using LMγ1E8 and LMγ1E8/EQ expression vectors as templates.

The pcDNA3.4+MCS vector was generated by inserting the multiple cloning site sequence derived from the expression vector pSecTag2A into the TOPO® cloning site of pcDNA3.4-TOPO® (Thermo Fisher

Scientific). Expression vectors for individual truncated E8 fragments of human LMα5, LMβ1, and LMγ1 (designated tLMα5E8, tLMβ1E8, and tLMγ1E8, respectively) were constructed as follows. Complementary DNAs encoding tLMα5E8 (E2655–A3327), tLMβ1E8 (D1714–L1786), and tLMγ1E8 (D1528–P1609) were amplified by PCR using individual E8 expression vectors as templates. The PCR products were digested with Nhe I and Not I, and then ligated into the Nhe I–Not I sites of pcDNA3.4+MCS. 6×His, HA, and FLAG tags, followed by a TEV protease recognition sequence, were added by extension PCR. The PCR products were digested with Nhe I and Not I, and then inserted into the corresponding restriction sites of pcDNA3.4+MCS. tLMα5E8/I2723C and tLMγ1E8/D1585C mutants were generated by extension PCR using tLMα5E8 and tLMγ1E8 expression vectors as the templates, respectively. The PCR products were digested with Nhe I/Not I and inserted into the corresponding restriction sites of pcDNA3.4+MCS.

An expression vector for the extracellular domain of human integrin α6 with C-terminal ACID peptide and FLAG tag sequences was prepared as described previously (*89*). An expression vector for the extracellular domain of human integrin β1 with a BASE peptide and a 6×His tag sequence at the C-terminus was prepared as described (*167*). Expression vectors for integrin β1 mutants, in which 19 residues located on the I-like domain were individually Cys-substituted, were kindly provided by Ms. Erika Yamashita and Yukimasa Taniguchi. The PCR products were digested with Bam HI/Not I and cloned into the same sites of the wild-type construct. All DNA sequences were verified using an ABI PRISM 3130xl Genetic Analyzer (Thermo Fisher Scientific).

Expression and purification of recombinant proteins

LM511E8 was transiently expressed in FreeStyle™ 293-F cells (Thermo Fisher Scientific) according to the manufacturer's instructions. Conditioned media were collected 72 h after transfection and loaded onto cOmplete™ His-Tag Purification Resin (Roche). The resin was washed with Hepes-buffered saline (HBS) (8.0) [20 mM Hepes and 137 mM NaCl (pH 8.0)], and bound protein was eluted with HBS (8.0) containing 250 mM imidazole. Fractions containing LM511E8 were further loaded onto DDDDK-tagged Protein Purification Gel (MBL). The resin was washed with HBS (7.4) (20 mM HEPES, 137 mM NaCl, pH 7.4), and the proteins were eluted with HBS (7.4) containing DDDDK peptide (100 μg/ml; MBL). Fractions containing LM511E8 were concentrated with an Amicon® Ultra-15 (Merck Millipore) and further purified on a Superdex™ 200 10/300 GL column (GE Healthcare) using HBS (7.4) as the running buffer.

tLM511E8 for crystallization was produced using FreeStyle™ 293-F cells and purified by affinity chromatography as for LM511E8. Fractions containing tLM511E8 were concentrated using an Amicon® Ultra-15 and digested with TEV protease (2000 U/ml) at 25°C for 24 hours. The reaction mixture was subjected to gel filtration on a Superdex™ 200 10/300 GL column using HBS (7.4) as the running buffer. Fractions containing TEV protease-treated tLM511E8 were concentrated with an Amicon® Ultra-2 (Merck Millipore) to ~30 mg/ml and stored at −80°C. Recombinant human α6β1 integrin was prepared as described previously (*93*). Intact α6β1 integrin for electron microscopic observation was prepared using the same expression system. The conditioned media were loaded onto ANTI-FLAG® M2 Affinity Gel (Sigma-Aldrich), and bound proteins were eluted with HBS (7.4) containing FLAG® peptide (100 μg/ml). Fractions containing α6β1 integrin were concentrated with an Amicon® Ultra-4 (Merck Millipore), and immediately subjected to gel filtration on a

Superdex™ 200 10/300 GL column using HBS (7.4) as the running buffer. Fractions containing α6β1 integrin were collected and stored at −80°C. Protein concentrations of all recombinant products were determined using a Pierce™ BCA Protein Assay Kit (Thermo Fisher Scientific) using bovine serum albumin (BSA) as the standard.

Solid-phase integrin binding assays

LM511E8 concentrations in conditioned media of transfected FreeStyle™ 293-F cells were determined by sandwich ELISA using anti-laminin α5 mAb 5D6. Briefly, mAb 5D6 was adsorbed onto 96-well microtiter plates (Thermo Fisher Scientific) at 1.2 μg/cm^2 overnight at 4°C. After blocking with tris-buffered saline (TBS) [20 mM tris and 137 mM NaCl (7.4)] containing 3% (w/v) BSA and 0.1% (v/v) Tween®-20, conditioned media were applied to the wells and incubated at room temperature for 1 hour. After washing with TBS containing 0.3% (w/v) BSA and 0.1% (v/v) Tween®-20 [W-buffer (0.1)], HRP-conjugated anti-HA mAb was allowed to react with captured LM511E8 at room temperature for 1hour. The amount of bound antibody was quantified by measuring the absorbance at 490 nm after incubation with *o*-phenylenediamine. A standard curve was plotted using four-parameter fitting.

Binding activities of α6β1 integrin to wild-type and mutant LM511E8s in conditioned media were measured by solid-phase binding assay as follows. mAb 5D6 was adsorbed onto 96-wel microtiter plates at 1.2 μg/cm^2 overnight at 4°C and then blocked with TBS containing 3% (w/v) BSA and 0.1% (v/v) Tween®-20 at room temperature for 1hour. For α6β1 integrin binding assay, conditioned media diluted to contain wild-type or mutant LM511E8 (0.63 nM) was allowed to react with the coated mAb 5D6 at room temperature for 1 hour. After three washes with TBS containing 1 mM $MnCl_2$, 0.3% (w/v) BSA, and 0.1% (v/v) Tween®-20 [Mn^{2+} buffer (0.1)], the plates were incubated with α6β1 integrin (30 nM) in Mn^{2+} buffer (0.1) at room temperature for 1 hour. Bound α6β1 integrin was detected after sequential incubations with biotinylated rabbit anti-Velcro pAb and HRP-conjugated streptavidin. The amount of bound α6β1 integrin was quantified by measuring the absorbance at 490 nm after incubation with *o*-phenylenediamine.

Binding activities of α6β1 integrin to purified wild-type and mutant LM511E8s including tLM511E8 and Cys-substituted LM511E8 were measured by solid-phase binding assays as follows. Wild-type or mutant LM511E8s were adsorbed onto 96-well microtiter plates at 10 nM overnight at 4°C and then blocked with TBS containing 3% (w/v) BSA and 0.02% (v/v) Tween®-20 at room temperature for 1 hour. The amounts of LM511E8s adsorbed on the plates were quantified with mAbs 5D6 and 4C7 to confirm the equality of the amounts of adsorbed proteins. After washing once with TBS containing 1 mM $MnCl_2$, 0.3% (w/v) BSA, and 0.02% (v/v) Tween®-20 [Mn^{2+} buffer (0.02)], the plates were incubated with serially diluted α6β1 integrin solution at room temperature for 3 hours in the presence of 1 mM $MnCl_2$ or 10 mM EDTA. After three washes with Mn^{2+} buffer (0.02) or TBS containing 10 mM EDTA, 0.3% BSA, and 0.02% Tween®-20, the plates were incubated with biotinylated rabbit anti-Velcro pAb (1.5 μg/ml) in Mn^{2+} buffer (0.02) at room temperature for 30 min. After three washes with Mn^{2+} buffer (0.02), the plates were incubated with streptavidin-HRP (0.53 μg/ml) for 15 min. After three washes with Mn^{2+} buffer (0.02), the amount of bound α6β1 integrin was

quantified by measuring the absorbance at 490 nm after incubation with *o*-phenylenediamine. The apparent dissociation constants were determined as described previously (*172*).

Cell lysate preparation

Forty-eight hours after transfection, FreeStyle™ 293-F cells were pelleted by centrifugation at 1,000 g at 4 °C for 5 min, washed with cold PBS, and repelleted. This was repeated three times. The pellet was lysed in a pre-cold buffer containing 1% (w/v) Triton X-100, 1% (w/v) sodium deoxy cholate, 0.1% (w/v) sodium dodecyl sulfate, 150 mM NaCl, 1 mM EDTA, 50 mM Tris-HCl (pH 7.5) and 1:2000 diluted Pefabloc SC (Roche). Lysates were centrifuged at 15,000 *g* at 4 °C for 30 min, and the protein concentrations of the clarified lysates were determined using Pierce™ BCA Protein Assay Kit (Thermo Fisher Scientific) using BSA as the standard. Equal protein amounts of the clarified lysates were subjected to SDS-PAGE and subsequent immunoblotting.

Electron microscopy and image processing of laminin-integrin complex

The LM511E8-α6β1 integrin complex was prepared and examined by electron microscopy by Dr. Yukimasa Taniguchi. The laminin-integrin complex was formed by mixing 200 pmol of purified LM511E8 and the same amount of purified α6β1 integrin at room temperature for 30 min in HBS (7.4) containing 1 mM $MnCl_2$. The complex was subjected to gel filtration on a Superose™ 6 10/300 GL column (GE Healthcare) preequilibrated with HBS containing 1 mM $MnCl_2$. The fractionated complex was incubated for 1 min at room temperature on glow-discharged carbon-coated grids (Nisshin EM). Samples were washed three times in ultrapure water containing 1 mM $MnCl_2$ and stained three times with 2% uranyl acetate for 30 s. After vacuum drying, grids were inspected with a Hitachi H-7650 transmission electron microscope operated at 80 kV.

Intermolecular disulfide bond formation between LM511E8 and α6β1 integrin

c-Myc–tagged LMα5E8 was used throughout the intermolecular disulfide formation assays. LM511E8/wild-type, LM511E8/I1606C, LM511E8/I1606C/EQ, LM511E8/K1608C, and LM511E8/K1608C/EQ were transiently coexpressed with wild-type or Cys-introduced α6β1 integrin using the FreeStyle™ 293 Expression System. Seventy-two hours after transfection, conditioned media were incubated with mAb 5D6 (1 μg/ml) at 4°C for 1 hour. Secreted laminin-integrin complexes were precipitated with Protein G Sepharose™ 4 Fast Flow (GE Healthcare). Immunoprecipitates were analyzed by SDS-PAGE under nonreducing conditions, followed by immunoblotting with anti-c-Myc mAb and anti-Velcro pAb.

Inhibition of α6β1 integrin binding to LM511E8

Wild-type LM511E8 was adsorbed onto 96-well microtiter plates at 10 nM overnight at 4°C and then blocked with 3% BSA at room temperature for 1 hour. Serially diluted synthetic peptide [γ1C5 or γ1C5(EQ)] or LM511E8 (wild-type or Δγ1C5) were incubated with α6β1 integrin (1 nM) in Mn^{2+} buffer (0.02) containing isotype control IgG or integrin β1 activating mAb TS2/16 (3 nM) at room temperature for 1 hour, then added to LM511E8-coated plates and allowed to bind to LM511E8 at room temperature for 1 hour. After three washes with Mn^{2+} buffer (0.02), the plates were incubated with biotinylated rabbit anti-Velcro pAb (1.5 μg/ml) in Mn^{2+}

buffer (0.02) at room temperature for 30 min. After three washes with Mn^{2+} buffer (0.02), the plates were incubated with streptavidin-HRP (0.53 μg/ml) for 15 min. After three washes with Mn^{2+} buffer (0.02), the amount of bound α6β1 integrin was quantified by measuring the absorbance at 490 nm after incubation with *o*-phenylenediamine. Half-maximal inhibitory concentration (IC_{50}) values were calculated using the equation

$$y = \frac{A - D}{1 + (x/C)^B} + D$$

where, "x" is peptide or LM511E8 concentration, "y" is activity (in percent) in the presence of inhibitors relative to the activity in the absence of inhibitors, "*A*" corresponds to the relative activity on the top plateau region of the curve, "*B*" corresponds to the slope, "*C*" corresponds to the inflection point of the curve, and "*D*" corresponds to the relative activity on the bottom plateau region of the curve. To obtain these four parameters, experimental raw data points were fitted to this equation using the "Curve Fitter" tool of ImageJ software (*173*). IC_{50} values were determined by substituting "$y = 50$" in the abovementioned equation.

Crystallization and diffraction data collection

Crystallization was performed at 20°C. Initial screening of crystallization conditions was performed using The Classics Neo Suite (QIAGEN). In this screen, a mosquito crystallization robot (TTP LabTech) was used to dispense 0.5 μl of protein solution mixed in a 1:1 ratio with the reservoir solution. Drops were equilibrated over 80 μl of reservoir solution using the sitting drop vapor diffusion method. The initial crystallization condition (0.2 M ammonium sulfate, 0.1 M sodium acetate, pH 4.6, and 25% polyethylene glycol 4000 at room temperature) was optimized using a 24-well crystallization plate with the hanging drop vapor diffusion method. Each well contained 500 μl of reservoir solution, and the drop volume was a mixture of 0.5 μl of protein solution and 0.5 μl of reservoir solution. Diffraction-quality crystals were obtained under conditions of 0.2 M ammonium sulfate, 0.1 M sodium acetate adjusted to pH 4.2 with acetic acid, and 19% polyethylene glycol 4000. Before X-ray diffraction experiments, crystals were soaked in reservoir solution containing an additional 20% glycerol and flash cooled in liquid nitrogen. The diffraction dataset for phasing was collected at BL-1A, Photon Factory (Tsukuba, Japan), and processed using the XDS package (*174*). In this data collection, three datasets of 720° each with the oscillation angle of 0.2° were merged. A higher resolution dataset for refinement was collected at BL44XU, SPring-8 (Hyogo, Japan), and processed using the HKL2000 package (*175*). The diffraction data statistics are shown in Table 1.

Structure determination

Solving the tLM511E8 structure was performed under the supervision of Drs. Yu Kitago and Takao Arimori. The crystal structure of tLM511E8 was solved by the single wavelength anomalous dispersion method using native crystals (S-SAD method). The coordinates of the substructure including the sulfur atoms and the calcium ion were determined using SHELXC and SHELXD (*176*). The phase calculation using these coordinates with phase improvement followed by automated initial model building was performed using the PHENIX program package (*177*). This initial model was then extended and refined by manual editing using COOT (*178*) with the

iterated implementation of refmac5 (*179*) on the higher resolution dataset. Finally, the crystal structure was refined to the R/R_{free} factors of 0.202/0.237 at a resolution of 1.80 Å validated with MOLPROBIDY (*180*). Refinement statistics are described in Table 1. All figures of the tLM511E8 model in this article were produced using PyMOL (www.pymol.org/).

List of reference sequences

name	species	RefSeq ID
laminin α1 chain	Homo sapience	NP_005550.2
laminin α2 chain	Homo sapience	NP_000417.2
laminin α3 chain	Homo sapience	NP_000218.3
laminin α4 chain	Homo sapience	NP_001098676.2
laminin α5 chain	Homo sapience	NP_0005551.3
laminin β1 chain	Homo sapience	XP_016867690.1
	Mus musculus	NP_032508.2
	Gallus gallus	XP_415943.3
	Xenopus tropicalis	XP_002933140.2
	Danio rerio (lamb1a)	NP_775382.1
	Danio rerio (lamb1b)	NP_001264059.1
laminin β2 chain	Homo sapience	NP_002283.3
	Mus musculus	NP_032509.2
	Gallus gallus	NP_989497.2
	Xenopus tropicalis	XP_004914156.1
	Danio rerio (lamb2)	NP_001229974.1
	Danio rerio (lamb2l)	XP_692838.6
laminin β3 chain	Homo sapience	NP_00219.2
	Mus musculus	NP_001264857.1
	Gallus gallus	XP_015154530.1
	Xenopus tropicalis	XP_012826649.1
	Danio rerio	XP_700808.6
laminin β chain (ancestal)	D. melanogaster (LanB1)	NP_476618.1
	C. elegans (lam-1)	XP_002165286.2
	Hydra vulgaris	XP_002168125.2
laminin γ1 chain	Homo sapience	NP_002284.3
	Mus musculus	NP_034813.2
	Gallus gallus	XP_001234659.2
	Xenopus tropicalis	NP_001090659.1
	Danio rerio	NP_775384.1
laminin γ2 chain	Homo sapience	NP_005553.2
	Mus musculus	NP_032511.3
	Gallus gallus	XP_015146029.1
	Xenopus tropicalis	XP_002937413.2
	Danio rerio	XP_003197932.2

name	species	RefSeq ID
laminin γ3chain	Homo sapience	NP_006050.3
	Mus musculus	NP_035966.2
	Gallus gallus	XP_415462
	Danio rerio	XP_687343.5
laminin γ chain (ancestal)	D. melanogaster (LanB2)	NP_524006.1
	C. elegans (lam-2)	NP_509204.3
α1 integrin	Homo sapience	NP_852478.1
α2 integrin	Homo sapience	NP_002194.2
α3 integrin	Homo sapience	NP_002195.1
α5 integrin	Homo sapience	NP_002196.4
α6 integrin	Homo sapience	NP_000201.2
α7X1 integrin	Homo sapience	NP_001138468.1
α7X2 integrin	Homo sapience	NP_002197.2
α10 integrin	Homo sapience	NP_001289969.1
α11 integrin	Homo sapience	NP_001004439.1
αE integrin	Homo sapience	NP_002199.3
αL integrin	Homo sapience	NP_001107852.1
αX integrin	Homo sapience	NP_000878.2
αM integrin	Homo sapience	NP_000623.2
αD integrin	Homo sapience	NP_001305114.1
β1 integrin	Homo sapience	NP_002202.2
β2 integrin	Homo sapience	NP_000202.3
β3 integrin	Homo sapience	NP_000203.2
β4 integrin	Homo sapience	NP_000204.3
β5 integrin	Homo sapience	NP_002204.2
β6 integrin	Homo sapience	NP_000879.2
β7 integrin	Homo sapience	NP_000880.1
β8 integrin	Homo sapience	NP_002205.1
VCAM1	Homo sapience	NP_001069.1
MAdCAM1	Homo sapience	NP_570116.2
fibronectin	Homo sapience	NP_997647.1
EMILIN-1	Homo sapience	NP_008977.1
polydom	Homo sapience	NP_699197.3
tenescin-C	Homo sapience	NP_002151.2
ADAM15	Homo sapience	NP_997074.1

Chapter 6: References

1. R. O. Hynes, The evolution of metazoan extracellular matrix. *J. Cell Biol.* **196**, 671-679 (2012).
2. R. Jayadev, D. R. Sherwood, Basement membranes. *Curr. Biol.* **27**, R207-R211 (2017).
3. P. D. Yurchenco, J. C. Schittny, Molecular architecture of basement membranes. *FASEB J.* **4**, 1577-1590 (1990).
4. F. L. Chan, S. Inoue, C. P. Leblond, The basement membranes of cryofixed or aldehyde-fixed, freeze-substituted tissues are composed of a lamina densa and do not contain a lamina lucida. *Cell Tissue Res.* **273**, 41-52 (1993).
5. F. L. Chan, S. Inoue, Lamina lucida of basement membrane: an artefact. *Microsc. Res. Tech.* **28**, 48-59 (1994).
6. R. Manabe, K. Tsutsui, T. Yamada, M. Kimura, I. Nakano, C. Shimono, N. Sanzen, Y. Furutani, T. Fukuda, Y. Oguri, K. Shimamoto, D. Kiyozumi, Y. Sato, Y. Sado, H. Senoo, S. Yamashina, S. Fukuda, J. Kawai, N. Sugiura, K. Kimata, Y. Hayashizaki, K. Sekiguchi, Transcriptome-based systematic identification of extracellular matrix proteins. *Proc. Natl. Acad. Sci. U.S.A.* **105**, 12849-12854 (2008).
7. P. D. Yurchenco, Basement membranes: cell scaffoldings and signaling platforms. *Cold Spring Harb. Perspect. Biol.* **3**, (2011).
8. E. Hohenester, P. D. Yurchenco, Laminins in basement membrane assembly. *Cell Adh. Migr.* **7**, 56-63 (2013).
9. P. D. Yurchenco, Y. S. Cheng, H. Colognato, Laminin forms an independent network in basement membranes. *J. Cell Biol.* **117**, 1119-1133 (1992).
10. E. Poschl, U. Schlotzer-Schrehardt, B. Brachvogel, K. Saito, Y. Ninomiya, U. Mayer, Collagen IV is essential for basement membrane stability but dispensable for initiation of its assembly during early development. *Development* **131**, 1619-1628 (2004).
11. I. Leivo, A. Vaheri, R. Timpl, J. Wartiovaara, Appearance and distribution of collagens and laminin in the early mouse embryo. *Dev. Biol.* **76**, 100-114 (1980).
12. J. Takagi, Y. Yang, J. H. Liu, J. H. Wang, T. A. Springer, Complex between nidogen and laminin fragments reveals a paradigmatic beta-propeller interface. *Nature* **424**, 969-974 (2003).
13. N. Gersdorff, E. Kohfeldt, T. Sasaki, R. Timpl, N. Miosge, Laminin gamma3 chain binds to nidogen and is located in murine basement membranes. *J. Biol. Chem.* **280**, 22146-22153 (2005).
14. M. Murshed, N. Smyth, N. Miosge, J. Karolat, T. Krieg, M. Paulsson, R. Nischt, The absence of nidogen 1 does not affect murine basement membrane formation. *Mol. Cell. Biol.* **20**, 7007-7012 (2000).
15. J. Schymeinsky, S. Nedbal, N. Miosge, E. Poschl, C. Rao, D. R. Beier, W. C. Skarnes, R. Timpl, B. L. Bader, Gene structure and functional analysis of the mouse nidogen-2 gene: nidogen-2 is not essential for basement membrane formation in mice. *Mol. Cell Biol.* **22**, 6820-6830 (2002).
16. M. Willem, N. Miosge, W. Halfter, N. Smyth, I. Jannetti, E. Burghart, R. Timpl, U. Mayer, Specific ablation of the nidogen-binding site in the laminin gamma1 chain interferes with kidney and lung development. *Development* **129**, 2711-2722 (2002).
17. B. L. Bader, N. Smyth, S. Nedbal, N. Miosge, A. Baranowsky, S. Mokkapati, M. Murshed, R. Nischt, Compound genetic ablation of nidogen 1 and 2 causes basement membrane defects and perinatal lethality in mice. *Mol. Cell. Biol.* **25**, 6846-6856 (2005).
18. K. Bose, R. Nischt, A. Page, B. L. Bader, M. Paulsson, N. Smyth, Loss of nidogen-1 and -2 results in syndactyly and changes in limb development. *J. Biol. Chem.* **281**, 39620-39629 (2006).
19. E. Arikawa-Hirasawa, H. Watanabe, H. Takami, J. R. Hassell, Y. Yamada, Perlecan is essential for cartilage and cephalic development. *Nat. Genet.* **23**, 354-358 (1999).
20. M. Costell, E. Gustafsson, A. Aszodi, M. Morgelin, W. Bloch, E. Hunziker, K. Addicks, R. Timpl, R. Fassler, Perlecan

maintains the integrity of cartilage and some basement membranes. *J. Cell Biol.* **147**, 1109-1122 (1999).

21. M. Hopf, W. Gohring, K. Mann, R. Timpl, Mapping of binding sites for nidogens, fibulin-2, fibronectin and heparin to different IG modules of perlecan. *J. Mol. Biol.* **311**, 529-541 (2001).
22. J. M. Whitelock, J. Melrose, R. V. Iozzo, Diverse cell signaling events modulated by perlecan. *Biochemistry* **47**, 11174-11183 (2008).
23. D. T. Behrens, D. Villone, M. Koch, G. Brunner, L. Sorokin, H. Robenek, L. Bruckner-Tuderman, P. Bruckner, U. Hansen, The epidermal basement membrane is a composite of separate laminin- or collagen IV-containing networks connected by aggregated perlecan, but not by nidogens. *J. Biol. Chem.* **287**, 18700-18709 (2012).
24. R. Timpl, H. Rohde, P. G. Robey, S. I. Rennard, J. M. Foidart, G. R. Martin, Laminin--a glycoprotein from basement membranes. *J. Biol. Chem.* **254**, 9933-9937 (1979).
25. M. Aumailley, L. Bruckner-Tuderman, W. G. Carter, R. Deutzmann, D. Edgar, P. Ekblom, J. Engel, E. Engvall, E. Hohenester, J. C. Jones, H. K. Kleinman, M. P. Marinkovich, G. R. Martin, U. Mayer, G. Meneguzzi, J. H. Miner, K. Miyazaki, M. Patarroyo, M. Paulsson, V. Quaranta, J. R. Sanes, T. Sasaki, K. Sekiguchi, L. M. Sorokin, J. F. Talts, K. Tryggvason, J. Uitto, I. Virtanen, K. von der Mark, U. M. Wewer, Y. Yamada, P. D. Yurchenco, A simplified laminin nomenclature. *Matrix Biol.* **24**, 326-332 (2005).
26. A. Domogatskaya, S. Rodin, K. Tryggvason, Functional diversity of laminins. *Annu. Rev. Cell Dev. Biol.* **28**, 523-553 (2012).
27. S. A. Nichols, W. Dirks, J. S. Pearse, N. King, Early evolution of animal cell signaling and adhesion genes. *Proc. Natl. Acad. Sci. U.S.A.* **103**, 12451-12456 (2006).
28. M. P. Sarras, Jr., L. Yan, A. Grens, X. Zhang, A. Agbas, J. K. Huff, P. L. St John, D. R. Abrahamson, Cloning and biological function of laminin in Hydra vulgaris. *Dev. Biol.* **164**, 312-324 (1994).
29. T. Sztal, S. Berger, P. D. Currie, T. E. Hall, Characterization of the laminin gene family and evolution in zebrafish. *Dev. Dyn.* **240**, 422-431 (2011).
30. Y. Miyagoe, K. Hanaoka, I. Nonaka, M. Hayasaka, Y. Nabeshima, K. Arahata, Y. Nabeshima, S. Takeda, Laminin alpha2 chain-null mutant mice by targeted disruption of the Lama2 gene: a new model of merosin (laminin 2)-deficient congenital muscular dystrophy. *FEBS Lett.* **415**, 33-39 (1997).
31. W. Kuang, H. Xu, P. H. Vachon, E. Engvall, Disruption of the lama2 gene in embryonic stem cells: laminin alpha 2 is necessary for sustenance of mature muscle cells. *Exp. Cell Res.* **241**, 117-125 (1998).
32. T. E. Hall, R. J. Bryson-Richardson, S. Berger, A. S. Jacoby, N. J. Cole, G. E. Hollway, J. Berger, P. D. Currie, The zebrafish candyfloss mutant implicates extracellular matrix adhesion failure in laminin alpha2-deficient congenital muscular dystrophy. *Proc. Natl. Acad. Sci. U.S.A.* **104**, 7092-7097 (2007).
33. A. E. Webb, J. Sanderford, D. Frank, W. S. Talbot, W. Driever, D. Kimelman, Laminin alpha5 is essential for the formation of the zebrafish fins. *Dev. Biol.* **311**, 369-382 (2007).
34. J. H. Miner, J. Cunningham, J. R. Sanes, Roles for laminin in embryogenesis: exencephaly, syndactyly, and placentopathy in mice lacking the laminin alpha5 chain. *J. Cell Biol.* **143**, 1713-1723 (1998).
35. J. H. Miner, P. D. Yurchenco, Laminin functions in tissue morphogenesis. *Annu. Rev. Cell Dev. Biol.* **20**, 255-284 (2004).
36. E. Klaffky, R. Williams, C. C. Yao, B. Ziober, R. Kramer, A. Sutherland, Trophoblast-specific expression and function of the integrin alpha 7 subunit in the peri-implantation mouse embryo. *Dev. Biol.* **239**, 161-175 (2001).
37. J. H. Miner, C. Li, J. L. Mudd, G. Go, A. E. Sutherland, Compositional and structural requirements for laminin and basement membranes during mouse embryo implantation and gastrulation. *Development* **131**, 2247-2256 (2004).
38. N. Smyth, H. S. Vatansever, M. Meyer, C. Frie, M. Paulsson, D. Edgar, The targeted deletion of the LAMC1 gene. *Annals of the New York Academy of Sciences* **857**, 283-286 (1998).
39. F. Alpy, I. Jivkov, L. Sorokin, A. Klein, C. Arnold, Y. Huss, M. Kedinger, P. Simon-Assmann, O. Lefebvre, Generation

of a conditionally null allele of the laminin alpha1 gene. *Genesis* **43**, 59-70 (2005).

40. J. H. Miner, C. Li, Defective glomerulogenesis in the absence of laminin alpha5 demonstrates a developmental role for the kidney glomerular basement membrane. *Dev Biol* **217**, 278-289 (2000).
41. N. M. Nguyen, D. G. Kelley, J. A. Schlueter, M. J. Meyer, R. M. Senior, J. H. Miner, Epithelial laminin alpha5 is necessary for distal epithelial cell maturation, VEGF production, and alveolization in the developing murine lung. *Dev Biol* **282**, 111-125 (2005).
42. P. Murray, D. Edgar, Regulation of programmed cell death by basement membranes in embryonic development. *J. Cell Biol.* **150**, 1215-1221 (2000).
43. S. Li, D. Harrison, S. Carbonetto, R. Fassler, N. Smyth, D. Edgar, P. D. Yurchenco, Matrix assembly, regulation, and survival functions of laminin and its receptors in embryonic stem cell differentiation. *J. Cell. Biol.* **157**, 1279-1290 (2002).
44. H. Fujiwara, Y. Hayashi, N. Sanzen, R. Kobayashi, C. N. Weber, T. Emoto, S. Futaki, H. Niwa, P. Murray, D. Edgar, K. Sekiguchi, Regulation of mesodermal differentiation of mouse embryonic stem cells by basement membranes. *J. Biol. Chem.* **282**, 29701-29711 (2007).
45. J. H. Miner, Renal basement membrane components. *Kidney Int.* **56**, 2016-2024 (1999).
46. Y. Kikkawa, Y. Mochizuki, J. H. Miner, T. Mitaka, Transient expression of laminin alpha1 chain in regenerating murine liver: restricted localization of laminin chains and nidogen-1. *Exp. Cell Res.* **305**, 99-109 (2005).
47. M. Aumailley, The laminin family. *Cell Adh. Migr.* **7**, 48-55 (2013).
48. J. Holmberg, M. Durbeej, Laminin-211 in skeletal muscle function. *Cell Adh. Migr.* **7**, 111-121 (2013).
49. L. F. Yousif, J. Di Russo, L. Sorokin, Laminin isoforms in endothelial and perivascular basement membranes. *Cell Adh. Migr.* **7**, 101-110 (2013).
50. P. Rousselle, K. Beck, Laminin 332 processing impacts cellular behavior. *Cell Adh. Migr.* **7**, 122-134 (2013).
51. U. Ott, E. Odermatt, J. Engel, H. Furthmayr, R. Timpl, Protease resistance and conformation of laminin. *Eur. J. Biochem.* **123**, 63-72 (1982).
52. D. T. Woodley, C. N. Rao, J. R. Hassell, L. A. Liotta, G. R. Martin, H. K. Kleinman, Interactions of basement membrane components. *Biochim. Biophys. Acta* **761**, 278-283 (1983).
53. J. Engel, E. Odermatt, A. Engel, J. A. Madri, H. Furthmayr, H. Rohde, R. Timpl, Shapes, domain organizations and flexibility of laminin and fibronectin, two multifunctional proteins of the extracellular matrix. *J. Mol. Biol.* **150**, 97-120 (1981).
54. K. Beck, I. Hunter, J. Engel, Structure and function of laminin: anatomy of a multidomain glycoprotein. *FASEB J.* **4**, 148-160 (1990).
55. M. Bruch, R. Landwehr, J. Engel, Dissection of laminin by cathepsin G into its long-arm and short-arm structures and localization of regions involved in calcium dependent stabilization and self-association. *Eur. J. Biochem.* **185**, 271-279 (1989).
56. J. C. Schittny, P. D. Yurchenco, Terminal short arm domains of basement membrane laminin are critical for its self-assembly. *J. Cell Biol.* **110**, 825-832 (1990).
57. P. D. Yurchenco, Y. S. Cheng, Self-assembly and calcium-binding sites in laminin. A three-arm interaction model. *J. Biol. Chem.* **268**, 17286-17299 (1993).
58. K. K. McKee, D. Harrison, S. Capizzi, P. D. Yurchenco, Role of laminin terminal globular domains in basement membrane assembly. *J. Biol. Chem.* **282**, 21437-21447 (2007).
59. H. Xu, X. R. Wu, U. M. Wewer, E. Engvall, Murine muscular dystrophy caused by a mutation in the laminin alpha 2 (Lama2) gene. *Nat. Genet.* **8**, 297-302 (1994).
60. H. Colognato, P. D. Yurchenco, The laminin alpha2 expressed by dystrophic dy(2J) mice is defective in its ability to

form polymers. *Curr. Biol.* **9**, 1327-1330 (1999).

61. U. Odenthal, S. Haehn, P. Tunggal, B. Merkl, D. Schomburg, C. Frie, M. Paulsson, N. Smyth, Molecular analysis of laminin N-terminal domains mediating self-interactions. *J. Biol. Chem.* **279**, 44504-44512 (2004).
62. A. Purvis, E. Hohenester, Laminin network formation studied by reconstitution of ternary nodes in solution. *J. Biol. Chem.* **287**, 44270-44277 (2012).
63. S. A. Hussain, F. Carafoli, E. Hohenester, Determinants of laminin polymerization revealed by the structure of the alpha5 chain amino-terminal region. *EMBO Rep.* **12**, 276-282 (2011).
64. F. Carafoli, S. A. Hussain, E. Hohenester, Crystal structures of the network-forming short-arm tips of the laminin beta1 and gamma1 chains. *PLoS One* **7**, e42473 (2012).
65. I. Hunter, T. Schulthess, M. Bruch, K. Beck, J. Engel, Evidence for a specific mechanism of laminin assembly. *Eur. J. Biochem.* **188**, 205-211 (1990).
66. J. Engel, I. Hunter, T. Schulthess, K. Beck, T. W. Dixon, D. A. Parry, Assembly of laminin isoforms by triple- and double-stranded coiled-coil structures. *Biochem. Soc. Trans.* **19**, 839-843 (1991).
67. I. Hunter, T. Schulthess, J. Engel, Laminin chain assembly by triple and double stranded coiled-coil structures. *J. Biol. Chem.* **267**, 6006-6011 (1992).
68. A. Morita, E. Sugimoto, Y. Kitagawa, Post-translational assembly and glycosylation of laminin subunits in parietal endoderm-like F9 cells. *Biochem. J.* **229**, 259-264 (1985).
69. B. P. Peters, R. J. Hartle, R. F. Krzesicki, T. G. Kroll, F. Perini, J. E. Balun, I. J. Goldstein, R. W. Ruddon, The biosynthesis, processing, and secretion of laminin by human choriocarcinoma cells. *J. Biol. Chem.* **260**, 14732-14742 (1985).
70. A. Utani, M. Nomizu, R. Timpl, P. P. Roller, Y. Yamada, Laminin chain assembly. Specific sequences at the C terminus of the long arm are required for the formation of specific double- and triple-stranded coiled-coil structures. *J. Biol. Chem.* **269**, 19167-19175 (1994).
71. A. Utani, M. Nomizu, S. Sugiyama, S. Miyamoto, P. P. Roller, Y. Yamada, A specific sequence of the laminin alpha 2 chain critical for the initiation of heterotrimer assembly. *J. Biol. Chem.* **270**, 3292-3298 (1995).
72. M. Nomizu, A. Otaka, A. Utani, P. P. Roller, Y. Yamada, Assembly of synthetic laminin peptides into a triple-stranded coiled-coil structure. *J. Biol. Chem.* **269**, 30386-30392 (1994).
73. K. Beck, T. W. Dixon, J. Engel, D. A. Parry, Ionic interactions in the coiled-coil domain of laminin determine the specificity of chain assembly. *J. Mol. Biol.* **231**, 311-323 (1993).
74. P. R. Macdonald, A. Lustig, M. O. Steinmetz, R. A. Kammerer, Laminin chain assembly is regulated by specific coiled-coil interactions. *J. Struct. Biol.* **170**, 398-405 (2010).
75. R. A. Kammerer, P. Antonsson, T. Schulthess, C. Fauser, J. Engel, Selective chain recognition in the C-terminal alpha-helical coiled-coil region of laminin. *J. Mol. Biol.* **250**, 64-73 (1995).
76. M. Nomizu, A. Utani, K. Beck, A. Otaka, P. P. Roller, Y. Yamada, Mechanism of laminin chain assembly into a triple-stranded coiled-coil structure. *Biochemistry* **35**, 2885-2893 (1996).
77. M. Aumailley, R. Timpl, A. Sonnenberg, Antibody to integrin alpha 6 subunit specifically inhibits cell-binding to laminin fragment 8. *Exp. Cell Res.* **188**, 55-60 (1990).
78. V. Nurcombe, M. Aumailley, R. Timpl, D. Edgar, The high-affinity binding of laminin to cells. Assignation of a major cell-binding site to the long arm of laminin and of a latent cell-binding site to its short arms. *Eur. J. Biochem.* **180**, 9-14 (1989).
79. M. Aumailley, M. Gerl, A. Sonnenberg, R. Deutzmann, R. Timpl, Identification of the Arg-Gly-Asp sequence in laminin A chain as a latent cell-binding site being exposed in fragment P1. *FEBS Lett.* **262**, 82-86 (1990).
80. J. F. Talts, Z. Andac, W. Gohring, A. Brancaccio, R. Timpl, Binding of the G domains of laminin alpha1 and alpha2

chains and perlecan to heparin, sulfatides, alpha-dystroglycan and several extracellular matrix proteins. *EMBO J.* **18**, 863-870 (1999).

81. R. Barresi, K. P. Campbell, Dystroglycan: from biosynthesis to pathogenesis of human disease. *J. Cell Sci.* **119**, 199-207 (2006).
82. A. Brancaccio, T. Schulthess, M. Gesemann, J. Engel, Electron microscopic evidence for a mucin-like region in chick muscle alpha-dystroglycan. *FEBS Lett.* **368**, 139-142 (1995).
83. A. Brancaccio, T. Schulthess, M. Gesemann, J. Engel, The N-terminal region of alpha-dystroglycan is an autonomous globular domain. *Eur. J. Biochem.* **246**, 166-172 (1997).
84. M. O. Sheikh, S. M. Halmo, L. Wells, Recent advancements in understanding mammalian O-mannosylation. *Glycobiology* **27**, 806-819 (2017).
85. D. Tisi, J. F. Talts, R. Timpl, E. Hohenester, Structure of the C-terminal laminin G-like domain pair of the laminin alpha2 chain harbouring binding sites for alpha-dystroglycan and heparin. *EMBO J.* **19**, 1432-1440 (2000).
86. D. Harrison, S. A. Hussain, A. C. Combs, J. M. Ervasti, P. D. Yurchenco, E. Hohenester, Crystal structure and cell surface anchorage sites of laminin alpha1LG4-5. *J. Biol. Chem.* **282**, 11573-11581 (2007).
87. D. C. Briggs, T. Yoshida-Moriguchi, T. Zheng, D. Venzke, M. E. Anderson, A. Strazzulli, M. Moracci, L. Yu, E. Hohenester, K. P. Campbell, Structural basis of laminin binding to the LARGE glycans on dystroglycan. *Nat. Chem. Biol.* **12**, 810-814 (2016).
88. H. Ido, K. Harada, S. Futaki, Y. Hayashi, R. Nishiuchi, Y. Natsuka, S. Li, Y. Wada, A. C. Combs, J. M. Ervasti, K. Sekiguchi, Molecular dissection of the alpha-dystroglycan- and integrin-binding sites within the globular domain of human laminin-10. *J. Biol. Chem.* **279**, 10946-10954 (2004).
89. H. Ido, K. Harada, Y. Yagi, K. Sekiguchi, Probing the integrin-binding site within the globular domain of laminin-511 with the function-blocking monoclonal antibody 4C7. *Matrix Biol.* **25**, 112-117 (2006).
90. Y. Kikkawa, T. Sasaki, M. T. Nguyen, M. Nomizu, T. Mitaka, J. H. Miner, The LG1-3 tandem of laminin alpha5 harbors the binding sites of Lutheran/basal cell adhesion molecule and alpha3beta1/alpha6beta1 integrins. *J. Biol. Chem.* **282**, 14853-14860 (2007).
91. R. Nishiuchi, J. Takagi, M. Hayashi, H. Ido, Y. Yagi, N. Sanzen, T. Tsuji, M. Yamada, K. Sekiguchi, Ligand-binding specificities of laminin-binding integrins: a comprehensive survey of laminin-integrin interactions using recombinant alpha3beta1, alpha6beta1, alpha7beta1 and alpha6beta4 integrins. *Matrix Biol.* **25**, 189-197 (2006).
92. F. Carafoli, N. J. Clout, E. Hohenester, Crystal structure of the LG1-3 region of the laminin alpha2 chain. *J. Biol. Chem.* **284**, 22786-22792 (2009).
93. H. Ido, A. Nakamura, R. Kobayashi, S. Ito, S. Li, S. Futaki, K. Sekiguchi, The requirement of the glutamic acid residue at the third position from the carboxyl termini of the laminin gamma chains in integrin binding by laminins. *J. Biol. Chem.* **282**, 11144-11154 (2007).
94. H. Ido, S. Ito, Y. Taniguchi, M. Hayashi, R. Sato-Nishiuchi, N. Sanzen, Y. Hayashi, S. Futaki, K. Sekiguchi, Laminin isoforms containing the gamma3 chain are unable to bind to integrins due to the absence of the glutamic acid residue conserved in the C-terminal regions of the gamma1 and gamma2 chains. *J. Biol. Chem.* **283**, 28149-28157 (2008).
95. A. Navdaev, V. Heitmann, K. Desantana Evangelista, M. Morgelin, J. Wegener, J. A. Eble, The C-terminus of the gamma 2 chain but not of the beta 3 chain of laminin-332 is indirectly but indispensably necessary for integrin-mediated cell reactions. *Exp. Cell Res.* **314**, 489-497 (2008).
96. R. O. Hynes, Integrins: bidirectional, allosteric signaling machines. *Cell* **110**, 673-687 (2002).
97. T. Miyazaki, S. Futaki, K. Hasegawa, M. Kawasaki, N. Sanzen, M. Hayashi, E. Kawase, K. Sekiguchi, N. Nakatsuji, H. Suemori, Recombinant human laminin isoforms can support the undifferentiated growth of human embryonic stem cells. *Biochem. Biophys. Res. Commun.* **375**, 27-32 (2008).

98. T. Miyazaki, S. Futaki, H. Suemori, Y. Taniguchi, M. Yamada, M. Kawasaki, M. Hayashi, H. Kumagai, N. Nakatsuji, K. Sekiguchi, E. Kawase, Laminin E8 fragments support efficient adhesion and expansion of dissociated human pluripotent stem cells. *Nat. Commun.* **3**, 1236 (2012).

99. S. Rodin, L. Antonsson, C. Niaudet, O. E. Simonson, E. Salmela, E. M. Hansson, A. Domogatskaya, Z. Xiao, P. Damdimopoulou, M. Sheikhi, J. Inzunza, A. S. Nilsson, D. Baker, R. Kuiper, Y. Sun, E. Blennow, M. Nordenskjold, K. H. Grinnemo, J. Kere, C. Betsholtz, O. Hovatta, K. Tryggvason, Clonal culturing of human embryonic stem cells on laminin-521/E-cadherin matrix in defined and xeno-free environment. *Nat. Commun.* **5**, 3195 (2014).

100. J. P. Xiong, T. Stehle, B. Diefenbach, R. Zhang, R. Dunker, D. L. Scott, A. Joachimiak, S. L. Goodman, M. A. Arnaout, Crystal structure of the extracellular segment of integrin alpha Vbeta3. *Science* **294**, 339-345 (2001).

101. N. A. Carrell, L. A. Fitzgerald, B. Steiner, H. P. Erickson, D. R. Phillips, Structure of human platelet membrane glycoproteins IIb and IIIa as determined by electron microscopy. *J. Biol. Chem.* **260**, 1743-1749 (1985).

102. T. Kelly, L. Molony, K. Burridge, Purification of two smooth muscle glycoproteins related to integrin. Distribution in cultured chicken embryo fibroblasts. *J. Biol. Chem.* **262**, 17189-17199 (1987).

103. M. V. Nermut, N. M. Green, P. Eason, S. S. Yamada, K. M. Yamada, Electron microscopy and structural model of human fibronectin receptor. *EMBO J.* **7**, 4093-4099 (1988).

104. J. Takagi, B. M. Petre, T. Walz, T. A. Springer, Global conformational rearrangements in integrin extracellular domains in outside-in and inside-out signaling. *Cell* **110**, 599-511 (2002).

105. C. K. Miranti, J. S. Brugge, Sensing the environment: a historical perspective on integrin signal transduction. *Nat. Cell. Biol.* **4**, E83-90 (2002).

106. C. Brakebusch, R. Fassler, The integrin-actin connection, an eternal love affair. *EMBO J.* **22**, 2324-2333 (2003).

107. J. O. Lee, L. A. Bankston, M. A. Arnaout, R. C. Liddington, Two conformations of the integrin A-domain (I-domain): a pathway for activation? *Structure* **3**, 1333-1340 (1995).

108. T. Xiao, J. Takagi, B. S. Coller, J. H. Wang, T. A. Springer, Structural basis for allostery in integrins and binding to fibrinogen-mimetic therapeutics. *Nature* **432**, 59-67 (2004).

109. J. Takagi, Structural basis for ligand recognition by integrins. *Curr. Opin. Cell Biol.* **19**, 557-564 (2007).

110. B. H. Luo, C. V. Carman, T. A. Springer, Structural basis of integrin regulation and signaling. *Annu. Rev. Immunol.* **25**, 619-647 (2007).

111. J. O. Lee, P. Rieu, M. A. Arnaout, R. Liddington, Crystal structure of the A domain from the alpha subunit of integrin CR3 (CD11b/CD18). *Cell* **80**, 631-638 (1995).

112. J. Emsley, C. G. Knight, R. W. Farndale, M. J. Barnes, R. C. Liddington, Structural basis of collagen recognition by integrin alpha2beta1. *Cell* **101**, 47-56 (2000).

113. M. Shimaoka, T. Xiao, J. H. Liu, Y. Yang, Y. Dong, C. D. Jun, A. McCormack, R. Zhang, A. Joachimiak, J. Takagi, J. H. Wang, T. A. Springer, Structures of the alpha L I domain and its complex with ICAM-1 reveal a shape-shifting pathway for integrin regulation. *Cell* **112**, 99-111 (2003).

114. C. G. Knight, L. F. Morton, D. J. Onley, A. R. Peachey, A. J. Messent, P. A. Smethurst, D. S. Tuckwell, R. W. Farndale, M. J. Barnes, Identification in collagen type I of an integrin alpha2 beta1-binding site containing an essential GER sequence. *J. Biol. Chem.* **273**, 33287-33294 (1998).

115. J. Kallen, K. Welzenbach, P. Ramage, D. Geyl, R. Kriwacki, G. Legge, S. Cottens, G. Weitz-Schmidt, U. Hommel, Structural basis for LFA-1 inhibition upon lovastatin binding to the CD11a I-domain. *J. Mol Biol.* **292**, 1-9 (1999).

116. G. Liu, J. R. Huth, E. T. Olejniczak, R. Mendoza, P. DeVries, S. Leitza, E. B. Reilly, G. F. Okasinski, S. W. Fesik, T. W. von Geldern, Novel p-arylthio cinnamides as antagonists of leukocyte function-associated antigen-1/intracellular adhesion molecule-1 interaction. 2. Mechanism of inhibition and structure-based improvement of pharmaceutical properties. *J. Med. Chem.* **44**, 1202-1210 (2001).

117. K. Last-Barney, W. Davidson, M. Cardozo, L. L. Frye, C. A. Grygon, J. L. Hopkins, D. D. Jeanfavre, S. Pav, C. Qian, J. M. Stevenson, L. Tong, R. Zindell, T. A. Kelly, Binding site elucidation of hydantoin-based antagonists of LFA-1 using multidisciplinary technologies: evidence for the allosteric inhibition of a protein--protein interaction. *J. Am. Chem. Soc.* **123**, 5643-5650 (2001).

118. J. P. Xiong, T. Stehle, R. Zhang, A. Joachimiak, M. Frech, S. L. Goodman, M. A. Arnaout, Crystal structure of the extracellular segment of integrin alpha Vbeta3 in complex with an Arg-Gly-Asp ligand. *Science* **296**, 151-155 (2002).

119. R. O. Hynes, A. T. Destree, D. D. Wagner, Relationships between microfilaments, cell-substratum adhesion, and fibronectin. *Cold Spring Harb. Symp. Quant. Biol.* **46 Pt 2**, 659-670 (1982).

120. M. D. Pierschbacher, E. Ruoslahti, Variants of the cell recognition site of fibronectin that retain attachment-promoting activity. *Proc. Natl. Acad. Sci. U.S.A.* **81**, 5985-5988 (1984).

121. J. Takagi, K. Strokovich, T. A. Springer, T. Walz, Structure of integrin alpha5beta1 in complex with fibronectin. *EMBO J.* **22**, 4607-4615 (2003).

122. J. Zhu, B. H. Luo, T. Xiao, C. Zhang, N. Nishida, T. A. Springer, Structure of a complete integrin ectodomain in a physiologic resting state and activation and deactivation by applied forces. *Mol. Cell* **32**, 849-861 (2008).

123. T. A. Springer, J. Zhu, T. Xiao, Structural basis for distinctive recognition of fibrinogen gammaC peptide by the platelet integrin alphaIIbbeta3. *J. Cell Biol.* **182**, 791-800 (2008).

124. J. Chen, A. Salas, T. A. Springer, Bistable regulation of integrin adhesiveness by a bipolar metal ion cluster. *Nat. Struct. Biol.* **10**, 995-1001 (2003).

125. B. H. Luo, T. A. Springer, J. Takagi, Stabilizing the open conformation of the integrin headpiece with a glycan wedge increases affinity for ligand. *Proc. Natl. Acad. Sci. U.S.A.* **100**, 2403-2408 (2003).

126. B. H. Luo, K. Strokovich, T. Walz, T. A. Springer, J. Takagi, Allosteric beta1 integrin antibodies that stabilize the low affinity state by preventing the swing-out of the hybrid domain. *J. Biol. Chem.* **279**, 27466-27471 (2004).

127. M. Nagae, S. Re, E. Mihara, T. Nogi, Y. Sugita, J. Takagi, Crystal structure of alpha5beta1 integrin ectodomain: atomic details of the fibronectin receptor. *J. Cell. Biol.* **197**, 131-140 (2012).

128. Y. Su, W. Xia, J. Li, T. Walz, M. J. Humphries, D. Vestweber, C. Cabanas, C. Lu, T. A. Springer, Relating conformation to function in integrin alpha5beta1. *Proc. Natl. Acad. Sci. U.S.A.* **113**, E3872-3881 (2016).

129. W. Yang, M. Shimaoka, A. Salas, J. Takagi, T. A. Springer, Intersubunit signal transmission in integrins by a receptor-like interaction with a pull spring. *Proc. Natl. Acad. Sci. U.S.A.* **101**, 2906-2911 (2004).

130. G. Weitz-Schmidt, T. Schurpf, T. A. Springer, The C-terminal alphaI domain linker as a critical structural element in the conformational activation of alphaI integrins. *J. Biol. Chem.* **286**, 42115-42122 (2011).

131. M. Sen, K. Yuki, T. A. Springer, An internal ligand-bound, metastable state of a leukocyte integrin, alphaXbeta2. *J. Cell Biol.* **203**, 629-642 (2013).

132. Y. Taniguchi, H. Ido, N. Sanzen, M. Hayashi, R. Sato-Nishiuchi, S. Futaki, K. Sekiguchi, The C-terminal region of laminin beta chains modulates the integrin binding affinities of laminins. *J. Biol. Chem.* **284**, 7820-7831 (2009).

133. D. Pulido, S. A. Hussain, E. Hohenester, Crystal Structure of the Heterotrimeric Integrin-Binding Region of Laminin-111. *Structure*, (2017).

134. Y. Taniguchi, S. Li, M. Takizawa, E. Oonishi, J. Toga, E. Yagi, K. Sekiguchi, Probing the acidic residue within the integrin binding site of laminin-511 that interacts with the metal ion-dependent adhesion site of alpha6beta1 integrin. *Biochem. Biophys. Res. Commun.*, (2017).

135. W. Xia, T. A. Springer, Metal ion and ligand binding of integrin alpha5beta1. *Proc. Natl. Acad. Sci. U.S.A.* **111**, 17863-17868 (2014).

136. J. F. Van Agthoven, J. P. Xiong, J. L. Alonso, X. Rui, B. D. Adair, S. L. Goodman, M. A. Arnaout, Structural basis for pure antagonism of integrin alphaVbeta3 by a high-affinity form of fibronectin. *Nat. Struct. Mol. Biol.* **21**, 383-388

(2014).

137. T. G. Kapp, F. Rechenmacher, S. Neubauer, O. V. Maltsev, E. A. Cavalcanti-Adam, R. Zarka, U. Reuning, J. Notni, H. J. Wester, C. Mas-Moruno, J. Spatz, B. Geiger, H. Kessler, A Comprehensive Evaluation of the Activity and Selectivity Profile of Ligands for RGD-binding Integrins. *Sci. Rep.* **7**, 39805 (2017).

138. N. Green, J. Rosebrook, N. Cochran, K. Tan, J. H. Wang, T. A. Springer, M. J. Briskin, Mutational analysis of MAdCAM-1/alpha4beta7 interactions reveals significant binding determinants in both the first and second immunuglobulin domains. *Cell Adhes. Commun.* **7**, 167-181 (1999).

139. P. Taylor, M. Bilsland, M. D. Walkinshaw, A new conformation of the integrin-binding fragment of human VCAM-1 crystallizes in a highly hydrated packing arrangement. *Acta Crystallogr. D Biol. Crystallogr.* **57**, 1579-1583 (2001).

140. A. Komoriya, L. J. Green, M. Mervic, S. S. Yamada, K. M. Yamada, M. J. Humphries, The minimal essential sequence for a major cell type-specific adhesion site (CS1) within the alternatively spliced type III connecting segment domain of fibronectin is leucine-aspartic acid-valine. *J. Biol. Chem.* **266**, 15075-15079 (1991).

141. J. M. Clements, P. Newham, M. Shepherd, R. Gilbert, T. J. Dudgeon, L. A. Needham, R. M. Edwards, L. Berry, A. Brass, M. J. Humphries, Identification of a key integrin-binding sequence in VCAM-1 homologous to the LDV active site in fibronectin. *J. Cell Sci.* **107 (Pt 8)**, 2127-2135 (1994).

142. G. Verdone, R. Doliana, A. Corazza, S. A. Colebrooke, P. Spessotto, S. Bot, F. Bucciotti, A. Capuano, A. Silvestri, P. Viglino, I. D. Campbell, A. Colombatti, G. Esposito, The solution structure of EMILIN1 globular C1q domain reveals a disordered insertion necessary for interaction with the alpha4beta1 integrin. *J. Biol. Chem.* **283**, 18947-18956 (2008).

143. C. Danussi, A. Petrucco, B. Wassermann, E. Pivetta, T. M. Modica, L. Del Bel Belluz, A. Colombatti, P. Spessotto, EMILIN1-alpha4/alpha9 integrin interaction inhibits dermal fibroblast and keratinocyte proliferation. *J. Cell Biol.* **195**, 131-145 (2011).

144. C. Danussi, L. Del Bel Belluz, E. Pivetta, T. M. Modica, A. Muro, B. Wassermann, R. Doliana, P. Sabatelli, A. Colombatti, P. Spessotto, EMILIN1/alpha9beta1 integrin interaction is crucial in lymphatic valve formation and maintenance. *Mol. Cell Biol.* **33**, 4381-4394 (2013).

145. R. Sato-Nishiuchi, I. Nakano, A. Ozawa, Y. Sato, M. Takeichi, D. Kiyozumi, K. Yamazaki, T. Yasunaga, S. Futaki, K. Sekiguchi, Polydom/SVEP1 is a ligand for integrin alpha9beta1. *J. Biol. Chem.* **287**, 25615-25630 (2012).

146. Y. Yokosaki, N. Matsuura, S. Higashiyama, I. Murakami, M. Obara, M. Yamakido, N. Shigeto, J. Chen, D. Sheppard, Identification of the ligand binding site for the integrin alpha9 beta1 in the third fibronectin type III repeat of tenascin-C. *J. Biol. Chem.* **273**, 11423-11428 (1998).

147. K. Eto, C. Huet, T. Tarui, S. Kupriyanov, H. Z. Liu, W. Puzon-McLaughlin, X. P. Zhang, D. Sheppard, E. Engvall, Y. Takada, Functional classification of ADAMs based on a conserved motif for binding to integrin alpha 9beta 1: implications for sperm-egg binding and other cell interactions. *J. Biol. Chem.* **277**, 17804-17810 (2002).

148. M. Huhtala, J. Heino, D. Casciari, A. de Luise, M. S. Johnson, Integrin evolution: insights from ascidian and teleost fish genomes. *Matrix Biol.* **24**, 83-95 (2005).

149. M. Shimaoka, A. Salas, W. Yang, G. Weitz-Schmidt, T. A. Springer, Small molecule integrin antagonists that bind to the beta2 subunit I-like domain and activate signals in one direction and block them in the other. *Immunity* **19**, 391-402 (2003).

150. R. Liu, L. Peng, H. Han, K. S. Lam, Structure-activity relationship studies of a series of peptidomimetic ligands for alpha(4) beta(1) integrin on Jurkat T-leukemia cells. *Biopolymers* **84**, 595-604 (2006).

151. L. Peng, R. Liu, J. Marik, X. Wang, Y. Takada, K. S. Lam, Combinatorial chemistry identifies high-affinity peptidomimetics against alpha4beta1 integrin for in vivo tumor imaging. *Nat. Chem. Biol.* **2**, 381-389 (2006).

152. R. J. Davenport, J. R. Munday, Alpha4-integrin antagonism--an effective approach for the treatment of inflammatory diseases? *Drug Discov. Today* **12**, 569-576 (2007).

153. Y. Yu, J. Zhu, L. Z. Mi, T. Walz, H. Sun, J. Chen, T. A. Springer, Structural specializations of alpha(4)beta(7), an integrin that mediates rolling adhesion. *J. Cell Biol.* **196**, 131-146 (2012).

154. A. De Arcangelis, M. Mark, J. Kreidberg, L. Sorokin, E. Georges-Labouesse, Synergistic activities of alpha3 and alpha6 integrins are required during apical ectodermal ridge formation and organogenesis in the mouse. *Development* **126**, 3957-3968 (1999).

155. Y. Kikkawa, J. H. Miner, Molecular dissection of laminin alpha 5 in vivo reveals separable domain-specific roles in embryonic development and kidney function. *Dev. Biol.* **296**, 265-277 (2006).

156. H. von der Mark, I. Williams, O. Wendler, L. Sorokin, K. von der Mark, E. Poschl, Alternative splice variants of alpha 7 beta 1 integrin selectively recognize different laminin isoforms. *J. Biol. Chem.* **277**, 6012-6016 (2002).

157. H. von der Mark, E. Poschl, H. Lanig, T. Sasaki, R. Deutzman, K. von der Mark, Distinct acidic clusters and hydrophobic residues in the alternative splice domains X1 and X2 of alpha7 integrins define specificity for laminin isoforms. *J. Mol. Biol.* **371**, 1188-1203 (2007).

158. E. T. Eng, B. J. Smagghe, T. Walz, T. A. Springer, Intact alphaIIbbeta3 integrin is extended after activation as measured by solution X-ray scattering and electron microscopy. *J. Biol. Chem.* **286**, 35218-35226 (2011).

159. J. Zhu, J. Zhu, T. A. Springer, Complete integrin headpiece opening in eight steps. *J. Cell. Biol.* **201**, 1053-1068 (2013).

160. B. L. Patton, J. H. Miner, A. Y. Chiu, J. R. Sanes, Distribution and function of laminins in the neuromuscular system of developing, adult, and mutant mice. *J Cell Biol* **139**, 1507-1521 (1997).

161. T. Sasaki, K. Mann, J. H. Miner, N. Miosge, R. Timpl, Domain IV of mouse laminin beta1 and beta2 chains. *Eur J Biochem* **269**, 431-442 (2002).

162. P. G. Noakes, M. Gautam, J. Mudd, J. R. Sanes, J. P. Merlie, Aberrant differentiation of neuromuscular junctions in mice lacking s-laminin/laminin beta 2. *Nature* **374**, 258-262 (1995).

163. P. G. Noakes, J. H. Miner, M. Gautam, J. M. Cunningham, J. R. Sanes, J. P. Merlie, The renal glomerulus of mice lacking s-laminin/laminin beta 2: nephrosis despite molecular compensation by laminin beta 1. *Nat. Genet.* **10**, 400-406 (1995).

164. J. H. Miner, G. Go, J. Cunningham, B. L. Patton, G. Jarad, Transgenic isolation of skeletal muscle and kidney defects in laminin beta2 mutant mice: implications for Pierson syndrome. *Development* **133**, 967-975 (2006).

165. J. A. Kreidberg, J. M. Symons, Integrins in kidney development, function, and disease. *Am. J. Physiol. Renal. Physiol.* **279**, F233-242 (2000).

166. B. L. Ziober, M. P. Vu, N. Waleh, J. Crawford, C. S. Lin, R. H. Kramer, Alternative extracellular and cytoplasmic domains of the integrin alpha 7 subunit are differentially expressed during development. *J. Biol. Chem.* **268**, 26773-26783 (1993).

167. J. Takagi, H. P. Erickson, T. A. Springer, C-terminal opening mimics 'inside-out' activation of integrin alpha5beta1. *Nat. Struct. Biol.* **8**, 412-416 (2001).

168. H. Fujiwara, Y. Kikkawa, N. Sanzen, K. Sekiguchi, Purification and characterization of human laminin-8. Laminin-8 stimulates cell adhesion and migration through alpha3beta1 and alpha6beta1 integrins. *J. Biol. Chem.* **276**, 17550-17558 (2001).

169. E. Engvall, G. E. Davis, K. Dickerson, E. Ruoslahti, S. Varon, M. Manthorpe, Mapping of domains in human laminin using monoclonal antibodies: localization of the neurite-promoting site. *J. Cell. Biol.* **103**, 2457-2465 (1986).

170. C. F. Tiger, M. F. Champliaud, F. Pedrosa-Domellof, L. E. Thornell, P. Ekblom, D. Gullberg, Presence of laminin alpha5 chain and lack of laminin alpha1 chain during human muscle development and in muscular dystrophies. *J. Biol. Chem.* **272**, 28590-28595 (1997).

171. K. Sekiguchi, S. Hakomori, M. Funahashi, I. Matsumoto, N. Seno, Binding of fibronectin and its proteolytic fragments to glycosaminoglycans. Exposure of cryptic glycosaminoglycan-binding domains upon limited proteolysis. *J. Biol. Chem.* **258**, 14359-14365 (1983).

172. R. Nishiuchi, O. Murayama, H. Fujiwara, J. Gu, T. Kawakami, S. Aimoto, Y. Wada, K. Sekiguchi, Characterization of the ligand-binding specificities of integrin alpha3beta1 and alpha6beta1 using a panel of purified laminin isoforms containing distinct alpha chains. *J. Biochem.* **134**, 497-504 (2003).

173. C. A. Schneider, W. S. Rasband, K. W. Eliceiri, NIH Image to ImageJ: 25 years of image analysis. *Nat. Methods* **9**, 671-675 (2012).

174. W. Kabsch, Xds. *Acta Crystallogr. D Biol. Crystallogr.* **66**, 125-132 (2010).

175. Z. Otwinowski, W. Minor, Processing of X-ray diffraction data collected in oscillation mode. *Methods Enzymol.* **276**, 307-326 (1997).

176. G. M. Sheldrick, A short history of SHELX. *Acta Crystallogr. A* **64**, 112-122 (2008).

177. P. D. Adams, P. V. Afonine, G. Bunkoczi, V. B. Chen, I. W. Davis, N. Echols, J. J. Headd, L. W. Hung, G. J. Kapral, R. W. Grosse-Kunstleve, A. J. McCoy, N. W. Moriarty, R. Oeffner, R. J. Read, D. C. Richardson, J. S. Richardson, T. C. Terwilliger, P. H. Zwart, PHENIX: a comprehensive Python-based system for macromolecular structure solution. *Acta Crystallogr. D Biol. Crystallogr.* **66**, 213-221 (2010).

178. P. Emsley, B. Lohkamp, W. G. Scott, K. Cowtan, Features and development of Coot. *Acta Crystallogr. D Biol. Crystallogr.* **66**, 486-501 (2010).

179. G. N. Murshudov, P. Skubak, A. A. Lebedev, N. S. Pannu, R. A. Steiner, R. A. Nicholls, M. D. Winn, F. Long, A. A. Vagin, REFMAC5 for the refinement of macromolecular crystal structures. *Acta Crystallogr. D Biol. Crystallogr.* **67**, 355-367 (2011).

180. V. B. Chen, W. B. Arendall, 3rd, J. J. Headd, D. A. Keedy, R. M. Immormino, G. J. Kapral, L. W. Murray, J. S. Richardson, D. C. Richardson, MolProbity: all-atom structure validation for macromolecular crystallography. *Acta Crystallogr. D Biol. Crystallogr.* **66**, 12-21 (2010).

Chapter 7: List of publications

- X. Li, H. Qian, M. Takizawa, H. Koga, A. Tsuchisaka, N. Ishii, T. Hayakawa, K. Ohara, C. Sitaru, D. Zillikens, K. Sekiguchi, Y. Hirako, T. Hashimoto, N-linked glycosylation on laminin gamma1 influences recognition of anti-laminin gamma1 pemphigoid autoantibodies. *J. Dermatol. Sci.* **77**, 125-129 (2015).

- Y. Taniguchi, S. Li, M. Takizawa, E. Oonishi, J. Toga, E. Yagi, K. Sekiguchi, Probing the acidic residue within the integrin binding site of laminin-511 that interacts with the metal ion-dependent adhesion site of alpha6beta1 integrin. *Biochem Biophys Res Commun* **487**, 525-531 (2017).

- M. Takizawa, T. Arimori, Y. Taniguchi, Y. Kitago, E. Yamashita, J. Takagi, K. Sekiguchi, Mechanistic basis for the recognition of laminin-511 by alpha6beta1 integrin. *Sci. Adv.* **3**, e1701497 (2017).

Chapter 8: Acknowledgements

This work was carried out under the direction of Professor Kiyotoshi Sekiguchi, Head of the Laboratory of Extracellular Matrix Biochemistry, now Division of Matrixome Research and Application, Institute for Protein Research, Osaka University (2011-2018).

My special thanks go to Prof. Kiyotoshi Sekiguchi for giving me the opportunity to carry out the challenging and interesting theme in his laboratory. In addition, I acknowledge for his firm guidance and for his readiness for scientific discussion on this work. I learned attitudes toward the research.

I'm very grateful to my excellent mentor, Dr. Yukimasa Taniguchi (Matrixome Inc.; Division of Matrixome Research and Application, Institute for Protein Research, Osaka University), for believing in my potential and for his constant motivation, patience, encouragement, discussions and comments during seven years. I extend thank to Dr. Yuya Sato (Laboratory of Stem Cell and Neuro-Vascular Biology, National Heart, Lung, and Blood Institute, National Institutes of Health). He has always given me scientific suggestions, comments and discussions for my research at the edge of lake.

I would like to express my sincere gratitude to all of my co-workers for supporting my research and helpful discussions, especially Prof. Junichi Takagi, Assistant Prof. Yu Kitago and Assistant Prof. Takao Arimori (Laboratory of Protein Synthesis and Expression, Institute for Protein research, Osaka University) for determination of the crystal structure of tLM511E8, and Ms. Erika Yamashita (Department of Immunology and Cell Biology, Graduate School of Medicine and Frontier Biosciences, Osaka University) for construction of many kinds of Cys-substituted mutants for intermolecular disulfide formation assays.

I would like to thank Prof. Junichi Takagi, Prof. Genji Kurisu, and Prof. Masato Okada for accepting to review my dissertation.

Many thanks go to my parents, brother, sister, aunt, and grandmother (Kenji Takizawa, Keiko Takizawa, Takeshi Takizawa, Yuka Takizawa, Yuko Senzaki and Akiko Senzaki) for their motivation, trust, encouragement. I'm sorry I'm not good at expressing my gratitude for them with words. Without them, this work could not have been completed. Let me take this opportunity to express my thanks for them. I also send big thanks to my nephews (Kohei Takizawa and Shohei Takizawa), who make me feel alive as well as my life colorful.

Finally, I thank the reader for reading my dissertation.

March 2018

Division of Matrixome Research and Application

Institute for Protein Research, Osaka University